INVESTIGATION OF SULFURIZATION TEMPERATURE EFFECTS ON Cu_2ZnSnS_4 THIN FILMS PREPARED BY MAGNETRON SPUTTERING METHOD ON FLEXIBLE TITANIUM FOIL SUBSTRATES FOR THIN FILM SOLAR CELLS

A Thesis Submitted to
The Graduate School of Engineering and Sciences of
İzmir Institute of Technology
In Partial Fulfilment of the Requirements for the Degree of

MASTER OF SCIENCE

in Material Science and Engineering

By
Dilara Gökçen Buldu

July, 2017
İZMİR

We approve the thesis of **Dilara Gökçen BULDU**

Examining Committee Members:

_____
Assoc. Prof. Dr. Gülnur AYGÜN ÖZYÜZER
Department of Physics, İzmir Institute of Technology

_____
Prof. Dr. Orhan ÖZTÜRK
Department of Physics, İzmir Institute of Technology

_____
Prof. Dr. Aysun AKŞİT
Department of Textile Engineering, Dokuz Eylül University

31 July 2017

_____
Assoc. Prof. Dr. Gülnur AYGÜN ÖZYÜZER
Supervisor, Department of Physics,
İzmir Institute of Technology

_____
Prof. Dr. Muammer Mustafa DEMİR
Head of the Department Material Science and
Engineering

_____
Prof. Dr. Aysun SOFUOĞLU
Dean of the Graduate School of
Engineering and Sciences

ACKNOWLEDGEMENT

I would like to thank to my advisor, Assoc. Prof. Dr. Gülnur AYGÜN for giving me a chance to work in the field of solar cells. I am grateful for her support, motivation and encouragement during my thesis.

Besides my advisor, I would like to thank Prof. Dr. Lütfi Özyüzer for sharing his advice and knowledge with me.

Especially, I am grateful to my laboratory colleagues for their support and helps during my work.

Lastly, I would like to dedicate my thesis to my mom because I could never succeed my thesis without her love and patience.

ABSTRACT

INVESTIGATION OF SULFURIZATION TEMPERATURE EFFECTS
ON Cu_2ZnSnS_4 THIN FILMS PREPARED BY
MAGNETRON SPUTTERING METHOD ON FLEXIBLE TITANIUM
FOIL SUBSTRATE FOR THIN FILM SOLAR CELLS

This thesis presents the effect of sulfurization temperature on Cu_2ZnSnS_4 (CZTS) thin films on flexible titanium (Ti) foil substrates. The CZTS films was produced by using a two-stage method. In the first step, the metallic precursor layers Cu/Sn/Zn/Substrate were deposited on Ti foil substrate by using DC magnetron sputtering method. In the second step, the deposited metal precursors were sulfurized in a graphite box under Argon (Ar) ambient inside a tubular furnace under a definite temperature. To understand the effects of temperature on the formation of the CZTS structure several analyses were performed. Our samples, each with a different sulfurization temperature; ranging from 530 to 580 $^{\circ}C$, were carried out and the structural properties of the absorber layer was determined. XRD measurements showed a sharp and intense peak coming from the (112) planes which was a strong evidence for good crystallinity. The intensity of (112) plane became a sharp and intense with increasing sulfurization temperature. Raman spectroscopy of the sulfurized thin films revealed that, the kesterite structure CZTS thin film were obtained with increasing sulfurization temperature. Electron Dispersive Spectroscopy (EDS) was also used for the compositional analysis of the thin films. EDS analysis showed that the films were grown with a Cu-poor Zn-rich composition. From these analyses we conclude that no interface formation occurred between the substrate and the CZTS thin films, hence, a buffer layer was not required. It was also seen that Ti foil was suitable as substrate for the growth of CZTS thin films with desired properties. We also conclude that the sulfurization temperature plays a crucial role for producing good quality CZTS thin films on Ti foil substrate.

ÖZET

SÜLFÜRLEME SICAKLIĞININ İNCE FİLM GÜNEŞ HÜCRELERİ İÇİN ESNEK TİTANYUM FOLYO ALTTAŞLARI ÜZERİNE MIKNATISSAL SAÇTIRMA YÖNTEMİYLE HAZIRLANAN Cu_2ZnSnS_4 İNCE FİLMLERE ETKİSİNİN İNCELENMESİ

Bu tez çalışmasında, sülfürleme sıcaklığının esnek titanyum (Ti) folyo alttaşları üzerine büyütülen Cu_2ZnSnS_4 (CZTS) ince filmler üzerine etkisi incelendi. CZTS filmler iki aşamalı metot kullanılarak üretildi. İlk aşamada, metalik öncü katmanlar olan Cu/Sn/Zn/ Ti folyo alttaşı üzerine DC magnetron püskürtme metodu kullanılarak büyütüldü. İkinci aşamada, kaplanan metal öncü katmanlar grafit kutuda, boru şeklindeki fırın içerisinde, Argon (Ar) ortamında belirlenen sıcaklık altında sülfürlendi. Sıcaklığın CZTS yapısı oluşumundaki etkisinin anlaşılması için pek çok farklı analiz kullanıldı. Örneklerimiz, 530 ile 580 ºC arasında değişen farklı sülfürleme sıcaklıklarına tabii tutuldu ve elde edilen her bir emici tabakanın yapısal özellikleri incelendi. XRD ölçümlerinde, yapının iyi bir kristal yapısına sahip olduğunu doğrulayan, (112) düzlemlerinden gelen keskin ve güçlü bir sinyal görüldü. Sülfürleme sıcaklığının artması ile (112) düzleminden gelen sinyalin güçlendiği görüldü. Sülfürlenen ince filmlerin Raman spektroskopisi sonuçları ise artan sülfürleme sıcaklığının artmasına bağlı olarak kesterite yapısındaki CZTS ince filmlerin üretildiğini gösterdi. İnce filmlerin kompozisyonlarının belirlenmesi için Elektron Dağılımlı Spektroskopi (EDS) ölçümleri yapıldı. EDS analizleri büyütülen filmlerin kompozisyonlarının Cu bakımında fakir, Zn bakımından zengin miktar içerdiğini gösterdi. Bu analizlerden yola çıkarak, CZTS ince filmi ile alttaş arasında bir arayüz oluşumu olmadığını, dolayısıyla, bir tampon katmanın gerekli olmadığını söyleyebiliriz. Ayrıca, istenen özelliklerde CZTS ince filmlerin üretilebilmesi için Ti folyo alttaşının uygun bir aday olduğu görüldü. Sonuç olarak, sülfürleme sıcaklığının, Ti folyo alttaş üzerinde yüksek kalitede CZTS ince filmlerin üretilmesinde önemli bir rol oynadığı gözlemlendi.

TABLE OF CONTENTS

LIST OF FIGURES

LIST OF TABLES

CHAPTER 1

INTRODUCTION

The increase in the world population in the last century has undoubtedly increased the need for energy. Most of the limited reserves of fossil and nuclear fuels are recently being used to meet the growing energy demand of the world, yet the shortage of these fuels are inevitable. Furthermore, burning these fuels have environmental impacts such as air pollution and the climate change. So, the utilization of clean energy sources has started to attract immerse attention in the energy generation sector in order to meet the growing demand for energy globally in a green and cost competitive manner.

The solar energy is most promising, economic and powerful one among the other clean and renewable energy sources because of the direct conversion of sunlight into electricity. The solar energy is of particular interest due to its capacity to provide up to terawatts of electricity, comparable to that of consumed in the world. However, in order to utilize the solar energy as the major source of the electricity supply, the current photovoltaic technology should be improvised to achieve a cost-competitive market with respect to the current sources of electricity.

1.1 Brief History of Thin Film Solar Cell

Currently, the dominant absorber layers in photovoltaic (PV) market are based on single-crystal (c-Si) or multi-crystalline (mc-Si) semiconductors. Si solar modules require a thickness about 200-300 µm and high energy intensive process. Although the high efficiency is observed using c-Si solar modules, the manufacturing costs of the structures are also quite high. Therefore, the low cost alternatives are being investigated by using cheap techniques with less material consumption. In this case, PV can compete with the current sources of electricity.

The thin film technology is the real competitor of Si solar cells, as this technology promises a vast range of applications and furthermore, other superior advantages such as portability, cost-effective production and the ease of installation. As an inevitable result of these superiorities, along with the advantages of thin (down to 1-3 µm thickness) films

including low weight and flexibility, the thin film solar cell technology has been a powerful alternative to Si wafer technology for contemporary applications. Latterly, two chalcopyrite semiconductor compounds, namely $Cu(In,Ga)Se_2$ (CIGS) and CdTe, have been in the hotspot of research to be commercially used in thin film solar cell industry as an absorber layer material. The highest power conversion efficiency report is 22.3% for CIGS and 22.1% for CdTe thin films (Green et al. 2016). Even though these compound semiconductor have high conversion efficiency, they have some disadvantages due to its constituent elements. Cadmium (Cd) is a toxic element and it causes environmental problems. Indium (In), Gallium (Ga) and Telluride (Te) are limited source so they are high cost materials. These disadvantages impose restrictions in the production of these thin film solar cells. To overcome these restrictions, Cu_2ZnSnS_4 (CZTS) has been suggested as a promising thin film semiconductor material, as its constituent elements are earth-abundant, non-toxic and cheap. The relation between the abundance and price of material can be seen in Figure 1.1.
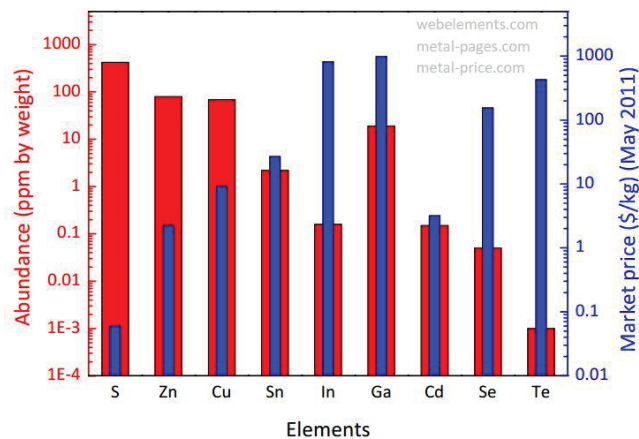
Figure 1.1. Thin film solar cell materials abundance and prices
(Source: Berg, 2012).

CZTS is one of the most promising candidate materials among many others as an absorber layer in the solar cells. Main reasons for that are that first, it has a low-cost production since it does not contain any rare elements, such as Ga and In, and second, it is environmentally friendly because it does not contain any toxic elements such as Cd. Thus, CZTS is a very important replacement material, especially more so, for conventional $Cu(In,Ga)Se_2$ (CIGS) thin film solar cells. CZTS is a p-type quaternary semiconductor compound with a large absorption coefficient, larger than 10^4 cm^{-1}, having a direct band gap with a gap energy of 1.5 eV (Katagiri et al. 1997) which makes it a

superior candidate to many others as an absorber layer in solar cell devices for the replacement of conventional Si whose band gap is indirect which limits its performance. Theoretically, the Shockley-Queisser limit of a single p-n junction with 1.52 eV bandgap is found the maximum solar conversion efficiency to be approximately 32% by using an AM 1.5 solar spectrum (Shockley and Queisser 1961). The last reported highest power conversion efficiency is 9.4% (Tajima et al. 2017) and 12.6% (Wang et al. 2014) for CZTS and $Cu_2ZnSn(S,Se)_4$ (CZTSSe), respectively. By concerning promising Shockley limit of semiconductor material, which has 1.52 eV band gap, and the last reported efficiency of CZTS, more research should be done to achieve higher efficiency with CZTS material.

1.2. Overview of CZTS Thin Film Solar Cell

CZTS was originally developed for thin film solar cells in 1998 by Ito and Nakazawa (Ito and Nakazawa 1988), using atom beam sputtering thin film deposition method. Several production methods have been used in the fabrication of CZTS thin film, such as electrodeposition (Scragg et al. 2008; Ennaoui et al. 2009), spray pyrolysis deposition (Yoo and Kim 2011; Tanaka et al. 2012), hydrazine-based solution (Wang et al. 2014), e-beam evaporation (Araki et al. 2008), co-evaporation (Hiroi et al. 2013), thermal evaporation (Zakaria et al. 2015), and magnetron sputtering (Yazici et al. 2015; Jimbo et al. 2007; Ericson et al. 2012; Liu et al. 2010; Fernandes et al. 2009) etc. Most of these techniques use a rigid substrate, such as, molybdenum (Mo) coated soda lime glass (SLG) substrates which restricts the area of applications. This limitation can be avoided with the use of a flexible substrate. In fact, it is possible to produce thin film solar cells fabricated on flexible substrates, such as aluminium (Al), Mo, stainless steel (SS) foils or flexible glass. The flexibility of these solar cells makes it possible to reduce the total thickness of the films and their cost. There are some reports of CZTS thin films on flexible metallic substrates as well (Yazici et al. 2015; Zhang et al. 2014; Khalil et al. 2016; Xu et al. 2014; Sun et al. 2016). For such a thin film on a Mo foil substrate grown by electrodeposition method, the highest conversion efficiency is 3.82% (Zhang et al. 2014). The thin film on a SS foil substrate grown by co-sputtering method, the highest conversion efficiency is 4.10% (Sun et al. 2016). However, the conversion efficiency of flexible CZTS thin film solar cells is still lower than the rigid CZTS thin film solar cells.Therefore, there is a need

for more research to understand growth mechanism of CZTS thin film on flexible substrates to improve their efficiencies beyond those of conventional ones.

The challenges are controlling the film composition during the growth process and phase stability of this compound during the sulfurization process. Phases such as $Cu_{2-x}S$ and $Cu_{2-x}Sn_xS_3$ are detrimental for device because of their behaviour, which could lead to shunting of cells. The other challenges are the grain size of CZTS thin film, and the conversion efficiency of thin films which is strongly related to the grain size due to the enhanced minority carrier diffusion lengths and built-in potentials in thin film solar cells (Mkawi et al. 2014; Shin et al. 2011). The grain boundaries act as recombination centres resulting in a decrease the efficiency of thin film solar cells (He et al. 2015; Xie et al. 2013). Therefore, studying the impact of the various growth parameter, especially the temperature in the sulfurization process, may provide to understand how to avoid phase existence and get large grain size.

In this thesis, firstly metallic precursor layers were deposited on Ti foil via magnetron sputtering method which is low-cost and easy adaptation to large-scale manufacturing. Then, sulfurization was carried out at various temperatures. Sulfurization temperature is one of the key point to produce good quality CZTS thin film. Thus, the effect of the sulfurization temperature has been investigated to understand how it affects the structural, composition and morphological properties of the thin film on Ti foil substrate. Additionally, Ti foil has been chosen because its thermal expansion coefficient is in similar order with CZTS absorber layer, and also it shows chemical inertness behaviour.

CHAPTER 2

THE PHYSICS OF SOLAR CELLS

Solar cell is a semiconductor device which converts solar radiant energy directly into electrical energy. When photon with energy equal to or higher than band gap of the solar cell semiconductor is absorbed, consequently electrons in the semiconductor become excited and they promote from valence band (E_v) to conduction band (E_c), leaving a free space (hole) in the valence band and electron-hole pair is created. When the electrons and holes are separated and electron-hole pairs are formed, the built-in electric field of p-n junction separates these electrons and holes; which result in free carriers inside the system. This is the basic mechanism behind the solar cell devices that convert the incident photon energy into electrical energy.

2.1. Types of Semiconductor

The type of semiconductor is defined according to the electron and hole distributions in energy band. Electrons and holes are able to move freely in a semiconductor. In the band diagram model, the level of Fermi Energy (E_f) is used to represent the hypothetical energy level of an electron at which there is a 50% probability of being occupied. The types of semiconductors are illustrated according to the location of their E_f at Figure 2.1. First type of semiconductor is intrinsic semiconductor, which has equal number of electrons and holes in the valence and conduction band, its E_f is located in the middle of the band gap. Second type of semiconductor is extrinsic semiconductor which can be p-type or n-type semiconductor. In an extrinsic semiconductor the plentiful carriers are named majority carrier, while the less abundant carriers are named minority carriers. In p-type semiconductors, the holes are majority carriers and electrons are the minority carriers. Their E_f is located close to the valence band, this results in less electrons at higher energies. In n-type semiconductors, the holes are minority carrier whereas the electrons are majority carriers. Their E_f is located close to the conduction band as a result of plentiful electrons at those energy level.
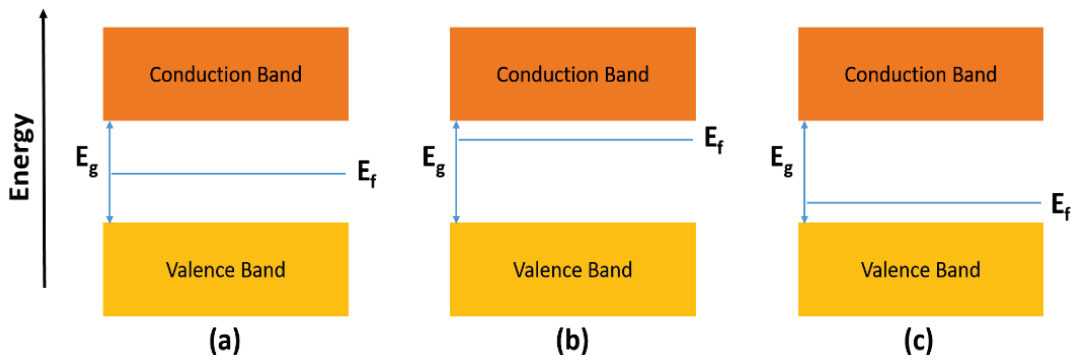
Figure 2.1. Semiconductor types (a) intrinsic, (b) n-type, and (c) p-type
semiconductor.

2.2. P-N Junction

When a p-type and an n-type semiconductor put into contact with each other, p-n junction is formed. When the two semiconductor are jointed with each other, the diffusion of majority carriers occurs across the barrier. The electrons move from n-type to p-type, leaving a positively charged donor ions and holes move from p-type to n-type, leaving a negatively charged acceptor ions. As a result, in the vicinity of the contact region, the space charge region (SCR) or depletion region (DR) is formed by fixed positive and negative charged ions. These fixed ions in the DR forms an electric field, which is known as built-in electric field (E_{in}), from the positive donor ions in the n-type region to the negative charge ions in the p-type region. As a consequence of the electrical field, drift current arise which counteracts the diffusion flow of respective charge carrier types. At equilibrium, the diffusion and drift current compensate each other. The E_f of p-type and n-type is aligned. As a result, the energy bands of these materials shift. The magnitude of this shift is equal to the built-in potential set by the p-n junction boundaries.

In the vicinity of an applied external voltage to the p-n junction, the equilibrium becomes disturbed; consequently the drift and the diffusion currents no longer compensate each other.

In forward bias, the positive terminal is connected to the p-type region and negative terminal is connected n-type region. The induced field and built-in field are in opposite direction so the resultant field is decreased. Thus, the potential difference within in the depletion region is reduced and the depletion region gets thinner.

In reverse bias, the negative terminal is connected the p-type region and positive terminal is connected n-type region. The induced field and built-in field are in the same,

so the resultant field is increased. Thus, the potential difference within in the depletion region is increased and the depletion region becomes thicker.

2.3. Principle of Solar Cells

2.3.1. Characteristic Parameters of Solar Cells

When a solar cell is illuminated under solar spectrum, additional electron-hole pairs are created resulting in photogenerated current (I_{ph}) is generated. The photocurrent causes a shift of the dark curve downward by amount of I_{ph}. The maximum current is obtained when the voltage across the solar cell is zero, as the solar cell is short circuited. It is called short-circuit current I_{sc}. The maximum voltage across the solar cell is obtained when the current is zero. It is called the open-circuit voltage (V_{oc}).

The Fill Factor (FF) determined the performance of solar cell. It is equal to ratio of the solar cell maximum actual power output ($P_{max} = V_{max}$ x I_{max}) versus the power product V_{oc} x I_{sc}. (Figure 2.2).

$$FF = \frac{P_{max.}}{V_{oc} \times I_{sc}} \tag{2.1}$$

The energy conversion efficiency (η) of solar cells is defined as the ratio between of electrical power output at the maximum operating point and the incident light power to which the cell the cell is exposed. The different parameters, such as the intensity of the incident light, the working temperature of the solar cell, affects the efficiency of solar cells.

$$\eta = \frac{P_{max.}}{P_{inc.}} = \frac{V_{oc} \times I_{sc} \times FF}{P_{inc}} \tag{2.2}$$
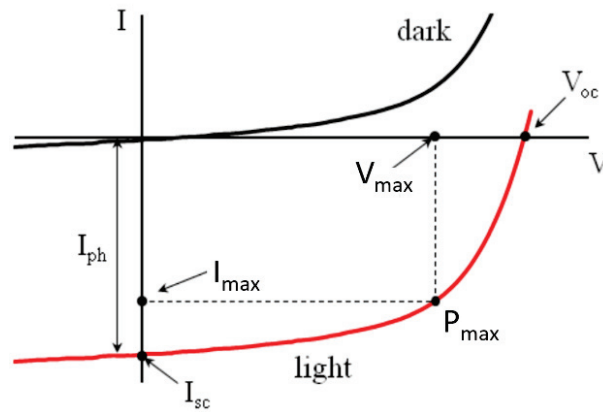
Figure 2.2. Current-voltage of p-n junction solar cell.

2.3.2. Losses in Solar Cells

Series (R_s) and shunt (R_{sh}) resistances cause the losses in the solar cells. The resistance of the front and back contacts, and the resistance at the interface of different layers, such as contact resistance between metal back contact and absorber layer, causes the R_s. High values of the R_s may reduce the I_{sc}, but it has no effect on V_{oc}. R_{sh} can cause an alternative paths, in particular short-circuits, for current. The non-perfect interface between the semiconductor layer and metal contacts, and the lattice defects in the depletion region can cause it. To prevent lost in V_{oc}, R_{sh} must be as highest as possible (Figure 2.3).
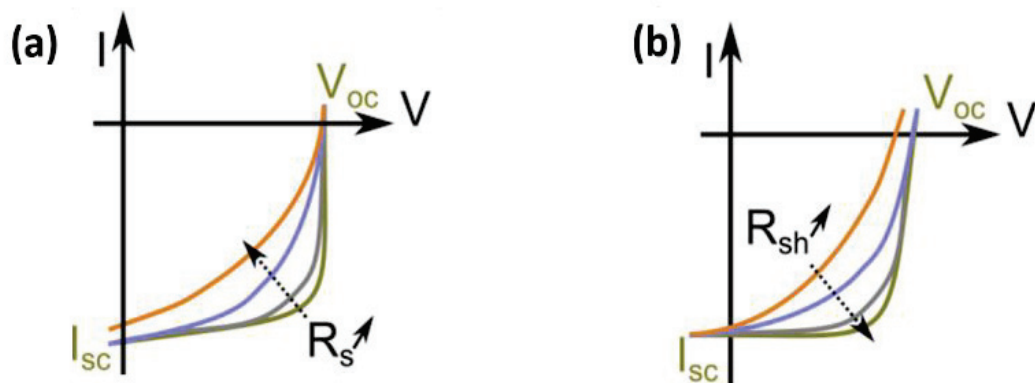
Figure 2.3. Effect of (a) R_s and (b) R_{sh} resistance on photovoltaic
(Source: Altamura, 2014).

The other loss is optical losses. All of the incident light cannot be absorbed and a part of incident light is reflected by the metal contacts and shade a portion of the front surface, thus not contributing to the generation of electron-hole pairs. Another part of

incident light is reflected at the front surface. To avoid the optical losses, an antireflective coating can be deposited.

Recombination is a reverse process of the generation of electron-hole pairs. In recombination process, photogenerated electron-hole pairs destroy each other before they are collected at the external cell electrodes. An excited electron falls down from the conduction band to the valance band and there, it recombines with an already-present hole and releases energy. This released energy is emitted either as a photon, or a phonon. In semiconductors, the recombination processes can be examined under two main processes: intrinsic and extrinsic recombination. Intrinsic transition, including band-band and band-band Auger recombination, are unavoidable and occur even in defect free semiconductors. The lattice defects or impurities in the semiconductor causes extrinsic transitions. Lattice defects or impurity atoms with energy level acts as a recombination centre and traps for charge carriers. For this reason, the total amount of free-charge carrier decreases and directly the I_{sc} and V_{oc} of the device are effected by recombination process. As a result, the FF is reduced also. Therefore, producing semiconductor materials with minimal impurities is crucial for obtaining efficient solar cells.

CHAPTER 3

THIN FILM SOLAR CELLS

Thin film technology has a fast growing rate in the PV market. Because thin film materials have direct band gap with having light absorption coefficients and are less material intensive to absorb the same amount of light so they overcome the limitation of Si-based solar cells. Besides the absorber layer material thickness is a few microns when it is compared with Si-based solar cells. The device can be fabricated on various substrates such as glass, plastic and metal foils, by the way, the thin film technology offers various fabrication process which is simpler and lower cost. Figure 3.1 shows the typically thin film PVs device.
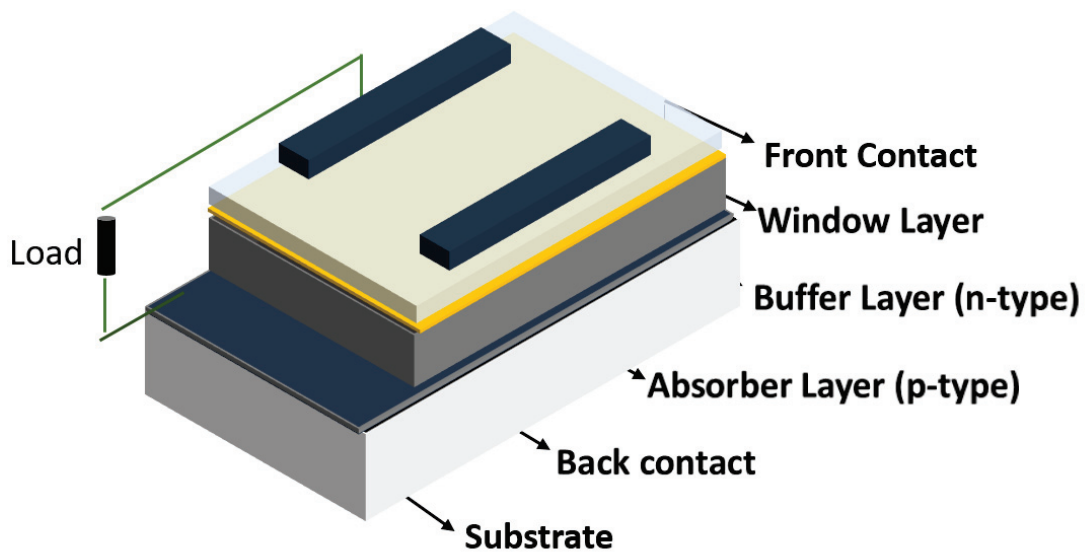
Figure 3.1. Typically thin film PVs device.

The working principle of thin film solar cell is similar to p-n heterojunction where dissimilar semiconductor is connected. A p-type semiconductor is deposited as an absorber layer, where the electron-hole pairs are formed, on back contact or metal foil substrate. A p-type semiconductor material is generally chosen as an absorber layer, because the diffusion length of electrons in p-type semiconductor is larger than the diffusion length of holes in an n-type semiconductor. Then a thin n-type semiconductor

is deposited as a buffer layer on it. The buffer layer must be thin and made of wide-band material for incident light to pass through to absorber layer without being absorbed. The transparent conducting oxide material is deposited as a window layer to draw the current to outer circuit.

To obtain high efficient thin film solar cells, each component behaviour should be understood. Because each layer is formed of different materials so it has different physical and chemical properties. The non-perfect interface can cause the defects, surface recombination, and stress formation.

3.1. Absorber Layer

P-type semiconductor materials are generally used as an absorber layer in thin film PVs. In order to convert a photon into an electron, an absorber layer is utilized in thin film solar cells. The theoretical high efficiency is 32.4% and to reach sufficient efficiency, the band gap should be in the range of 1.1-1.7 eV. At this moment, cadmium telluride (CdTe) and copper indium gallium sulphide (CIGS) are used as an absorber layer in the thin film PV. However, these absorber layers have some disadvantages due to the elements it contains. Cadmium is a toxic element, gallium and telluride are rare elements in the Earth. In this manner, these thin films are not ideal candidates for sustainable energy due to these disadvantages. To eliminate these disadvantages, Cu_2ZnSnS_4 (CZTS) has been suggested as a promising thin film semiconductor material, as its constituent elements are earth-abundant, non-toxic and cheap elements.

3.1.1. Cadmium telluride (CdTe)

In thin film PVs market, CdTe has been used as an optimal absorber layer candidate (Chaar et al. 2011) due to its chemical stability and high absorption coefficient ($>10^4$ cm^{-1}) with having direct band gap of about 1.45 eV (Bai et. al., 2011). The material can be both as p- or n-type, but p-type CdTe is used as an absorber layer for solar cells. The highest record of 22.1% for CdTe cell (Green et al. 2016). Although CdTe thin film solar cell is produced cost-effectively and with high efficiency, the toxicity of cadmium and the rarity of tellurium which could negative impact in the production of PVs.

3.1.2. Cu(In,Ga)Se$_2$ (CIGS)

The quaternary compound copper gallium indium diselenide Cu$_2$InGaSe$_2$ (CIGS) has direct bandgap with high absorption coefficient and its bandgap can be tuned by ranging indium diselenide CuInSe$_2$ (1.0 eV) to copper gallium diselenide CuGaSe$_2$ (1.7 eV) (Jackson et al. 2011).These chalcopyrite semiconductors have direct bandgap with high absorption coefficient which makes them suitable for PV applications. The first CuInSe$_2$ thin film was demonstrated in 1976 with 4.5% efficiency (Kazmerski, and Morgan 1976). Later, gallium was included in CuInSe$_2$ to produce CIGS and the highest efficiency is 22.3% (Green et al. 2016) for CIGS thin film solar cell. The rarity of indium causes negative impact in PV application because the high price of indium affects to produce cell and module costs.

3.1.3. Cu$_2$ZnSnS$_4$ (CZTS)

Thin film modules suffer from shortage of raw materials such as Te and In and toxicity of Cd, or low efficient a-Si. In this regard, CZTS appears to be a promising candidate as an absorber layer material in thin film solar cells because it contains earth-abundant and non-toxic elements unlike CdTe and CIGS. CZTS is a p-type semiconductor with a direct band gap around 1.5 eV, having a large absorption coefficient, which makes it a suitable absorber layer for thin film solar cell applications (Ito and Nakazawa 1988). Theoretically, the Shockley-Queisser limit of a single p-n junction with 1.52 eV bandgap is found the maximum solar conversion efficiency to be approximately 32% by using an AM 1.5 solar spectrum (Shockley and Queisser 1961).

The quaternary CZTS can be derived from II-V compound which is zinc-blende (ZnS). Zn atom is replaced with one Cu atom which is group-I atom and one In atom which is group-III atom so the ternary compound semiconductor (I-III-VI$_2$) such as CuInS$_2$ is formed. Then, the half of In atom is replaced with one Zn atom which is group-II atom and the other half with Sn atom which is group-IV atom, resulting CZTS is produced. The derivation of CZTS from ZnS can be seen in Figure 3.2.
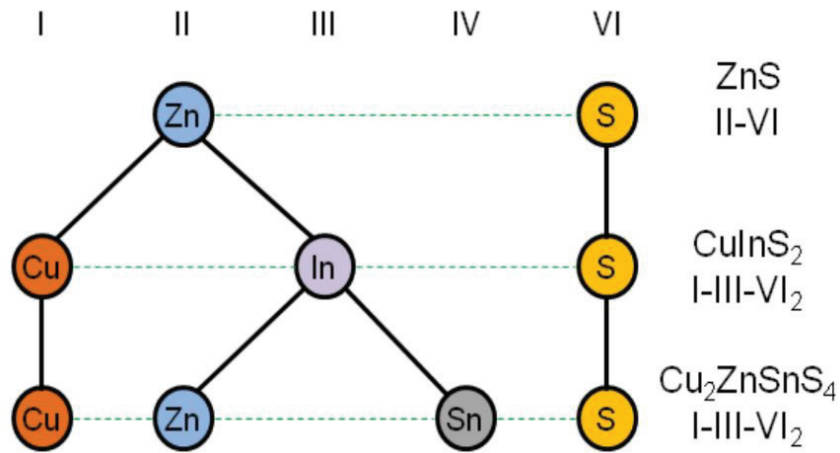
Figure 3.2. Derivation of CZTS from ZnS
(Source: Abusnina, 2016).

3.1.3.1. Crystal structure

CZTS can crystallize in two main structure form which is either kesterite (space group $I\bar{4}$) or stannite structure (space group $I\bar{4}2m$). Both crystal structures are tetragonal structures, consisting of cubic closed faced array of sulfur anions, with cations occupying one half on the tetrahedral voids, with a stacking similar to the zinc blend. The arrangements of cation atoms give rise to two different structures formation. In kesterite CZTS structure, the cation layers CuSn, CuZn, CuSn, CuZn alternate at z = 0, $^1/_4$, ½ and ¾, respectively, whereas in the stannite CZTS structure, ZnSn layer alternate with Cu_2 layers. Sn is located at the same structural site for both kesterite and stannite structure (Hall et al. 1978; Paier et al. 2009). Both kesterite and stannite structure are body-centered tetragonal with c ≈ 2a and the lattice constants a and c are similar for both of them (Paier et al. 2009). The crystal structure of kesterite and stannite CZTS is can be seen in Figure 3.3. The ab-initio calculations shows that the kesterite CZTS structure is more stable than stannite CZTS structure, and it is also more likely to form due to the low energy cost (Chen et al. 2009; Persson, 2010).
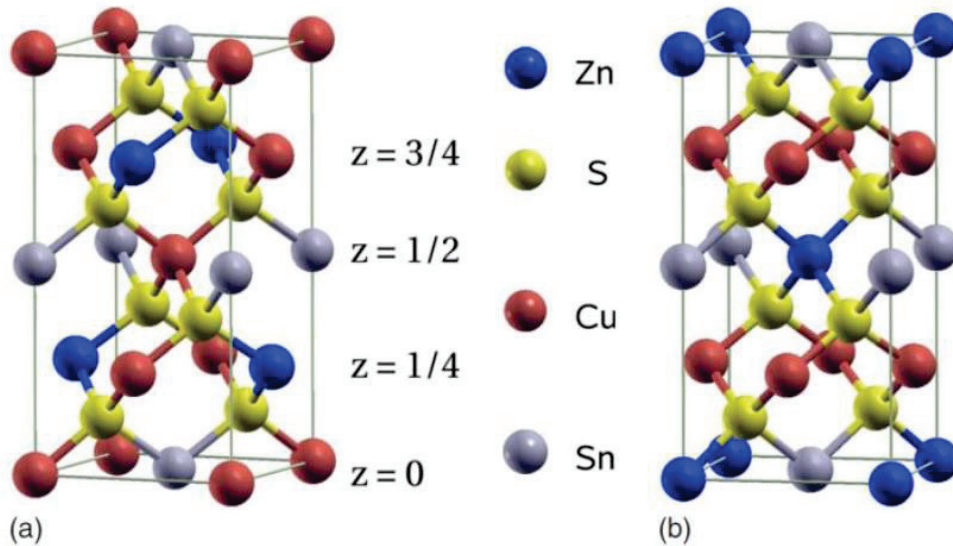
Figure 3.3. Crystal structures of (a) kesterite, (b) stannite CZTS
(Source: Paier et al. 2009).

Moreover, the tetragonal structure modifications have been shown in the literature (Paier et al. 2009; Chen et al. 2009). These modifications of the kesterite attribute to the tetragonal space groups which are P$\bar{4}$2c, P$\bar{4}$2$_1$m and P2. By exchanging two ions on the cation sublattice, these modifications can be observed. When copper and zinc atoms in the layer z=1/4 are exchanged, the structure, which belongs to P$\bar{4}$2c space group, is formed. Cu atoms in the layer z =1/2 and Zn atoms in the layer z=3/4 are exchanged, the structure which belongs to P$\bar{4}$2$_1$m space group is formed. In the last structure which is P2, a Cu atom at z=1/2 is exchanged with Zn atom at z=3/4. The structures can be seen in Figure 3.4.
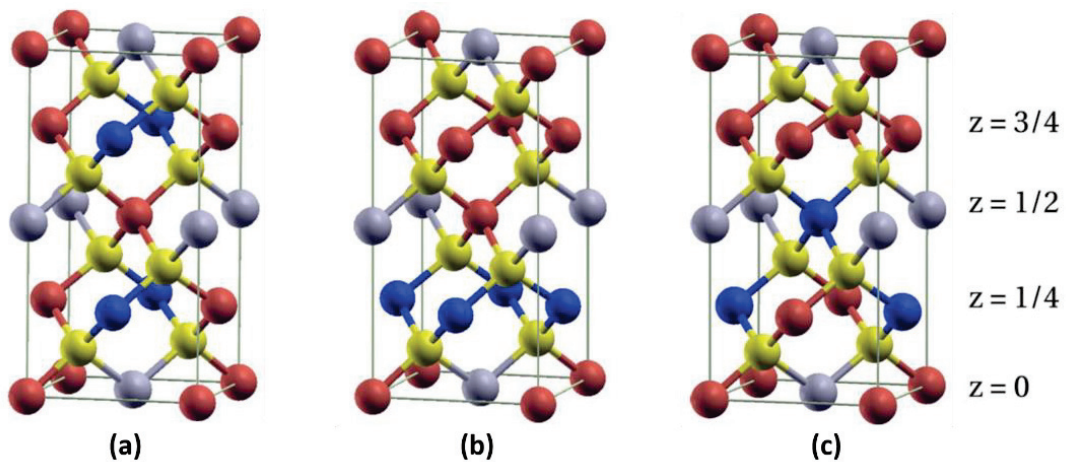
Figure 3.4. Three structural modification of kesterite which belongs to (a) P$\bar{4}$2c, (b) P$\bar{4}$21m and (c) P2 space group are shown (Source: Paier et al. 2009).

14

3.1.3.2. Intrinsic Defects

CZTS is quanternary compound semiconductor and due to its complexity, the several intrinsic defects are possible that can form during the growth process. These include vacancies (V_{Cu}, V_{Zn}, V_{Sn}, V_s), antisite defects (Cu_{Zn}, Zn_{Cu}, Cu_{Sn}, Sn_{Cu}, Zn_{Sn}, and Sn_{Zn}), and interstitial defects (Cu_i, Zn_i, and Sn_i). These defects can form shallow donor and acceptor level, mid gap level, and can acts like traps or recombination center within the band gap of CZTS material. The formation of acceptor defects are lower than the formation of donor defects. Copper vacancies (V_{Cu}) and copper on zinc antisite (Cu_{Zn}) form an acceptor level. The V_{Cu} acceptor has a shallower level just above valence band maximum. The Cu_{Zn} acceptor level is deeper than V_{Cu} but actually, the absolute position is not a deep level. Both of defects are beneficial to improve the p-type nature of CZTS and device efficiency. The other acceptor defects, such as Cu_{Sn}, Zn_{Sn}, V_{Zn}, V_{Sn}, form multiple level within the band gap of CZTS because of the high energy formation. Their contribution could be negligible for single phase crystal but they could act as recombination centers. The deep donor defects, which are Sn_{Cu}, Sn_{Zn}, Zn_i and V_s, can act as electron-hole pair recombination center thus these defects could affect the device performance. The ionization level of intrinsic defects within the band gap of CZTS are shown in Figure 3.5.
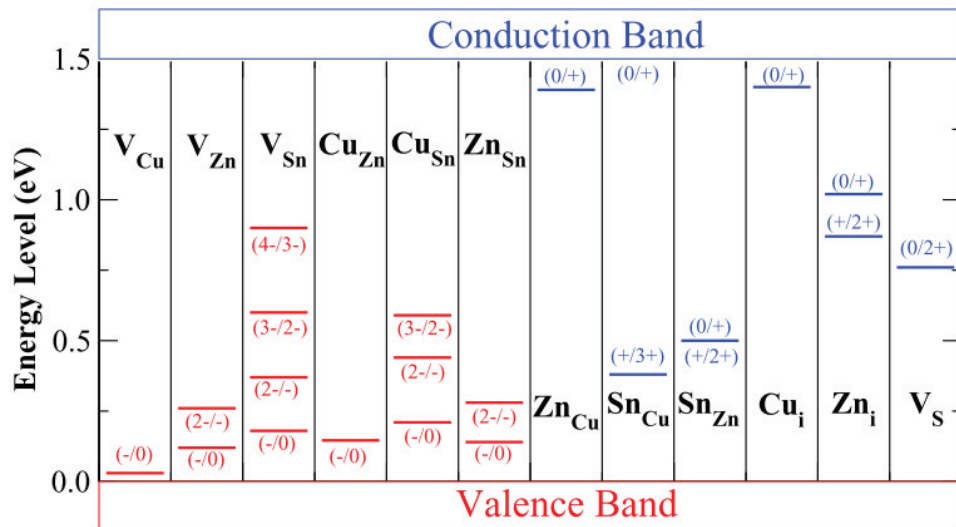
Figure 3.5. The ionization level of intrinsic defects within the band gap of CZTS
(Source: Chen et al. 2013).

Beside these defects, defect clusters can form in CZTS. The defect clusters are self-compensate defects that form because of the presence of donor and acceptor vacancies, interstitial and antisite defects. Their formation energy is lower than individual antisite defect. The understanding of these defects is important because they affect the optical and electronic properties of CZTS (Chen et al. 2010). Defect clusters can be characterized as stoichiometric and non-stoichiometric defects. The stoichiometric defect clusters are $[Cu_{Zn}+Zn_{Cu}]$, $[Sn_{Zn}+Zn_{Sn}]$, $[Cu_{Sn}+Sn_{Cu}]$ and the non-stoichiometric defect clusters are $[V_{Cu}+Zn_{Cu}]$, $[Zn_{Sn}+2Zn_{Cu}]$, $[2Cu_{Zn}+Sn_{Zn}]$. Two of stoichiometric defect clusters, which are $[Sn_{Zn}+Zn_{Sn}]$, $[Cu_{Sn}+Sn_{Cu}]$, decrease the band gap in CZTS thus they affect the electronic structure, and they are not taken as benign defects. However, $[Cu_{Zn}+Zn_{Cu}]$ defect clusters do not have significant impact on the electronic and optical properties, and they can be thought as benign defects (Chen et al. 2013), but the disorder in the kesterite Cu-Zn layer can be explained by this defect clusters (Schorr et al. 2007). The non-stoichiometric defect cluster have a significant effect on stoichiometry of CZTS. The high population of $[2Cu_{Zn}+Sn_{Zn}]$ defect clusters can be in CZTS material due to their low formation energies. They decrease the band gap of CZTS, and induce electron-hole trapping level in CZTS result in introducing a detrimental impact on device performance (Chen et al. 2012). The $[V_{Cu}+Zn_{Cu}]$ defect clusters can be beneficial for CZTS because they can facilitate the separation of electron-hole pair (Chen et al. 2013). The formation of stoichiometric defect clusters are not dependent of stoichiometric variation in CZTS, whereas the non-stoichiometric defect clusters have impact on stoichiometry of CZTS. The both works shows under Cu-poor and Zn-rich composition condition gives high efficiency of CZTS solar cells.

3.1.3.3. Phase stability and controlling of CZTS composition

The phase stability and controlling of chemical composition of a quanternary compound CZTS is challenging because, it has for constituents and each of which can be varied independently. To explain the Cu-Zn-Sn-S quanternary system, four dimensional diagram is required but the chalcogen, which is sulphur, is not an independent variable so it allows to represent the alloy in a ternary phase diagram. The amount of sulphur in the alloy depends on the amount of metals and their valance such as Cu(I), Zn(II) and Sn(IV). The ratios of atomic percentages Cu/(Zn+Sn) and Zn/Sn are used to represent the

composition of the metallic elements in the alloy. When the both ratios are equal to one, it can be said that the material is stoichiometric. In particular case, these ratios do not clearly show stoichiometric deviation because they are not independent. The pseudo-ternary system Cu_2S-ZnS-SnS_2 was investigated by Olekseyuk et al. (Olekseyuk et al. 2004), who showed that the single-phase CZTS only forms in a very small region of composition, and a small deviation from stoichiometric composition gives rise to the formation of binary and/or ternary secondary phases. This phase diagram was developed for an equilibrium at 400 ℃. The simplified ternary phase diagram, by using the based on study of Oleksyuk and on the assumption that the sulfur content is not an independent variable in the alloy was suggested by Scragg et al. (Scragg, 2010). This ternary phase diagram can be seen in Figure 3.6.
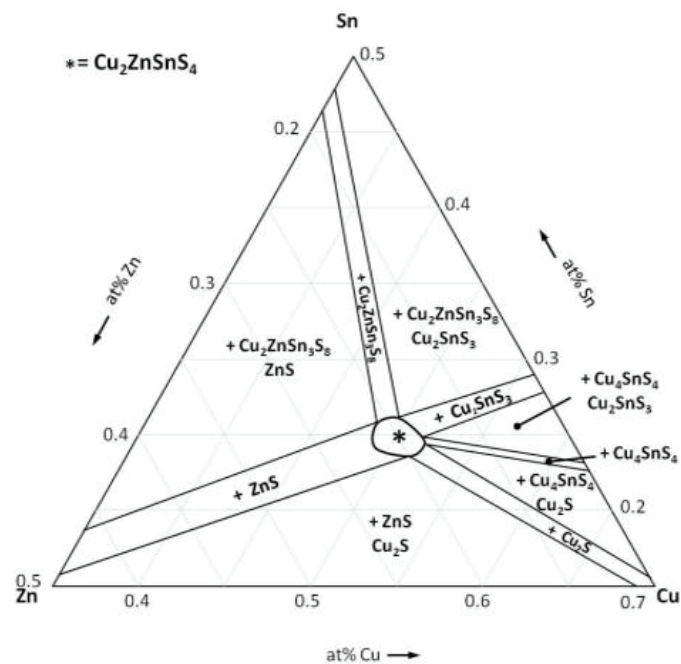
Figure 3.6. Ternary phase diagram and the expected secondary phases
(Source: Scragg, 2010).

The phase diagram includes ten fields. Each field includes secondary phase formation in addition on CZTS formation. The eleventh region in the middle, marked with a star, is the place where pure CZTS formation is possible.

The point defects in the form of cationic substitution are related to the non-stoichiometry in CZTS absorber (Lafond et al. 2012; Choubrac et al. 2012). Three of non-stoichiometric defect cluster give rise to different type formation which is related the composition of CZTS. Cu-poor Zn-rich composition can be observed as A-type and B-

type formation. $[V_{cu}+Zn_{Cu}]$ and $[2Zn_{Cu}+Zn_{Sn}]$ defect cluster give rise to the A-type formation and B-type formation, respectively. For Cu-rich Zn poor composition the C-type formation is observed where $[2Cu_{Zn}+Sn_{Zn}]$ defect cluster is (Choubrac et al. 2012; Valle Rios et al. 2016). The type formations are related to the Cu_2S-ZnS-SnS$_2$ ternary phase diagram also to the metallic ratios Cu/(Zn+Sn) and Zn/Sn (Figure 3.7). The connection between composition ratios and conversion efficiencies has investigated by Katagiri et al., and the highest efficiency cells were observed when Cu/(Zn+Sn) and Zn/Sn ratios were 0.85 and 1.1-1.3, respectively (Katagiri and Jimbo 2011). Furthermore, efficiencies of CZTS are reported for thin film with metallic ratio of Cu/(Zn+Sn) ~ 0.8 and Zn/Sn ~1.2 which appears that Cu-poor Zn-rich composition of CZTS (Todorov et al. 2010; Repins et al. 2012; Shin et al. 2013; Todorov et al. 2011; Ericson et al. 2013).
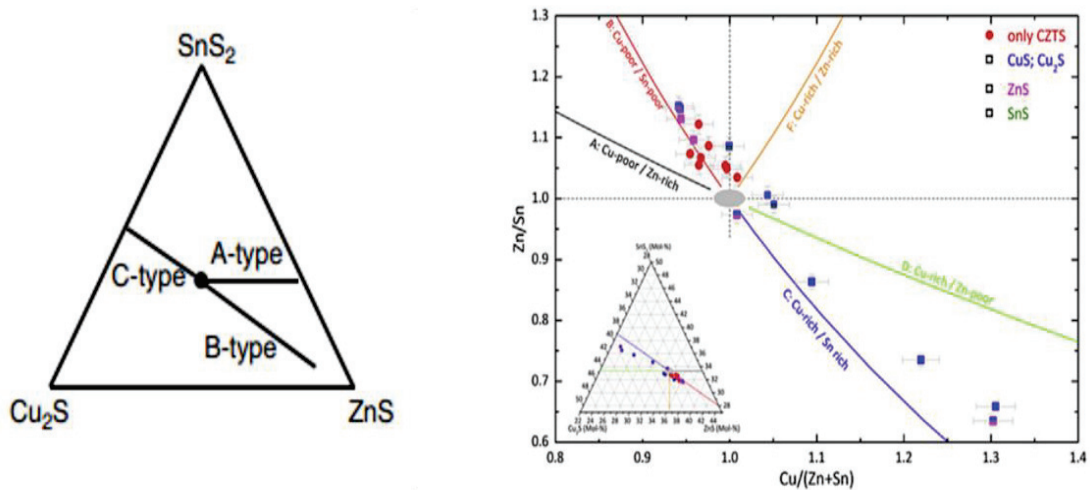
Figure 3.7. The type formations within Cu_2S-ZnS-SnS$_2$ ternary phase diagram (Source: Choubrac et al. 2012) and the metallic ratio of CZTS (Source: Valle Rios et al. 2016).

3.1.3.4. Secondary Phases

Due to the small region of single-phase CZTS formation, binary and ternary secondary phase easily form in addition to CZTS during the growth process. Controlling of secondary phase formation plays a key role to reach high efficiency CZTS solar cell.

3.1.3.4.1. Cu₂S secondary phase

Copper sulphides (Cu_2S) can be formed in the Cu-rich as well as Sn- and Zn-poor condition. Cu_2S is highly conductive and it causes shunt in the solar cell. Moreover, this phase within a solar cell can present a problem because it enhances the recombination.

3.1.3.4.2. SnS and SnS₂ secondary phases

Tin sulphide (SnS_2) is a n-type semiconductor with a band gap 2.2 eV (Kumar et al. 2015). This secondary phase could act as an insulator which can cause high photocarrier recombination. When the high amount SnS_2 in the CZTS, it may form a secondary diode within the absorber layer, which could act as a barrier to carrier collection and reduce the fill factor so it affects the solar cell performance. Also, another secondary phase is SnS which is p-type semiconductor with a band gap 1.1eV.

3.1.3.4.3. Copper Tin Sulfide (CTS) secondary phase

Cu_2SnS_3 (CTS) is another secondary phase occurred in CZTS absorber under Zn-poor conditions. CTS is a p-type semiconductor with a metallic behaviour (Wu et al. 2007; Tiwari et al. 2013). Like Cu_2S, CTS is detrimental for solar cells because it has high conductivity which could decrease the shunt resistance, and it has low band gap which could reduce the V_{oc} (Siebentritt and Schorr 2012).

3.1.3.4.4. ZnS secondary phase

Zinc sulphide (ZnS) is a secondary phase occurred in CZTS absorber under Cu-poor Zn-rich condition. It is a wide gap (3.54 eV) material and it acts like insulator so it can reduce the active area, where the electron-hole pairs are generated, and current collection (Kumar et al. 2015). The V_{oc} of device is not affected due to low conductivity of ZnS, whereas it can cause high series resistance in the solar cells (Siebentritt and Schorr 2012).

3.1.3.5. Detecting Secondary Phases in CZTS

X-ray diffraction is used to identify the secondary phase formation and crystal structure. Cu-S and Sn-S secondary phases can be detected easily using X-ray diffraction because the diffraction peaks are clearly distinct from the diffraction peaks of CZTS. However, ZnS and CTS secondary phases are difficult to distinguish from CZTS phases because these phases have same diffraction peaks at the same position due to similarity in the crystal structure and lattice parameters (Fernandes et al. 2011; Cheng et al. 2011). Figure 3.8 shows overlap XRD peaks of kesterite CZTS, CTS and ZnS (Walsh et al. 2012).
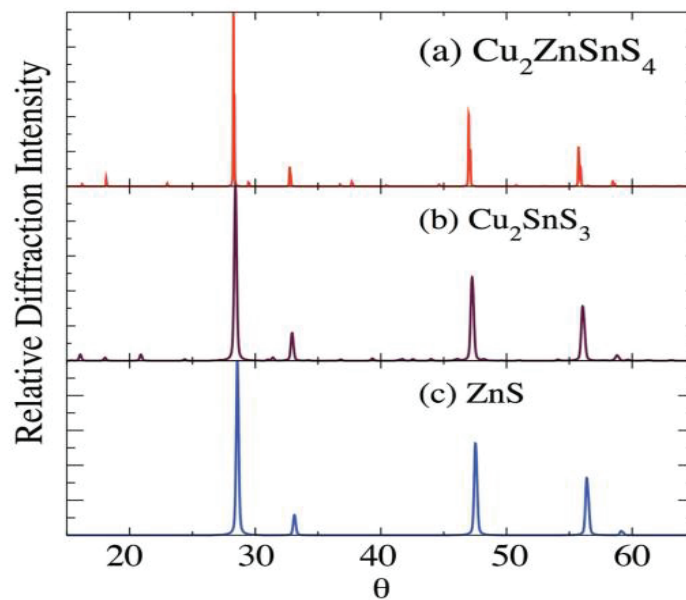
Figure 3.8. Overlap XRD peaks of kesterite CZTS, CTS and ZnS structure
(Source: Walsh et al. 2012).

Another techniques are Raman spectroscopy to identify the secondary phases in CZTS. Raman spectroscopy is more reliable characterization technique to detect the secondary phases. The kesterite CZTS exhibits prominent peaks at 288-289 cm^{-1}, and 338-339 cm^{-1}, a shoulder at 351 cm^{-1}, and a broad peak between 368-374 cm^{-1} (Altosaar et al. 2008; (Fernandes et al. 2011; Fernandes et al. 2009). Raman peaks of tetragonal Cu_2SnS_3 are observed at 297, 337 and 352 cm^{-1} (Fernandes et al. 2011), and cubic Cu_2SnS_3 at 267, 303, and 356 cm^{-1} (Fernande et al. 2010a; Fernandes et al. 2010b). The weak Raman peak of cubic ZnS appears at 275 cm^{-1} and strongest peak at 352 cm^{-1} (Fernandes et al. 2011). However, the strongest peak of ZnS is almost the same position

of CZTS peak at 351 cm^{-1}, thus it makes it difficult to distinguish ZnS from CZTS when using an excitation wavelength below the band gap of ZnS (Berg et al. 2014). ZnS secondary phase can be clearly distinguished from CZTS using an ultraviolet excitation wavelength of 325 nm (Fontane et al. 2011). To identify ZnS secondary phase in CZTS absorber, energy-dispersive X-ray spectroscopy (EDS) can be used to determine the chemical composition of area or of individual grains. The high Zn concentration in detected regions or grain implies the presence of this phase (Abusnina 2016).

3.2. Fabrication Methods for CZTS Thin Film

To achieve high-quality CZTS thin film for solar cell application, many fabrication methods have been used by several groups. The main objectives are to make high quality material that is homogenous single-phase films with large grains and no voids or cracks, and a low-cost fabrication process. CZTS can be produced using vacuum or non-vacuum deposition method which can be a one- or two-step fabrication process. In the one-step process, each element (Cu, Zn, Sn, S) is deposited simultaneously on a substrate. The substrate is heated because the high temperatures enables the interdiffusion of the elements. In the two-step process, firstly, a precursor, which could be contain only metals or all elements including sulphur, is deposited on the substrate at room temperature and secondly, the precursor is annealed at high temperatures in sulphur atmosphere. When the two-step and one–step process is compared, the two-step process demonstrates better device performance of CZTS thin film (Figure 3.9).
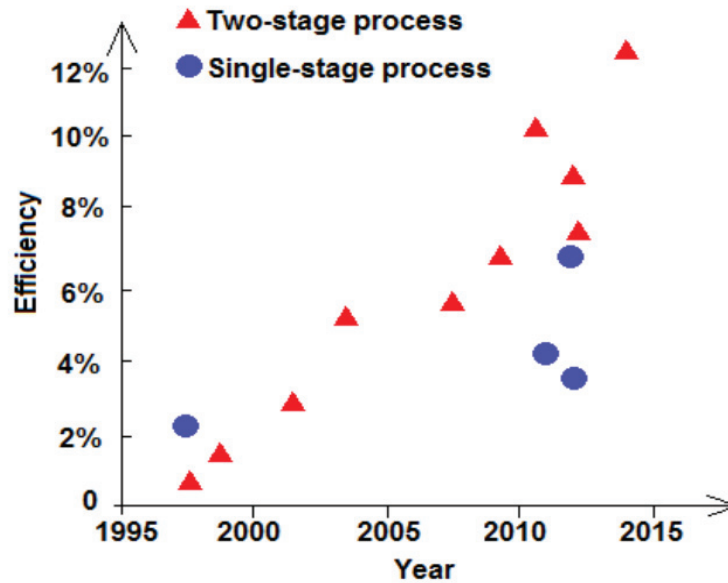
Figure 3.9. The comparison of one-step and two-step process for CZTS thin film device performance (Source: Wang, 2016).

3.3. Flexible Substrate for Thin Film Solar Cells

The flexible substrates offer various advantages for solar cell manufacturing as well as application when they are compared to solar cell on rigid substrate. Flexible and lightweight solar modules are suitable for roll-to-roll process, thus they have considerable potential to be cost effective solar modules. Different types of flexible substrates, can be used, such as polymer or metal foils, however the choice of substrate is a critical point for the processing methods. The chosen substrate must endure vacuum conditions, and should not degas nor degrade during the deposition process. Additionally, it should be chemically inert, means it must not corrode or decompose during the process, furthermore, it must not react with S, not release impurities into the absorber. Also, thermal stability is important because most of deposition techniques require high temperature in range 400-600 °C. Substrate material should be chosen in the similar range to thermal expansion coefficient (CTE) of absorber layer to avoid delamination and adhesion problems because the sample shows a rapid change in temperature during the process. The adhesion problem may occur due to the high CTE of the substrate, whereas the defects as a crack formation may take place due to low CTE of substrate. The mismatch of CTE causes stress between the different layers that can create cracks in the absorber. The performance of device is influenced by crack formation that creates shunt

path between the back and front contacts (Bremaud et al. 2007). Table 3.1. shows properties of substrate and material (Kessler and Rudmann 2004; Adachi 2015).

Table 3.1. Properties of substrate and material

Material	CTE $(10^{-6}K)$	Density (g/cm^3)
Substrate		
SLG	9	2.5
Steel	11-16	7.8
Ti	8.6	4.5
Al	23.1	2.7
Polyimide	12-24	1.5
Solar cell material		
Mo	4.8	10.2
CZTS	7.4/8.6	4.5
CdS	4.5	4.8
ZnO	4.75/2.9	5.6

Flexible substrate can be categories as a polymer and metal foils. The used polymers are usually special heat resistance polyimides such as Upilex or Kapton. They can resist temperatures up to 450-550 ºC, unfortunately which is still ~100 ºC lower than usual deposition temperature on glass. On the other hand the metal foils such as stainless steel (SS), titanium (Ti), molybdenum (Mo), can be used at higher temperature without no deterioration of substrate, but there are still other problems that need to be solved. One is the diffusion of impurities from substrate into the absorber layer that affects the photovoltaic properties of solar cells negatively. An additional barrier layer can be used between the substrate and the back contact to eliminate or reduce the impurities diffusion. Additionally, the barrier layer can be utilize to provide conductivity as substrate is not conductive. Nevertheless, all barrier layers should resist to high temperature process because if any crack forms in these layer, crack formation will be detrimental. The other important point is surface smoothness because rapid changes in the surface topography such as spikes or cavities can be lead to shunts between the front and back contact, and the impurity diffusion barrier can be deposited easier or more successful on a smooth

substrate. Among the suitable metal foil substrates, the pure metallic foil substrate such as chromium (Cr) and Ti can be used without diffusion barrier because their diffusion rate into absorber layer are lower than others (Hartmann et al. 2000). However, an improvement in the efficiency of solar cell is observed when the diffusion barrier layer is deposited on Cr-steel foil, but there is no significant change in the efficiency of solar cell when diffusion barrier layer is deposited on Ti foil and still has higher efficiency than Cr-steel (Herz et al. 2003). Therefore, it can be said that it is a low cost because Ti foil substrate does not require additional layer.

The back contact layer has to be chemically inert with optimum electrical properties to achieve high efficient solar cells. For example, in the case where Mo is used as a back contact, the sulfurization process at elevated temperatures gives rise to decomposition of the CZTS absorber layer, consequently, a MoS_2 phase occurs between the absorber layer and back contact (Scragg et al. 2012; Scragg et al. 2013). This intermediate layer can affect the V_{oc} and change the bad alignment between the Mo back contact and CZTS absorber layer. Furthermore, a back-contact blocking (Schottky) barrier is formed between the MoS_2 and Mo layer that restrict the hole transport across the Mo to absorber layer interface (Wang et al. 2010; Yang et al. 2014). Additionally, in case of SS back contact, Fe atoms of SS foil substrate react with sulfur and form FeS layer during the sulfurization process. This formation may affect the normal sulfurization reaction of CZTS, leading to absence of CZTS structure (Xu et al. 2014). Besides, the diffusion of impurities can occur from the SS substrate to CZTS. The short circuit density J_{sc} is influenced by medium Fe concentrations and the open circuit voltage V_{oc} decreases at very high Fe concentration in CZTS absorber layer (Wuerz et al. 2009).

Recently, CTZS absorber layer has grown on various metallic foils via different growth methods. The CZTS absorber layer has been grown on flexible Mo foil via electrodeposition method and the efficiency of solar cell is found to be 3.82% that is the highest efficiency by using Mo foil substrate (Zhang et al. 2014). Furthermore, CZTS absorber layer has been grown on flexible SS foil via sputtering techniques and the efficiency of solar cell reached up to 3.07% that is the highest efficiency by using SS foil substrate without sodium layer (Sun et al. 2016).

In light of these information, the choice of substrate plays a key role to achieve high efficient solar cell and reduce the manufacturing costs for the high throughput fabrication of thin film solar cells. Most of metallic foil substrates (SS, Mo etc.) require the barrier layer to prevent the diffusion of impurities from the substrates to absorber

layer, Ti foil does not require barrier layer thus it reduces the manufacturing cost. It is important to note here that, accordingly with the reserve of the element in the Earth, the cost of the commercial metal foils change with the purity level, and Ti element has more reserve than others. Consequently, Ti foil is much cheaper due to its high abundance. The aim of this thesis to present a perspective for efficient CZTS absorber layer on Ti foil substrate investigating sulfurization temperature.

CHAPTER 4

EXPERIMENTAL PROCEDURES

In this thesis, two-step fabrication process was used to fabricate the metallic precursor which is first step of the growth mechanism, magnetron sputtering technique was used that offers a wide advantages such as easy adaptation to large scale, and reproducible manufacturing and easy control of film composition (Tuna et al. 2010); (Wang, 2011). In second step, deposited metallic precursor on Ti foil substrate was annealed in sulfur atmosphere, which is known as sulfurization process, to convert the metallic film into CZTS thin film. The various sulfurization temperatures (530-580 ºC) were investigated to present a perspective to achieve good quality CZTS absorber layer on Ti foil substrate, and efficient solar cell applications.

4.1. Substrate Preparation

There are many striking advantages that flexible substrates present compared to the solar cells fabricated on rigid soda lime glass. The rigid substrate gives rise to limitations for building applications. However this limitations can overcome using flexible foils. Besides, flexible substrates easily adapt roll-to-roll process that is important for industry. In this thesis Ti foil was used as a substrate due to its advantages which mentioned in Chapter 3.3. CZTS absorber layers have been deposited on flexible metallic Ti foil. The surface smoothness of foil substrate is one of the most important parameter for high-efficient CZTS solar cell applications. Ti surfaces are known to possess a high affinity to react with O_2, thus TiO_2 layers are readily present on Ti foils. When the Ti is exposed to the air at room temperature, a passive oxide layer is formed rapidly on Ti surface. This native oxide, passive film has an amorphous structure and is almost 5-10 nm in thickness, and formed of three layers. The layer in contact with the metallic titanium substrate is formed of TiO, second one is Ti_2O_3 layer, and last one is anatase TiO_2 layer which is in contact with the environment. A transition of this oxide layer from amorphous structure to anatase phase occurs at about 276 ºC, and this anatase structure remains in

the range 276-457 °C. Between 457 °C and 718 °C, the film consist anatase and rutile sublayer, and beyond at 718 °C pure rutile is observed (Gemelli and Camargo 2007).

To remove this oxide layer, a mixed acid solution treatment is carried out. The HF and HNO$_3$ mixed acid solution or just HF acid in deionized water is used to remove oxide layer (Walker and Tarn 1991). For that reason, Ti foil substrates were chemically etched for 1.5 min in 90.0 ml deionized water and 10.0 ml diluted HF acid mixed solution at room temperature to remove oxide layer before the sputtering process. Ti foils with a thickness of 200 µm before the chemical etching process and 0.8 x 2.5 cm^2 in size were used as substrates. After, Ti foils were chemically etched, the thickness of Ti foil was about 150 µm. Surface morphology of Ti foil was examined by SEM before and after the chemical etching process.

4.2. Fabrication of Metallic Precursors

This part is the first stage to fabricate the CZTS thin films. The metallic precursors which contain Cu-Sn-Zn metallic layers, were deposited using magnetron sputtering system. The Ti foil of ≥99.9% pure and Grade 1 was used as a metallic foil substrate. The metallic layers of precursors were deposited by dc magnetron sputtering from 2-inch target of Zn (99.99%), Sn (99.999%), and Cu (99.999%) at room temperature, respectively (Figure 4.1).

In this procedure, firstly rough pump (RP) was evacuated the chamber, and then the turbo molecular pump (TMP) was started. Before sputtering, the pressure in the chamber was lowered down to below 10^{-6} Torr. During the sputtering, pure argon gas with a 30 sccm flow was fed into the chamber and the working pressure was maintained at 1.5x10^{-2} Torr, pre-sputtering was performed for 5 min to remove contamination of the surface of the targets. The layer of metallic precursors Cu/Sn/Zn were deposited on Ti foil substrate using rotational holder. The distance between target and substrate was fixed at 8 cm. After deposition process, the pumps turned off and then the substrate holder was removed from the chamber when the pressure of the chamber reached to atmospheric pressure. The thickness of the metallic precursor is 609 nm after sulfurization process the thickness of films is around 1.2 µm.
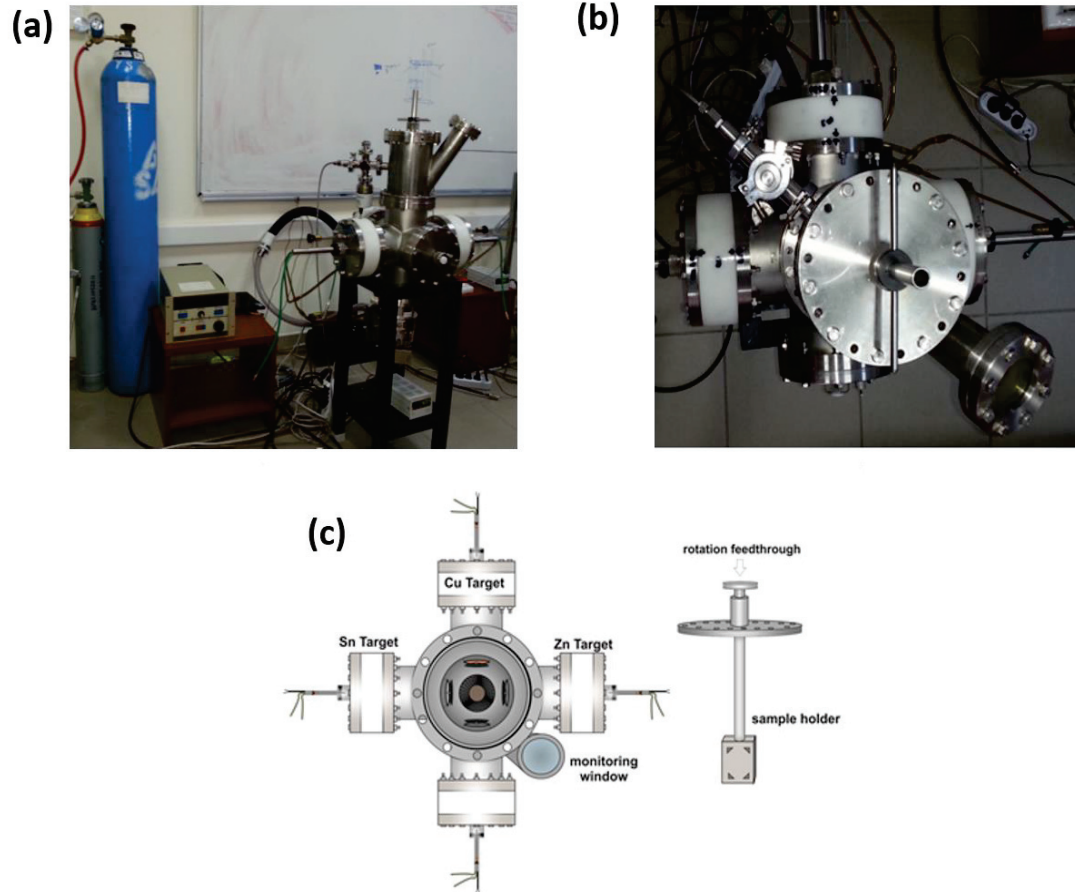
Figure 4.1. The pictures of system were demonstrated in (a) and (b), (c) the schematic diagram of top view of sputtering system and holder apparatus within the sputtering system (Source: Yazici et al. 2015).

The magnetron sputtering method provides ease of control by means of layer thickness and composition of the precursor. The deposition power and time were optimized for desired thickness for each layer to obtain Cu-poor and Zn-rich composition which is the most efficient CZTS according to the literature. The each thickness of metallic precursor layers were determined using the density and atomic weight of metals. The stacking order of metallic precursor is an important point because the compositional ratio of CZTS thin film can easily control. Besides, the stacking order of layers have an effect on formation of CZTS and prevent the Zn, Sn loss during sulfurization process. When the literature survey was made, it showed that when Cu layer is deposited as a first layer, it migrates to upper surface which gives rise to the void formation between the substrate and film, for that reason, the Cu layer should be placed as a top layer (Yoo and Kim 2010). The loss of Sn and Zn are obtained in during the sulfurization process due to its volatile nature of Zn and Sn, however, these losses can be prevented by depositing Cu

layer as a top layer (Thota et al. 2017). On the other hand, the thickness of Cu layer was investigated to understand the effects on CZTS thin films, and Sn and S loss for precursor having thicker Cu to layer were observed, whereas having thinner Cu top layer, Zn loss was observed (Koseoglu, 2017). Araki et al. investigated six different stacking order to understand effects of stacking order on CZTS thin film formation. This study showed that the CZTS thin film formation is required that CTS and ZnS phase have to react with each other during the sulfurization process, but if Cu layer is not adjacent to Sn layer, the CTS phase formation becomes difficult and that affects the formation of CZTS (Araki et al. 2008).

In the light of these information, the stacking order was chosen as a Cu/Sn/Zn. To obtain desired Cu-poor Zn-rich composition, thickness of the layers were optimized. The power values of DC-power supply were 41, 40, and 20 watts for Cu, Sn, Zn, respectively. The thickness of each metallic layers were obtained as 126, 290 and 193 nm for Cu, Sn, and Zn, respectively (Figure 4.2). Table 4.1 lists the growth parameters of metallic layers of precursor.

Table 4.1. Growth parameters of metallic layers

Target	DC-Power (W)	Sputtering Time (s)
Zn	20	200
Sn	40	360
Cu	41	300
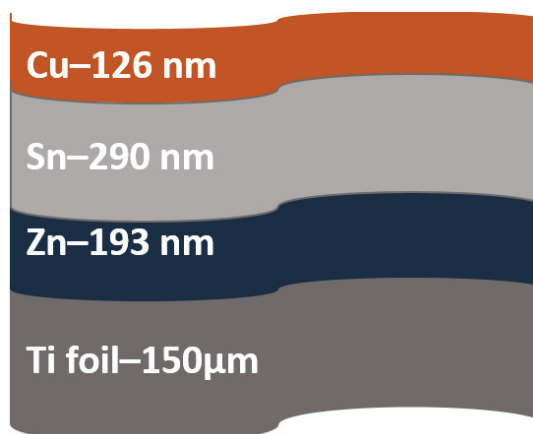
Figure 4.2. Schematically illustrated metallic precursor on the Ti foil substrate.

4.2.1. Magnetron Sputtering Technique

The thin film layers can be deposited onto a substrate with many different techniques which can be divided into two groups as vacuum-based and non-vacuum based technique. In this present thesis, magnetron sputtering method, which is a vacuum-based technique, was used during the experimental work.

Sputtering, which is a physical vapor deposition method, is the one of the most utilized technique to deposit the thin film layers onto a substrate. The working principle of this technique is based on bombarding a source material (target) with energetic ions, surface atoms of source material are ejected, and ejected atoms are condensed onto the substrate.

The sputter chamber is evacuated to a base pressure of 10^{-5}-10^{-6} Torr before the sputtering. At the beginning of the sputtering, a chamber is filled with inert gas, generally argon, to bombard the target material with the energetic ions. After reaching the working pressure, around 1 to10 mTorr, high DC potential is applied between the target material (cathode) and substrates (anode). However, RF potential also can be used for insulator target but in the RF sputtering, the deposition rate is low, as a result of this, it requires the longer deposition times that is not desirable for production. Under proper condition of working pressure and applied voltage, the gas is converted into a plasma discharge consisting neutral gas atoms, ions and electrons. The electric field near the target accelerated the energetic Ar^+ ions toward the target to collide with the target atoms. The incident ions with high kinetic energy eject atoms from the target surface and the ejected atoms condense on the substrate to build the desired layer. However, there are other particles such as ions and electrons ejected from the source material addition to sputtered atoms. The electrons ejected from the target, known as secondary electrons, are accelerated back to the plasma charge and collide with the neutral Ar gas atoms, resulting the ejection of the outer shell electrons of the gas atom, therefore, more positively charged Ar ions are generated. Besides, the high amount of the secondary electrons move through the plasma and reach to the anode, and they hit the substrate surface, consequently, they cause the substrate heating.

The difference between DC and magnetron sputtering is, in the magnetron sputtering method, a strong magnetic field is applied near the target by placing magnets. In this way, the secondary electrons are confined in the vicinity of the target surface. By

confining the secondary electrons near the target surface, the possibility of collision between the Ar atoms and these electrons is increased. This result in the greater ionization of the sputter-gas atoms, a denser plasma, and higher deposition rate.

4.3. Sulfurization Process

In order to incorporate sulfur and to convert the metallic precursor into CZTS thin film, the sulfurization process, which includes the annealing of the metal precursor in a sulfur atmosphere, is required. The parameters of sulfurization process such as sulfurizaton temperature and duration, heating rate, vapor pressure inside the tube and carrier gas flux were investigated in the literature. However, most of the published works investigated on the impact of sulfurization temperature and duration on the growth mechanism and properties of CZTS thin film. Emrani et al. investigated the sulfurization temperature between 500 ℃ and 575 ℃ for 3-4 hours, and this study showed that lower temperatures showed voids and small grains with consisting of some secondary phases and higher temperature gave rise to rough surface morphology due to coarsening of grains (Emrani et al. 2013). Amal et al. sulfurized sputtered metal precursors at 530 ℃, 550 ℃, 570 ℃ for 30 min, and it showed that lower temperature caused the void and higher temperature gave rise to secondary phases in films (Ikhlasul Amal and Kim 2013).The sulfurization temperature plays a key role to convert precursor into CZTS thin film. On the other hand, Yang et al. investigated the same sulfurization temperatures with Amal et al., and they showed that higher sulfurization temperature improved the morphology and crystallinity of films, and also the secondary phases formation were suppressed (Yang et al. 2015). In addition the sulfurization temperature, the duration of sulfurization has also been reported to have effects on CZTS thin film. The various sulfurization durations 5 min to 40 min were investigated by Singh et al., and the secondary phase was observed in long sulfurization process due to the decomposition of CZTS thin film (Singh et al. 2014). Most of the published works show that the sulfurization temperature has a critical role to improve the crystallinity, uniformity and composition of the films, agree that the properties of the film such as morphological and structural are improved with increasing sulfurization temperature.

The sulfurization process was performed in a Lindberg/Blue M tube furnace. The sulfurization process was carried out in a quartz tube, 2.6 cm in diameter and 60 cm in

length, placed in the tubular hole in the middle of a furnace. Before the sulfurization, the quartz tube was cleaned with 150 sccm (standard cubic centimeters per minute) argon gas flow for 15 min. Ar gas was chosen as a carrier and as a proactive gas instead of N_2 gas because Ti could react with N_2 which could lead to formation of TiN interface and this formation could cause deterioration in the CZTS formation on foil substrate. Figure 4.3 (a) shows the sulfurization system and the used graphite box is shown in the inset, and (b) shows the illustration of sulfurization process.
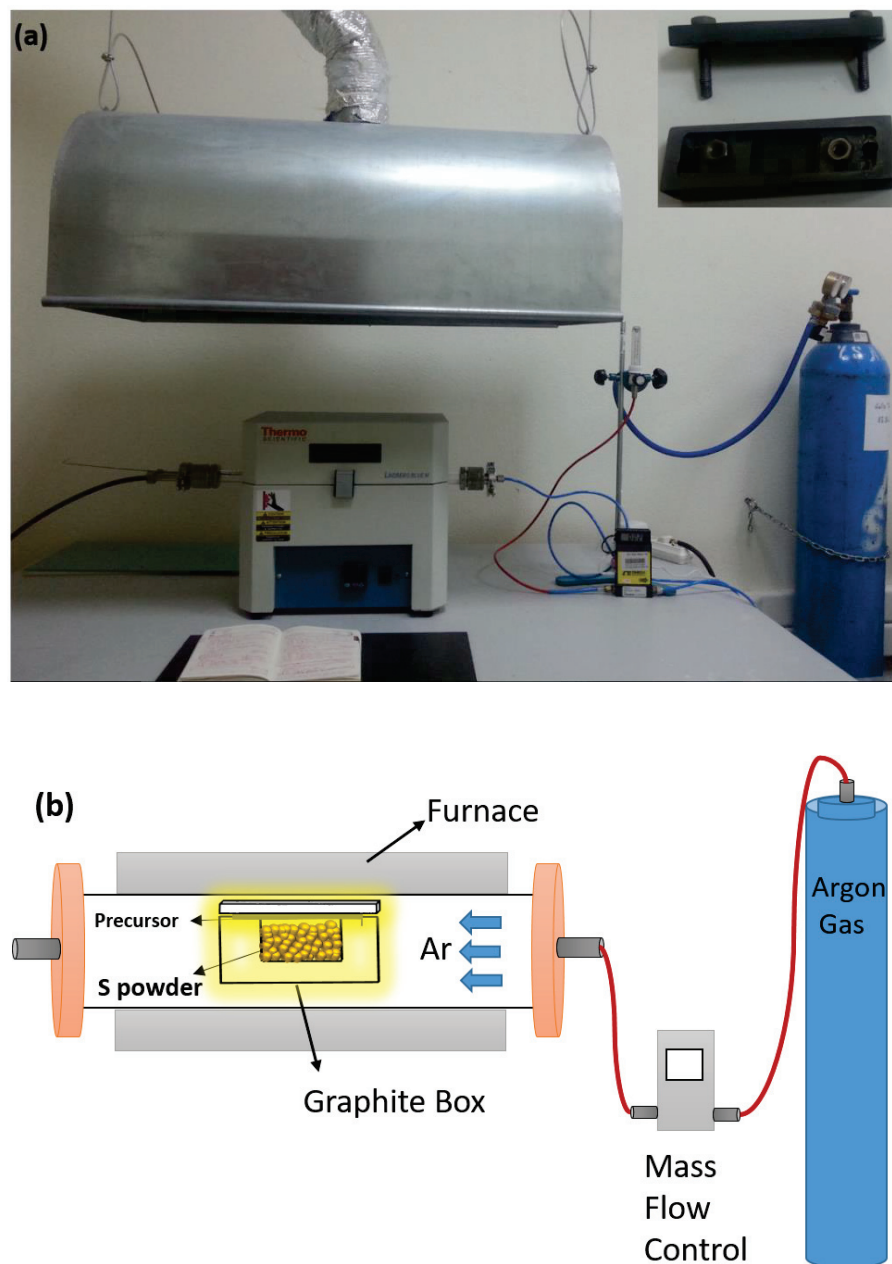
Figure 4.3. (a) The sulfurization system and the used graphite box is shown in the inset, and (b) the illustration of sulfurization process.

The mentioned works above have different sulfurization systems for that reason, it can be said that the films show different properties at the same temperature with depending on sulfurization system. In this light of these information, in this study, the short sulfurization duration was used for high-throughput production and the various sulfurization temperatures were investigated. During the preliminary experiments to improve the material quality, various sulfurization durations were carried out. It observed that when the duration of sulfurization was kept shorter or longer than optimized duration, the adhesion problem and loss of Zn in the films were observed. Based on the results of our preliminary experiments, sulfurization duration was selected in 20 min to produce CZTS thin films. In this study, the effect of sulfurization temperature was investigated, and it is the first study to understand effects of temperature on CZTS thin film on Ti foil substrate.

A 250 mg sulfur powder (99.98%) was placed in the middle of a graphite box, then, the metallic precursor was placed to cover the sulfur powder. After the lid of the graphite box was closed, it was placed in the middle of the quartz tube in the furnace. The furnace was set to 15 min to reach a desired sulfurization temperature. The sulfurization duration was kept constant as 20 min for all samples. The sulfurization temperature, fixed for each sample, was varied from 530 ºC to 580 ºC from sample to sample. During the sulfurization process, a pure argon gas of 47 sccm flowed through the quartz tube as a carrier and protective gas. The sulfurization process was carried at the atmospheric pressure. After the sulfurization process, the samples were naturally cooled down in Ar atmosphere. Figure 4.4 represents the sulfurization parameters of CZTS films.
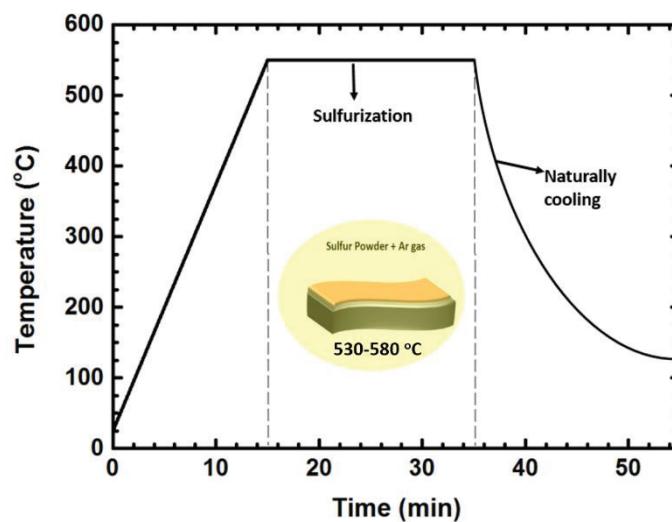
Figure 4.4. Sulfurization parameters of samples.

4.4. Characterization Methods

4.4.1. Scanning Electron Microscopy (SEM)

SEM is important analysis technique used to investigate the morphology of films. It gives us the first information about crystal formation which is microstructure morphology of thin films. The working principle of an electron microscope is similar to optical microscope. Electrons are used in SEM instead of light therefore, it provides higher resolution due to much smaller wavelength of electrons.

The working principle of scanning electron microscope is based on bombarding the sample with focused beam of electrons that is accelerating and generating in electron gun. The beam is focused by magnetic lenses or electrostatic lenses instead of glass in the optical microscope. The electron beam scan over the sample. The secondary and /or backscattered electrons emitted from the sample surface as consequence of the interaction of the electrons and the sample are then detected and converted to signal, consequently the images are created.

In this study, the CZTS thin film morphology was investigated using a Scanning Electron Microscope (SEM; Phillips XL 30S FEG) which is able to do Energy Dispersive Spectroscopy (EDS; EDAX), and SEM images were taken under a 5 kV acceleration voltage.

4.4.2. Energy Dispersive X-ray Spectroscopy (EDS)

EDS enables to get information about the elemental composition of the sample. Each element has unique atomic structures for that reason it allows to observe the individual peaks which belongs the each element, on X-ray emission spectrum. The working principle of EDX is that high energy beam of incident electrons is focused into the sample, and they excite the bound electrons in the sample to leave the atomic shell. As a result, the vacancies are created in the atomic shell, which are filled up by the electrons from the higher shells. Therefore, X-ray photons with the specific energies, which belongs the characteristic element, are produced and detected to determine the content.

EDS measurements were done using an EDX detector with HV resolution in 15 kV and 5 spot size in high vacuum to determine the elemental composition of the CZTS thin film and the atomic cation Zn/Sn and Cu/(Zn+Sn) ratios.

4.4.3. X-Ray Diffraction (XRD) Analysis

X-ray diffraction is widely used to analyse the crystal structure of materials. The working principle of XRD relies on the diffraction of an incident X-ray waves by a crystal lattice. The wavelength of the incident light wavelength has to be in the same order of the lattice constant for the diffraction occurrence.

The XRD was operated in the Bragg-Brentano focusing geometry from 20º to 80° on a Phillips X'Pert Pro X-Ray diffractometry with Cu Kα radiation (λ=1.5406 Å) using a step size of 0.016° and a time step of 15 min. XRD diffraction was used to analyze the crystal structure and identify the secondary phases in the films. Besides, other structural characteristic properties can be determined such as internal strain, crystallite size, and the quality of thin films by using XRD. We determined the size of crystallites by XRD. The average of the crystallite size in the films can be estimated using Scherrer's equation given as:

$$d = \frac{k\lambda}{\beta cos\theta} \qquad (3.1)$$

where λ is the wavelength of X-ray source in nanometers, k is a constant related to crystallite shape, generally taken as 0.9 (Monshi et al. 2012), β is the full width of half maximum the diffraction peak at half maximum height (FWHM) in radians, and Ɵ is the Bragg's diffraction angle.

The XRD diffraction analysis is not enough to determine the crystal structure because second phases ZnS (JCPDS: 00-05-0566) and Cu_2SnS_3 (JCPDS: 00-027-0198) peaks overlap with the kesterite structure CZTS (JCPDS: 026-0575), we mentioned this situation in Chapter 3.1.3.5. Therefore, Raman spectroscopy was also needed to obtain a reliable analysis.

4.4.4. Raman Spectroscopy

Raman spectroscopy is a powerful technique to investigate the crystal structure of material, and it is a useful complementary technique for XRD in defining secondary phases. When a sample is illuminated by a laser beam, the monochromatic light from a laser interacts with molecular vibration or phonons in the sample material and scatter from the surface material. If the wavelength of scattered light is the same with the wavelength of the incident monochromatic light that illuminates the sample, this is called Rayleigh (elastic) scattering. However, if the wavelength of scattered light is different from wavelength of the incident monochromatic light that illuminates the sample, it is called Raman (inelastic) scattering, as a result Raman-shifted wavelengths occur, and are detected by the photodetector. The wavelengths of scattered light give an information about the vibrational modes in the sample to identify the structure.

In this work, micro-Raman spectroscopy system (S&I Mono Vista) equipped with a 100 mW Melles-Griot Ar ion laser, and a 750 mm focal length monochromator (Princeton Instrument, Acton SP2750 0.750mm Imaging Triple Grating Monochromator) was used. Raman signal was collected with a high resolution CCD camera with 1600x200 pixels. To be able to see the Raman active phonon modes of CZTS films and the vibrational modes of some other possible phases, 514.5 nm excitation wavelength was chosen.

4.4.5. X-Ray Photoelectron Spectroscopy (XPS)

XPS analysis is used to get information about the composition the chemical bonding of elements since the electron binding energy is influenced by its chemical surroundings. The working principle of XPS is based on photoelectric effect. XPS photons, which are X-ray, interacts with core level electrons of the sample. Electrons can be ejected from any orbital with photoemission when the energy of the X-ray photons are higher than the binding energy. The binding energy is identified by the energy difference between the kinetic energy of the ejected photoelectrons and incident X-ray energy, and the spectrometer work function. The binding energy depends on the X-ray energy, thus the incident X-ray energy should be monochromatic. The compound is recognized by comparing experimental and reference data. Each atom has a characteristic binding

energy for core electron. Thus, chemical compounds and elements are determined by the location of energy peaks on the XPS spectrum. The XPS peaks are originated from the ejected electron with kinetic energy in the core level and valance band. XPS is surface sensitive analysis because ejected photoelectrons originate from the near surface (0.5-5 nm) due to low photoelectron energy.

Core levels in XPS spectra is defined by using the nomenclature *nlj* where n is the principle quantum number, *l* is angular momentum quantum number and *j* is the total angular momentum quantum number. The total angular momentum quantum number equals to summation of the spin angular momentum number (s) and angular momentum quantum number. If *l* equals to zero, the singlet XPS peak is observed. If *l* is bigger than one, it gives rise to a doublet peaks because of the two possible states having different binding energies. This is known as spin-orbit splitting (l-s coupling). Besides, the based on the degeneracy of each spin state, the peaks have specific area ratios. These ratios have to be taken in consideration when analyzing spectra. The schematic drawing of XPS setup with a photon source and the energy band diagram of XPS method are shown in Figure 4.5 (a)-(b).
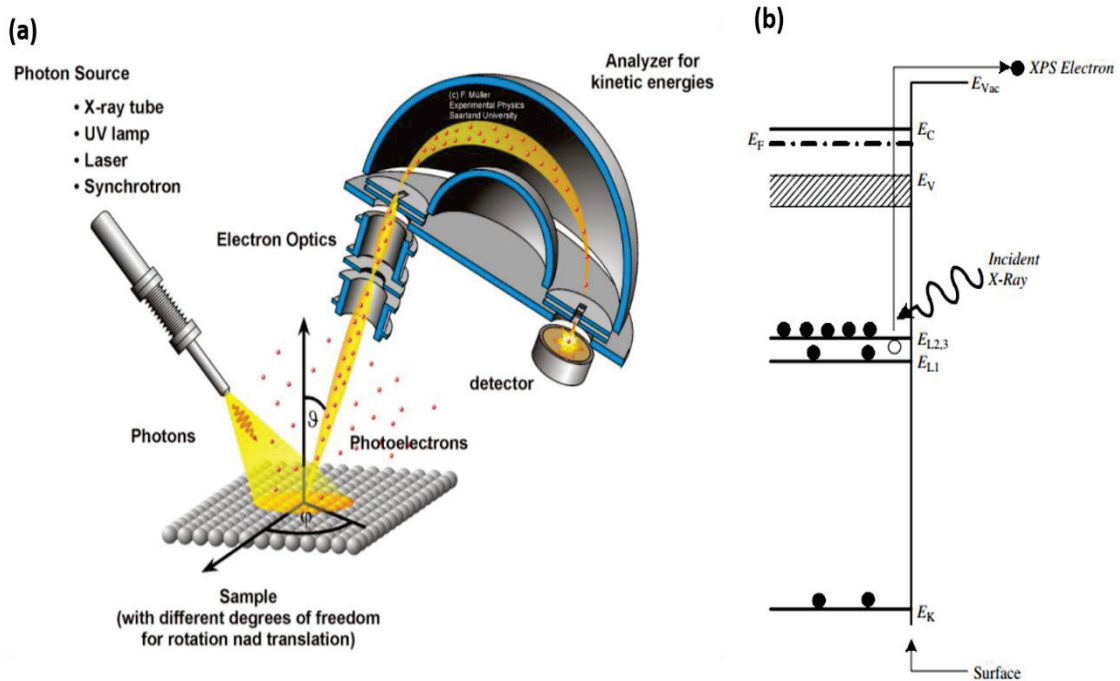
Figure 4.5. (a) The schematic drawing of XPS setup with a photon source, and (b) the energy band diagram of XPS method (Source: Schroder 2006).

In this thesis, X-ray Photoelectron Spectroscopy (XPS; SPECS Phoibos 150 3D-DLD) analysis was carried out to determine the chemical bonding and secondary phase formations. XPS measurements were performed with a monochromatized Mg K_α radiation source (hv=1254 eV) with powers of 200 W and 1.5 kW. The pressure in the sample chamber was set to be between $10^{-9} - 10^{-10}$ Torr. High-resolution scans of each element in CZTS were conducted at a 30 eV pass energy with a scan rate of 0.05 eV/s with a 2 second dwell time. The spectra were calibrated with respect to C $1s$ line at 284.6 eV which is characteristic for aromatic/aliphatic carbons (Cantas Bagdas, 2017). For the analysis, a Shirley-type background was used and the curves were fitted with Gaussian/Lorentzian product profile functions using a CasaXPS software.

CHAPTER 5

RESULT AND DISCUSSION

In this chapter, we will discuss the results, and give a perspective about the effect of sulfurization temperature on CZTS absorber layer on Ti foil substrate. Table 5.1 shows the parameters of samples.

Table 5.1. Growth parameters of samples

Sample Name	Layer Order	Sulfurization Temperature (ºC)	Sulfurization Duration (min)
Sample A	Cu/Sn/Zn	530	20
Sample B	Cu/Sn/Zn	540	20
Sample C	Cu/Sn/Zn	550	20
Sample D	Cu/Sn/Zn	560	20
Sample E	Cu/Sn/Zn	570	20
Sample F	Cu/Sn/Zn	580	20

5.1. Surface Analysis of Ti Foil Substrate

The surface of metallic Ti foil substrate is important issue because its morphology influences the morphology of metallic precursor while deposition process. As mention in Chapter 4.1, to remove the oxide layer, diluted HF and deionized water mixed solution was used for chemical etching of Ti foil. Surface morphology of Ti foil was examined via SEM spectroscopy before and after etching, and also morphology of metallic precursor on etched Ti foil substrate (Figure 5.1). After chemical etching, cavities were observed in some place on the surface of Ti foil. Some of these cavities were coverage and levelled up, after metallic precursor deposition but still grown metallic precursor layer imitated the morphology of the substrate. However, it is well known surface topography of

substrate such as spikes or cavities may cause to shunt between the front and back contact (Kessler and Rudmann, 2004). Besides, surface roughness affects growth of absorber layer and other subsequent layers, and also grain morphology of absorber layer (Hodges, 2008). The chemical etching process caused the cavities but it required good adhesion because the cleanliness of the substrate strongly affects the adhesion.
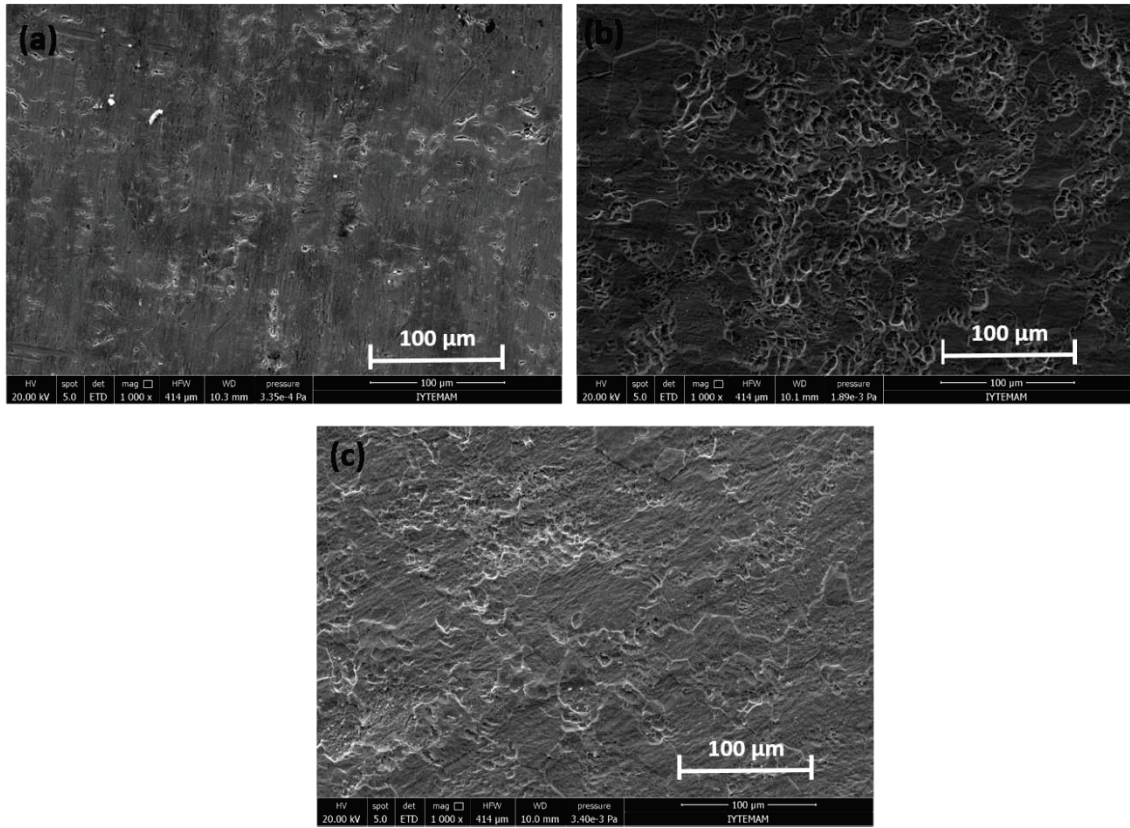
Figure 5.1. SEM images of (a) non-etched Ti foil, (b) etched Ti foil, and (c) CZT precursor on etched Ti foil.

5.2. Morphological Analysis

In this thesis, thickness of individual metallic layers were adjusted via molecular weight and density of each element to fabricate Cu_2ZnSnS_4. Due to complex structure of CZTS, systematic controlling of deposition and sulfurization process play an important role to get good quality of CZTs thin film. In the first stage of the process, the sputtering method enable to provide controlling each layer of the metallic precursor by adjusting sputtering power and time (Chapter 4.2). In the second stage which is sulfurization process, sulfurization process and duration play a key role in formation of the CZTS compound. We investigated the effect of sulfurization temperature on CZTS thin film on

Ti foil substrate for short sulfurization process. The short sulfurization process is important for high output. Figure 5.2 shows plane SEM images of the sulfurized films in different sulfurization temperatures. When the SEM images were examined, we did not see notable microstructure changes, all films had CZTS islands (bumps in the film), they may occur because of the sulfurization temperature or the films may imitate the substrate morphology. However, at 540 $^{\circ}$C, crack formation was observed between the CZTS islands and valley. All samples expect sulfurization temperature at 540 $^{\circ}$C showed dense bulk structure with some variation grain size. The microstructure changes with sulfurization temperature was more clearly observed in tilted cross-sectional SEM images (Figure 5.3). From the tilted SEM images of the film which is sulfurized at 530 $^{\circ}$C (Sample A), it is understood that the grain sizes of this film are smaller than the other grain size of the sulfurized films at other temperatures. The small bright grains were ZnS secondary phase and the EDS results also proved with high Zn/Sn ratio, under Zn-rich composition condition the ZnS and Cu_2S secondary phases are expected (Scragg 2010). Beside this, it may indicate an incomplete crystallization. At the 540 $^{\circ}$C, the grains started to coalesce to form CZTS structure, and larger grains were observed. Over 540 $^{\circ}$C, the grain sizes became larger and showed dense packing as result the crystallization was enhanced with increasing temperature. At 570 $^{\circ}$C, the largest grains and the more dense morphology were observed. However, it was observed that the grain size were reduced at 580 $^{\circ}$C. We thought that this is due to decomposition of CZTS into binary phases at higher temperature (Guilin et al. 2017), CZTS decomposes into Cu_2S and ZnS secondary phases, and Sn loss is occurred due to the SnS evaporation (Weber et al. 2010). Our other analysis were in agreement with these case for Sample F.
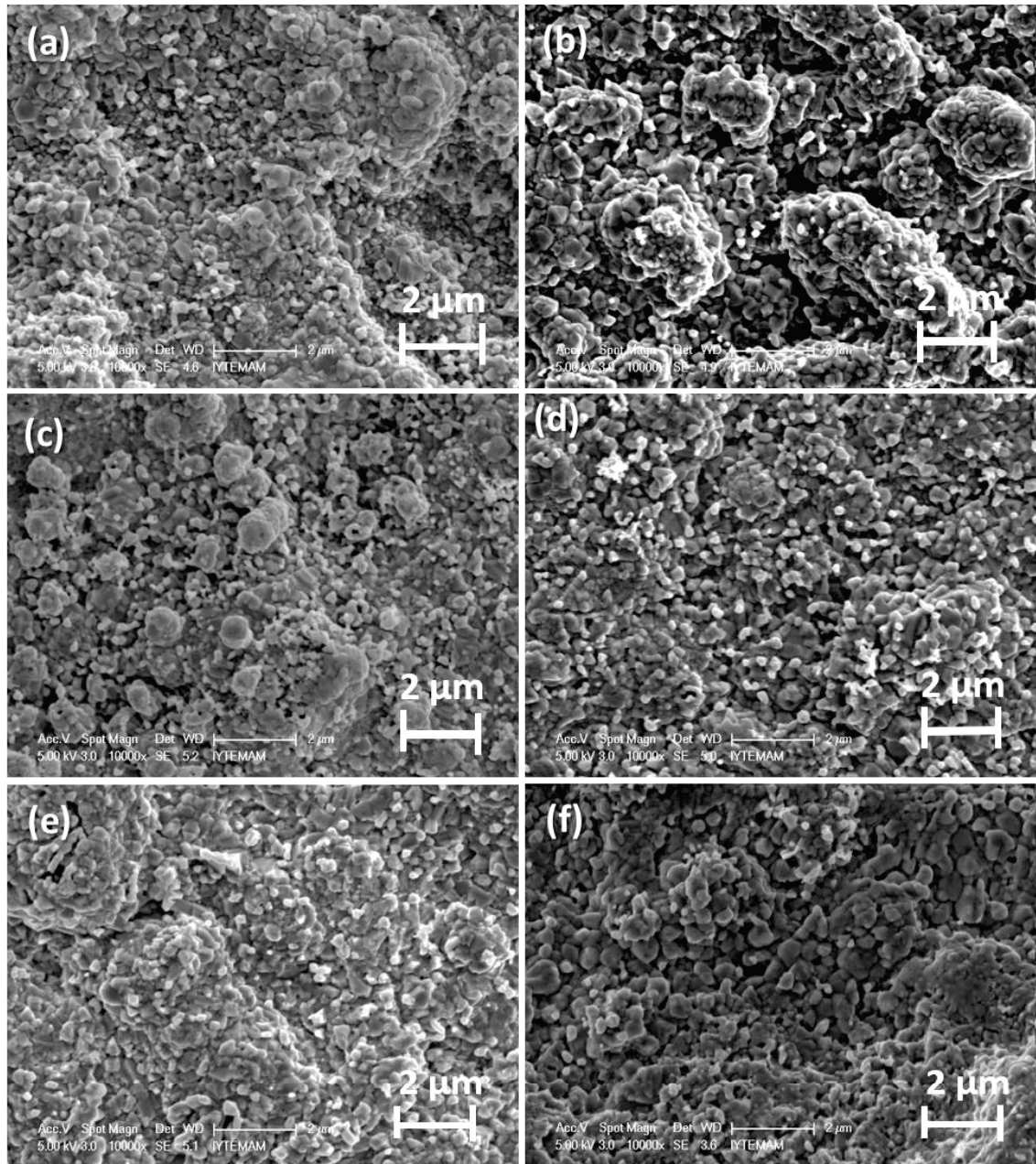
Figure 5.2. Tilted SEM images of sulfurized thin films on Ti foil in (a) 530 ºC, (b) 540 ºC (c) 550 ºC, (d) 560 ºC, (e) 570 ºC, and (f) 580 ºC.
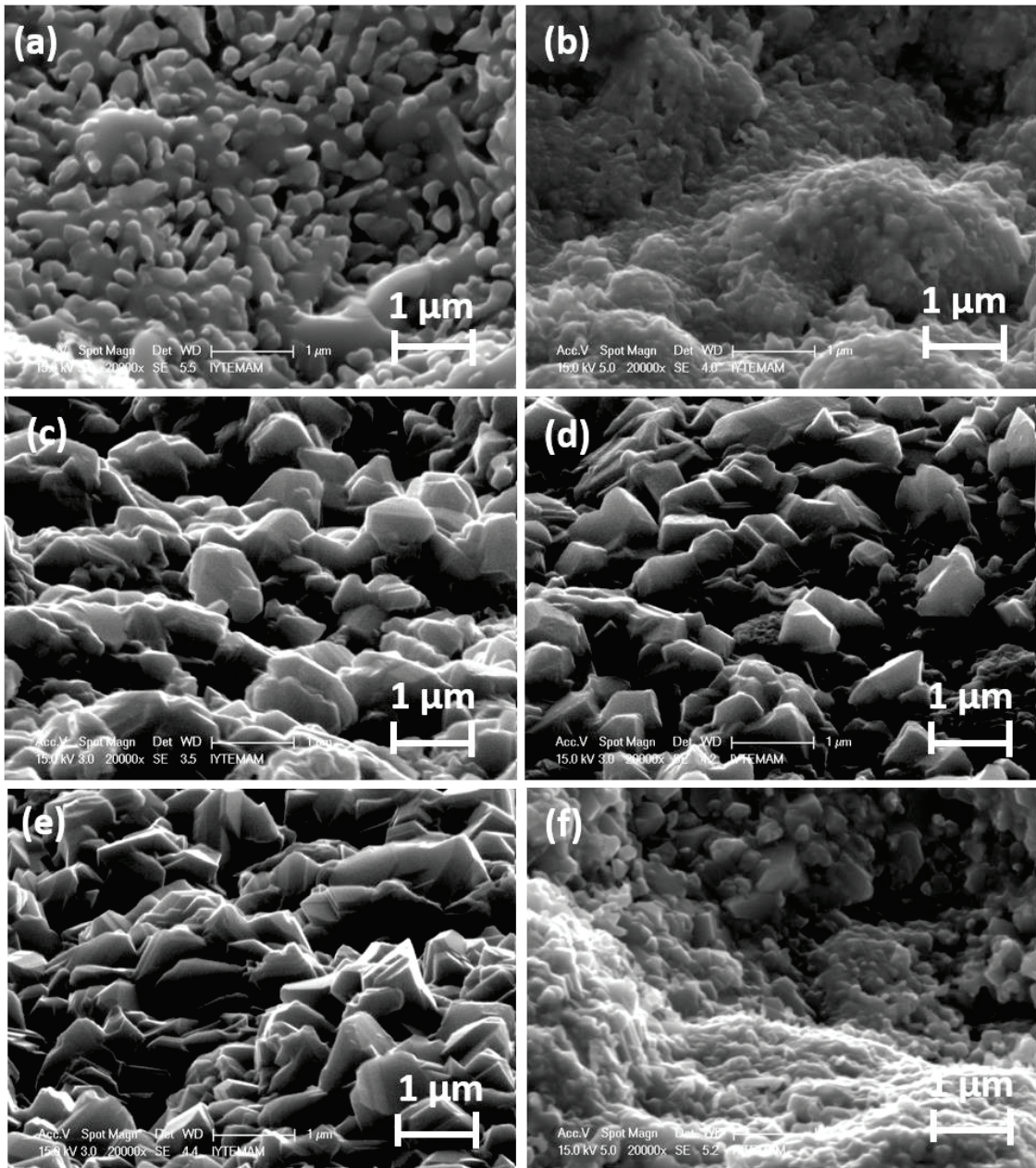
Figure 5.3. The SEM images of sulfurized thin films on Ti foil in (a) 530 $^{\circ}$C, (b) 540 $^{\circ}$C (c) 550 $^{\circ}$C, (d) 560 $^{\circ}$C, (e) 570 $^{\circ}$C, and (f) 580 $^{\circ}$C.

5.3. Chemical Composition Analysis

The thickness of each layer in metallic precursor was adjusted to grow CZTS thin film which has Cu-poor/Zn-rich composition during the sulfurization process because Cu-poor Zn-rich CZTS films have higher performances, since a Cu-poor composition enhances the formation of Cu vacancies, which produces shallow acceptors in films (Chen et al. 2010). The reported studies shows that CZTS films with Cu-poor and Zn-rich compositions have better device performances and higher efficiencies (Katagiri et al. 2009a; Platzer-Björkman et al. 2012). The report elemental ratio for Zn/Sn and Cu/(Zn+Sn) are 1.2 and 0.8, respectively (Katagiri et al. 2009b; Shin et al. 2013; Tajima et al. 2017). Elemental compositional analysis was done by carrying out EDS measurements. The structural quality and stoichiometry play a key role in the solar cell performance. Table 5.2 lists the atomic percentages of each element and the Zn/Sn and Cu/(Zn+Sn) ratios for different sulfurization temperatures

Table 5.2. EDS results showing the atomic percentages of the constituent elements and some component ratios for sulfurized CZTS thin film on Ti foil

Elements	Atomic percentages for different temperatures (ºC)					
	530 ºC	540 ºC	550 ºC	560 ºC	570 ºC	580 ºC
Cu	23.83	29.41	26.30	27.39	27.12	27.34
Zn	20.25	15.20	17.07	14.01	16.14	16.87
Sn	11.46	12.74	12.57	12.74	12.69	12.08
S	44.46	42.65	44.06	45.86	44.06	43.71
Ratios						
Zn/Sn	1.76	1.20	1.36	1.09	1.27	1.38
Cu/(Zn+Sn)	0.75	1.04	0.88	1.02	0.94	0.94

When we examined the metallic ratios of the sulfurized films at 540 ºC-580 ºC (Sample B to Sample F) have a similar ratios to those reported in the literature. However, Sample A has a considerably higher Zn/Sn ratio than the reported ones and this indicates the presence of ZnS phase in the CZTS film. It shows that loss of Sn could not be prevented, even though Cu layer deposited on Sn layer to prevent Sn loss. Based on the metallic ratios we can say that in our samples, thin films sulfurized at 540 ºC and 560 ºC show C-type off-stoichiometric CZTS formation due to the $Cu_{Zn}+Sn_{Zn}$ intrinsic defects, it means the films have Cu-rich/Zn-poor composition while the films sulfurized at 530

°C, 550 °C, 570 °C, and 580 °C showed B-type off-stoichiometric CZTS formation due to the $V_{Cu}+Zn_{Cu}$ intrinsic defects, it means the films have Cu-poor/Zn-rich composition. When the relation between the metallic ratios and sulfurization temperature is examined, no significant increase or decrease tendency of the metallic ratios with sulfurization temperature can be observed. However, the sulfurized film at 570 °C is more suitable than the other films for device application because its metallic ratio is similar to reported ones.

5.4. Structural Analyses

5.4.1. XRD Analysis

XRD analysis was carried out to reveal information about the crystal structure and existing phases. However, XRD analysis is not enough to identify the CZTS structure, since Cu_2SnS_3 (CTS) and ZnS secondary phases have similar a crystal structure with kesterite CZTS structure, and their peaks can overlap. Therefore, to get more reliable identification another analysis is required, and Raman analysis is an auxiliary way to a characterization of the phase structure. During the XRD characterization of the films, CZTS (JCPDS-26-0575) data base was used to identify the structure of our films. Figure 5.4 shows the XRD patterns of sulfurized films in different sulfurization temperature. The diffraction peaks were observed from the (110), (112), (103), (200), (105), (220), (312), (224), (008), and (332) planes, respectively. The observed XRD patterns match quite well with the standard XRD pattern of kesterite Cu_2ZnSnS_4 (JCPDS 26-0575), indicating the formation of kesterite CZTS for all sulfurization temperatures. Besides, the peaks belong the Ti substrate (JCPDS 44-1294) were observed at $2\Theta = 38.31, 40.13, 52.93$, and 70.94°, and the small peaks belong the rutile phase of titanium (JCPDS 44-1294) were observed at $2\Theta = 27.34$ and 36.12°. In addition the preferential (112) peak and other CZTS structure related peaks, the films showed some secondary phases such as SnS_2, $Cu_{2-x}S$ and Cu_2SnS_3 in samples with sulfurization temperatures up to 550 °C. Above 550 °C, no secondary phase was detected.
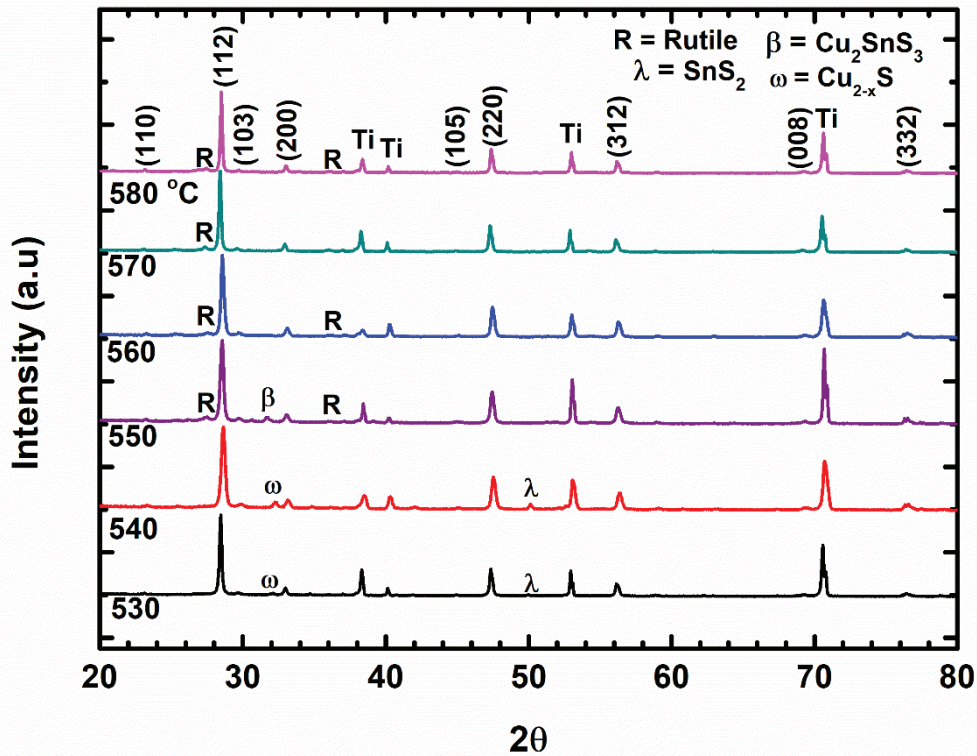
Figure 5.4. Normalized XRD patterns of thin films sulfurized at (a) 530 ºC, (b) 540 ºC (c) 550 ºC, (d) 560 ºC, (e) 570 ºC, and (f) 580 ºC (Source: Buldu et al. 2017).

The average crystallite size can be found by using Scherrer's formula $d = k\lambda/\beta cos\theta$, where λ is 0.1506 nm which is the wavelength of X-ray used, k is a constant generally taken as 0.9 (Monshi et al. 2012), β is the full width of half maximum the diffraction peak at half maximum height (FWHM) in radians, and Θ is the Bragg's diffraction angle. Figure 5.5 shows the variation of the crystallite size with the sulfurization temperature. Beyond 540 ºC, the crystallite size of the films increase with the sulfurization temperature, and the sulfurized thin films at 570 and 580 ºC have larger crystalline size 50.60 nm. Sample A (530 ºC) had 63.1 nm crystallite size, but due to the presence of high amount ZnS phase in the film, a large crystallite size could be observed. Beyond 540 ºC, the crystallite size of the films increase with the sulfurization temperature, and the sulfurized thin films at 570 and 580 ºC have larger crystallite size 50.60 nm. The diffraction peak intensities that belong to (112) plane and FWHM of the samples are shown in Figure 5.6 as a function of sulfurization temperature. Beyond 540 ºC, the intensity of (112) plane increase, and FWHM of diffraction peak of (112) plane of the samples decrease with the increasing sulfurization temperature. However, the sulfurized film at 530 ºC (Sample A) and 580 ºC Sample F showed a different tendency.

We thought that the (112) plane intensity of Sample F may have been reduced due to the decomposition of CZTS, we mentioned when we discussed about the morphological analysis.
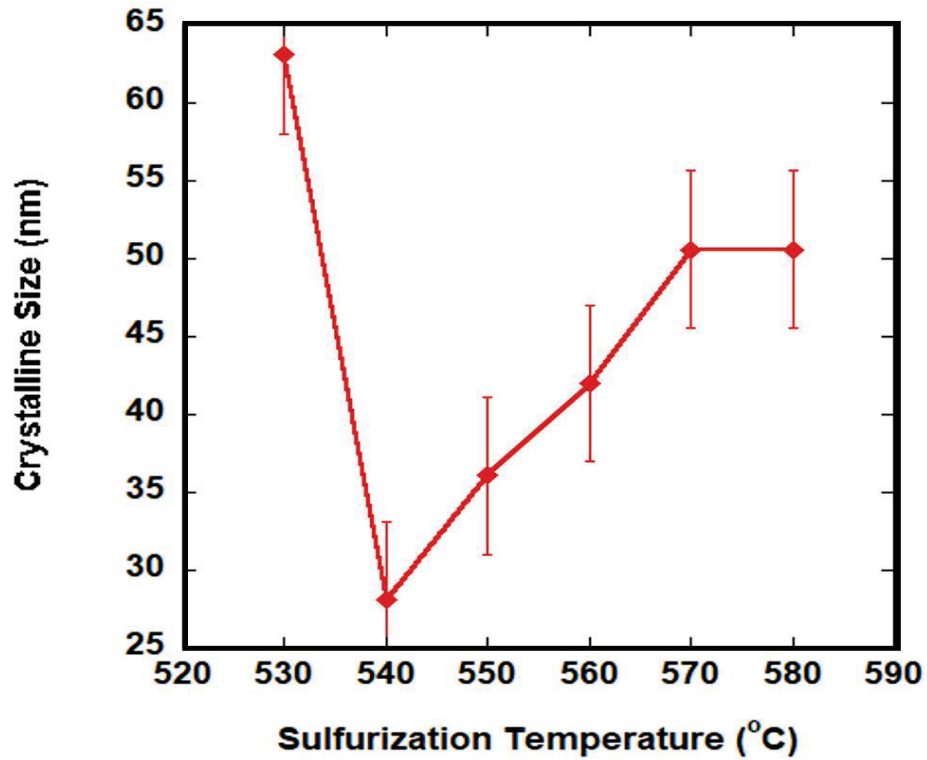
Figure 5.5. The variation of crystallite size with the sulfurization temperature.
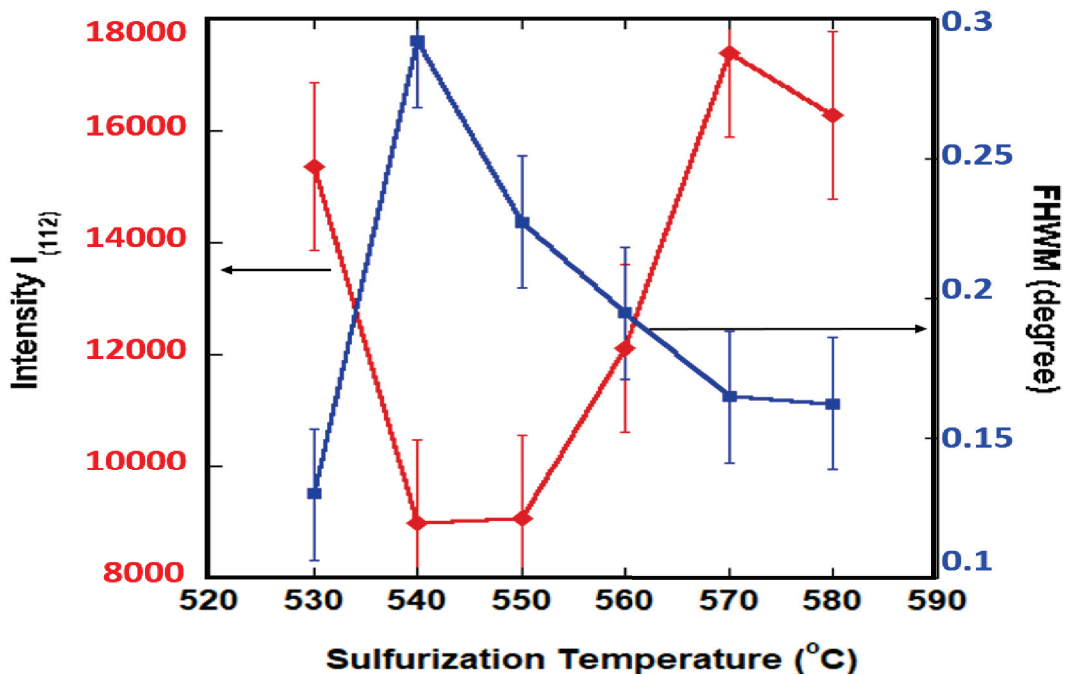
Figure 5.6. The (112) diffraction intensity and FWHM of (112) diffraction peak of films as a function of different sulfurization temperatures.

When we conclude this analysis, we saw that the sulfurization temperature plays a critical role in the crystallization of the CZTS films. As the sulfurization temperature increased, more intense and sharp peaks were observed, which means that the crystallization has become better with increasing the sulfurization temperature. As a result of the analysis so far, Sample E (570 ºC) is more suitable for solar cell applications due to its better properties.

5.4.2. Raman Spectroscopy Analysis

Raman spectroscopy measurements were performed for reliable structural characterization of CZTS thin films and the identification of secondary phases. The Raman spectra of thin films are shown in figure 5.7. Each Raman spectrum is the average of measurements taken from 4 different place on each sample to indicate homogeneity and the measurements show similar spectra which indicate homogeneity in our films.
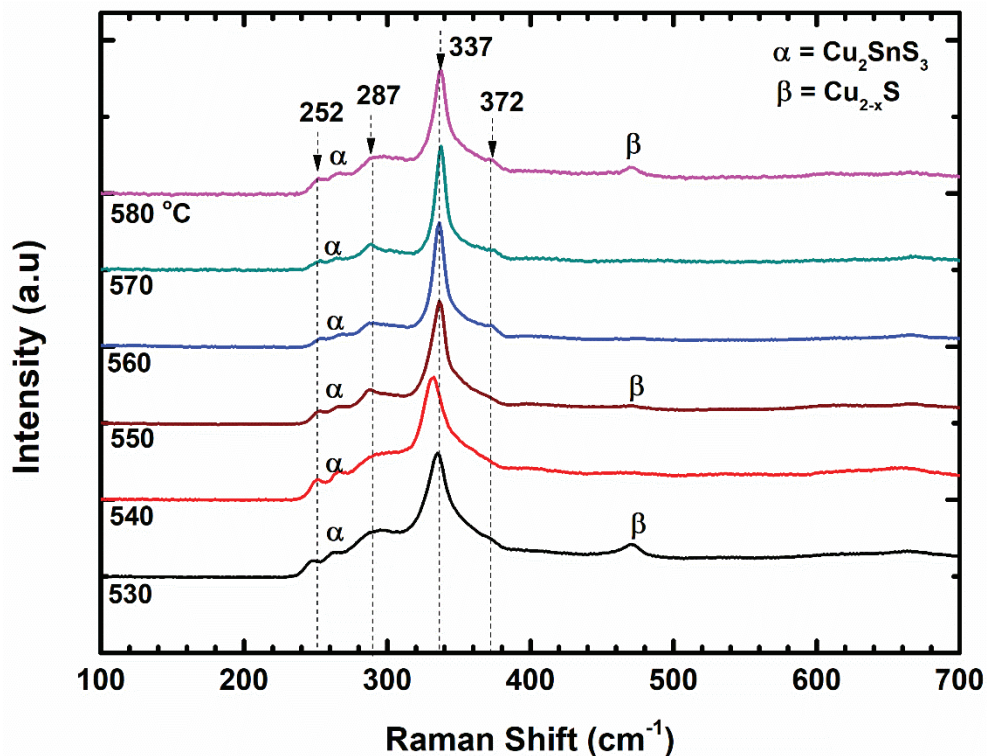
Figure 5.7. Raman spectra of thin films for the sulfurization temperatures (a) 530 ºC, (b) 540 ºC (c) 550 ºC, (d) 560 ºC, (e) 570 ºC, and (f) 580 ºC.

The Raman spectra of thin films is shown in figure 5.7 gives a prior knowledge of the structure of CZTS thin film. The characteristic Raman peaks of Cu_2ZnSnS_4 are nearly at 252, 287, 337, and 372 cm^{-1} (He et al. 2014; Yoo and Kim 2010) indicating the structure of the films is kesterite. The weak peak at 267 cm^{-1} was observed for all films and attributed to the Cu_2SnS_3 secondary phase (Fernandes et al. 2011). We notice that the peak for the secondary phase Cu_2SnS_3 is hardly visible for the sample with the sulfurization temperature of 570 °C. The weak peak detected at 470 cm^{-1} belongs the $Cu_{2-x}S$ secondary phase (Kumar et al. 2015) which was observed for sulfurized films at 530, 550, 580 °C. Two broad shoulders were observed near the strongest peak for that reason Lorentzian curve fit was applied between 200 cm^{-1} and 500 cm^{-1} wavelength so that the structure of CZTS films could be characterized more deeply. Figure 5.8 belong to Sample A (530 °C) and shows the Raman peaks with curve fitting.
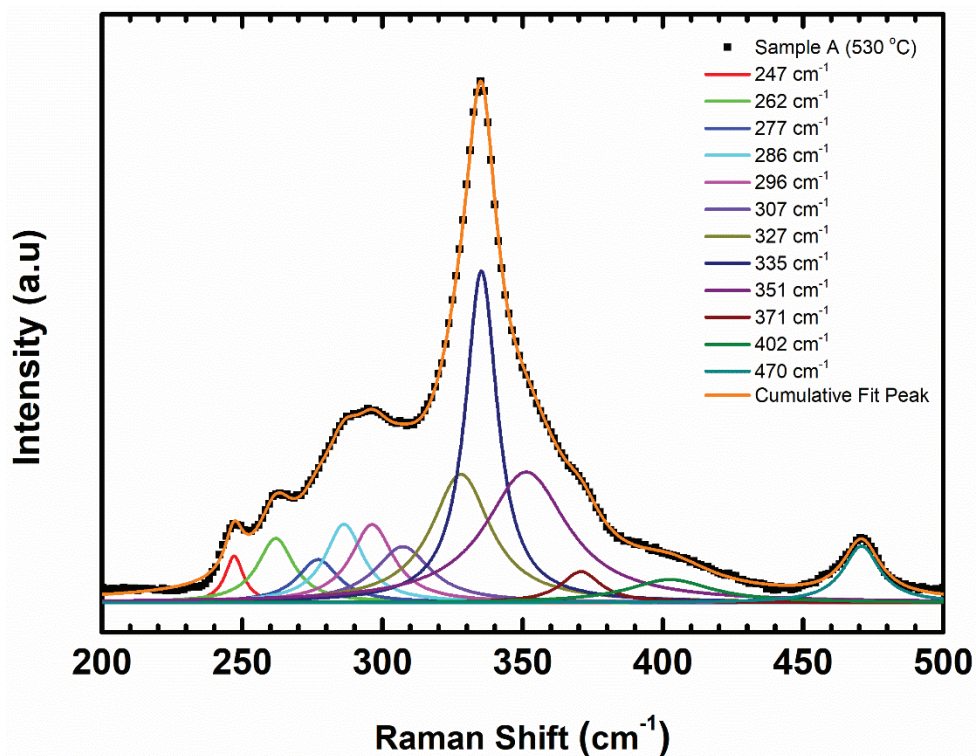
Figure 5.8. Raman spectra of Sample A.

The strongest peak was observed at 335 cm^{-1} (Gurel et al. 2011) which belong the A mode kesterite CZTS. The other kesterite CZTS peaks were observed at 247, 262, 286, 307, 351 and 371 cm^{-1} (Guc et al. 2016; Fontané et al. 2012). However, we observed other additional peaks which do not belong the kesterite CZTS structure when we applied curve fitting. The peaks of stannite CZTS were observed at 277 and 327 cm^{-1} (Khare et al.

2012a; Altamura et al. 2014). In the broad shoulder between 280-290 cm^{-1}, the peak maximum was observed at 296 cm^{-1} which belongs Cu_2SnS_3 secondary phase (Chalapathi et al. 2015). The other additional peak was observed at 402 cm^{-1} when the curve fitting was applied, and it belongs the anatase TiO_2 (Wang et al. 2015).
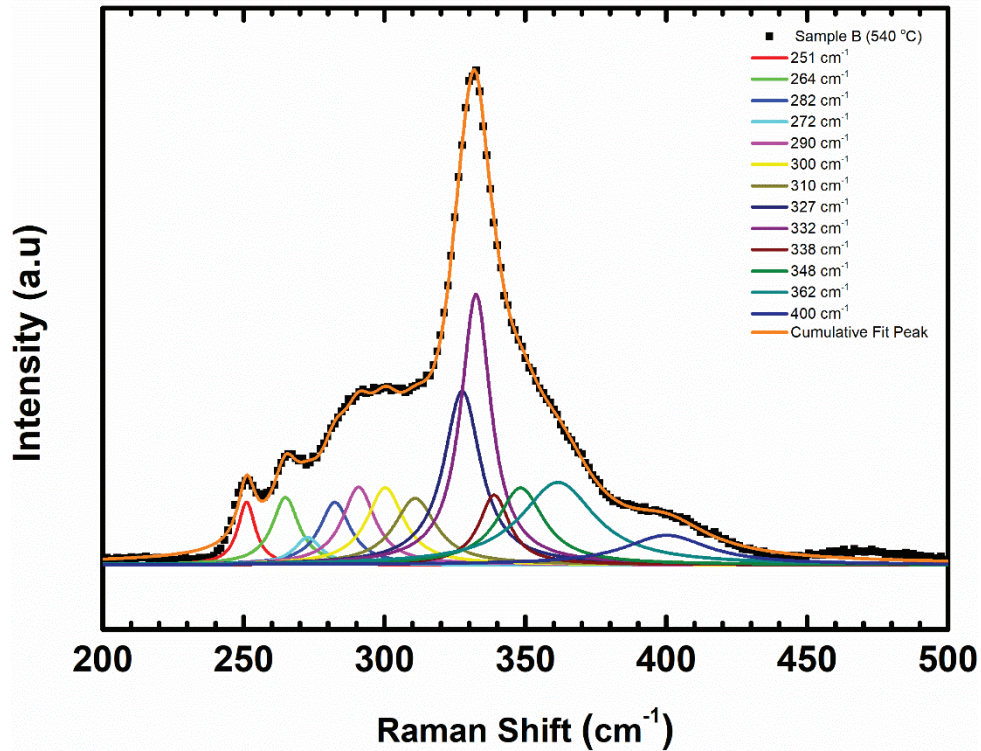
Figure 5.9. Raman spectra of Sample B.

The Raman spectra of Sample B showed in figure 5.9. The stronger peaks were located at 332 and 327 cm^{-1} which belongs the A_1 mode of stannite structure (Gurel et al. 2011; Altamura et al. 2014) . The other stannite CZTS structure peaks were observed at 264 and 282 cm^{-1} (Khar et al. 2012a). The presence of an additional Raman peaks at 338 cm^{-1} that is A mode of kesterite CZTS, and other kesterite CZTS peaks at 272 and 362 cm^{-1} (Khare et al. 2012a; Himmrich and Haeuseler 1991). The result of curve fitting, it could be said that the stannite structure was dominant in Sample B thin film. Furthermore, the film consisted secondary phases such as Cu_2SnS_3 at 290 and 300 cm^{-1} (Fontane et al. 2011; Scragg et al. 2014), and SnS_2 at 310 cm^{-1} (Yazici et al. 2015), and ZnS at 348 cm^{-1} (Calderón et al. 2015). Cu_2SnS_3 and ZnS secondary phases could not be detected in XRD analysis due to overlap structural peaks, however the XRD analysis matched with Raman analysis for SnS_2 secondary phase.
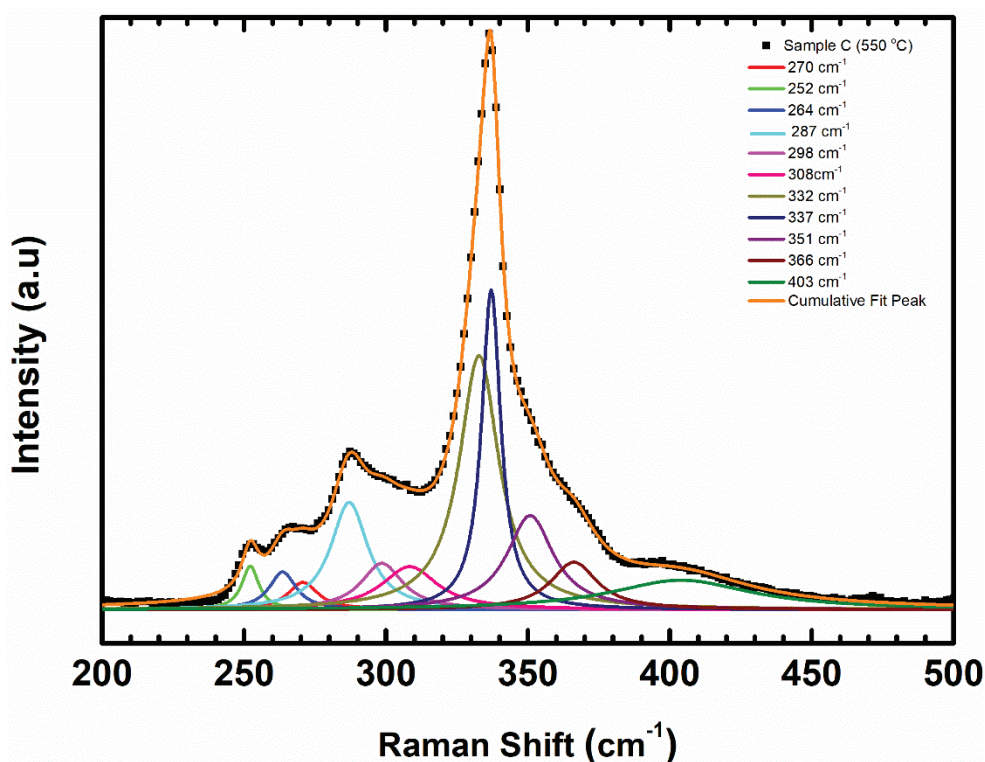
Figure 5.10. Raman spectra of Sample C.

The dominant peak was observed at 337 cm^{-1} which is A mode of kesterite CZTS structure (Valakh et al. 2013), and additional peak was observed at 332 cm^{-1} (Gurel et al. 2011) which can be either A$_1$ mode of stannite or B(LO) mode of kesterite CZTS. The additional peak at 332 cm^{-1} can be attributed to the disorder kesterite structure, and may be attributed the stannite phase. However, we cannot say the exact atomic displacements. We can say that our film is composed of two types of structure, and that one of them is dominant. The other kesterite structure peaks were observed at 252, 272, 287 and 366 cm^{-1} (Khare et al. 2012a; Khare et al. 2012b). The peak of secondary phases were observed at 264 and 299 cm^{-1} which belong to the Cu$_{2-x}$S phase and Cu$_2$SnS$_3$ phase, respectively (Berg 2012); (Ge et al. 2012). XRD and Raman analysis were matched with each other for secondary phases.

The Raman spectra of Sample D is given in Figure 5.11. The strongest peak was observed at 336 cm^{-1} which is B(LO) mode of kesterite structure (Gurel et al. 2011), additional peak was found at 334 cm^{-1} that is A$_1$ mode of stannite structure (Khare et al. 2012a). This circumstances could be occurred due to the disorder kesterite structure.
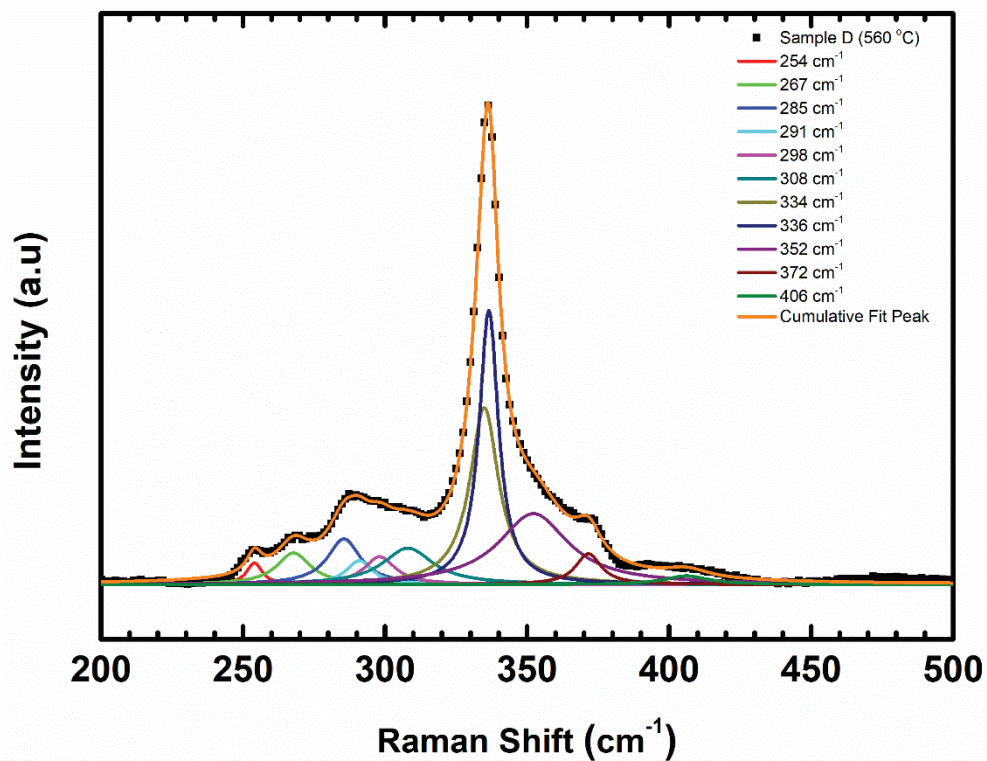
Figure 5.11. Raman spectra of Sample D.

The other characteristic of kesterite CZTS structure were observed at 254, 285, 308, 352, and 371 cm^{-1} (Fontané et al. 2012). The peaks of Cu_2SnS_3 secondary phase were observed at 267 cm^{-1} (Chalapathy et al. 2013), 291 cm^{-1} (Berg et al. 2012), and 298 cm^{-1} (Ge et al. 2012). This phase could not be determined in the XRD analysis due to overlap with CZTS structure. It can be said that the film is constituted by a mixing of two type of structures.

The Raman spectra of Sample E can be seen in Figure 5.12. The strongest and dominant peak was observed at 337 cm^{-1} which is A mode of kesterite structure (Jawhari et al. 2014), and the other characteristic kesterite peaks were observed at 252, 287, 354 and 372 cm^{-1} (Gurel et al. 2011; Fontané et al. 2012). The peaks of Cu_2SnS_3 secondary phase were observed at 266 and 304 cm^{-1} (Chalapathy et al. 2013). We observed that, this sample did not contain stannite structure when the curve fitting was applied, and secondary phase was barely visible (Figure 5.7). That means Sample E can be more suitable film for applications.
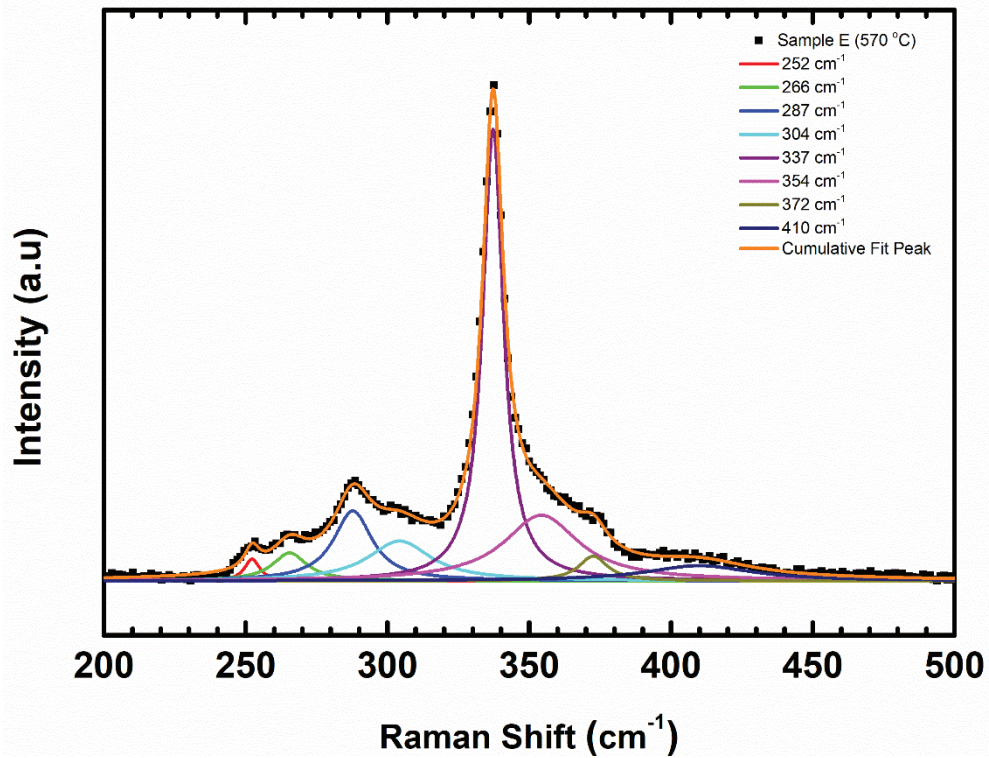
Figure 5.12. The Raman spectra of Sample E.

Figure 5.13 shows the Raman spectra of Sample F. The main peak was observed at 337 cm^{-1} which belongs the A mode of kesterite structure (Jawhari et al. 2014). However, additional peak was found at 331 cm^{-1}. This peak is thought to have arisen from a high concentration of intrinsic defects in Cu-poor CZTS thin films, especially regarding Zn_{Cu} and V_{Cu} antisite defect (Walsh et al. 2012; Schorr and Gonzalez-Aviles 2009). It is also noted that this peak might be attributed to the presence of a high degree disorder in the cation sublattice (Schorr et al. 2007; Valakh et al. 2013). As a result of the disorder kesterite structure, the space of kesterite structure changes and becomes the same as the stannite (Washio et al. 2011). In the view of such information, we can say that Sample F has a disorder kesterite structure. Furthermore, the other kesterite structure peaks were observed at 252, 271, 287, 309, 352 and 371 cm^{-1} (Khare et al. 2012a; Fontané et al. 2012; He et al. 2015). The presence of the secondary phases were determined at 264 and 472 cm^{-1}, and 297 cm^{-1} which belong the Cu_{2-x} and CuS secondary phase, and Cu_2SnS_3 secondary phase, respectively (Fernandes et al. 2009; Chaudhari et al. 2016).
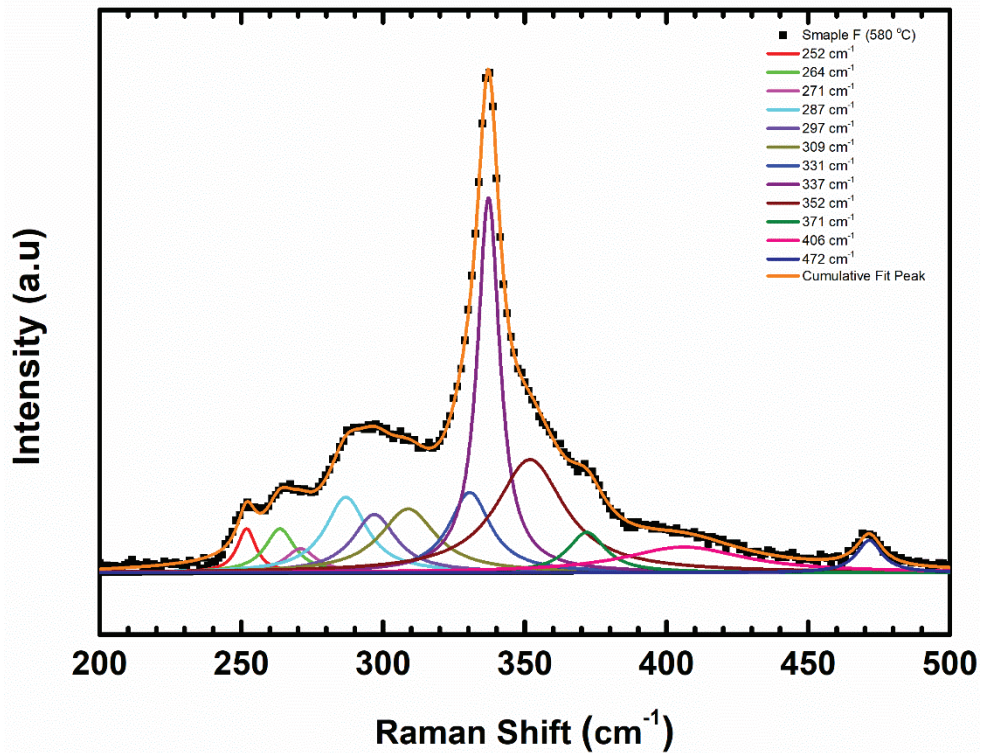
Figure 5.13 The Raman spectra of Sample F.

The Raman spectroscopy analysis with a Lorentzian curve fitting showed that the main peak of the films started to change with the sulfurization temperature. The blue shift was observed with increasing the sulfurization temperature, but the Sample B did not include this blue shift because of its stannite structure. The mixed phase structure (kesterite structure with stannite structure) was observed expect Sample E that means Sample E has better quality CZTS film. The sulfurization temperature does not have significant effect on secondary phases but the secondary phases were barely visible in the Sample E when it was compared with other samples. This shows that in two stage CZTS film fabrication, sulfurization process plays a critical role to reduce secondary phases. However, it is a big challenge producing single phase kesterite CZTS film due to its complex structure but better quality films can be obtained with optimal sulfurization process. Also we can say our XRD and Raman analysis were matched with each other.

5.5. Chemical Analysis

The compound elements, secondary phase formation and surface atomic concentration of the sulfurized CZTS films on Ti foil were determined using XPS. As mention earlier XPS is surface sensitive analysis for that reason XPS cannot be matched with the EDS results.

The high resolution spectra of Zn $2p$, Cu $2p$, Sn $3d$, and S $2p$ valance regions were measured. Figure 5.14 shows a series of XPS spectra for various compositional elements. Figure 5.14 (a)-(d) show Zn $2p$, Cu $2p$, Sn $3d$, and S $2p$ bands, respectively.
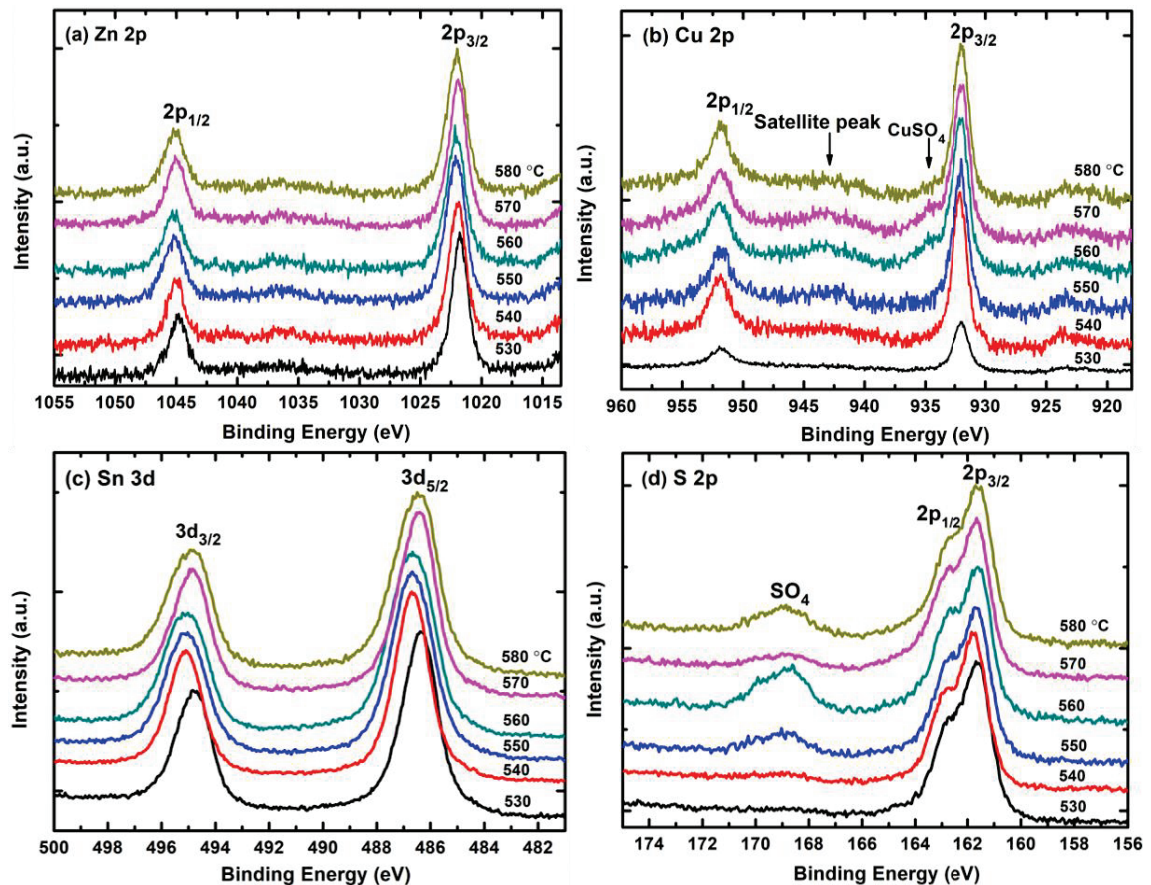
Figure 5.14. High resolution XPS spectra of (a) Zn 2p, (b) Cu 2p, (c) Sn 3d, and (d) S 2p bands.

To determine the surface chemical state and secondary phases, Shirley-type background was used for the high resolution spectra of each elements and then the curves were fitted with Gaussion/Lorentzian product GL(p) function. The $2p$ band was fitted using a 2:1 peak area ratio for the $2p_{3/2}$ to $2p_{1/2}$ peak area ratio whereas the $3d$ band was fitted with a 3:2 peak area ratio for $3d_{5/2}$ to $3d_{3/2}$ peak area ratio. For fittings, the

spin-orbit splitting energy value for each element was chosen as a constant parameter. The signs of the chemical shifts during a bonding process indicate an electron transfer which results in a net charge exchange (Moholkar et al. 2011). However, little to no shift was observed in the binding energies for the same element in different CZTS films. Hence, we conclude that no charge transfer occurred which indicate no phase change. The curve fitting results for observed peak positions at sulfurized films at different sulfurization temperatures are given in Table 5.3. All $2p$ and $3d$ bands are doublets as $2p_{3/2}$, $2p_{1/2}$ and $3d_{5/2}$, $3d_{3/2}$, respectively.

Table 5.3. Curve fitting results for high resolution XPS spectra

Sulfurization Temperature (ºC)						
	580	**570**	**560**	**550**	**540**	**530**
Zn 2p₁/₂	1045.1	1044.9	1045.1	1045.1	1045.0	1044.8
Zn 2p₃/₂	1022.1	1021.9	1022.1	1022.1	1022.0	1021.8
Cu 2p₁/₂	951.8	951.8	951.8	951.8	951.9	951.7
Cu 2p₃/₂	932.0	932.0	932.0	932.0	932.1	931.9
Cu 2p₁/₂	953.3	954.6	954.5	953.0	-	-
Cu 2p₃/₂	933.5	934.8	934.7	933.2	-	-
Sn 3d₃/₂	494.9	494.8	495.0	495.1	495.1	494.8
Sn 3d₅/₂	486.5	486.4	486.4	486.7	486.7	486.4
Sn 3d₃/₂	-	-	-	-	496.6	495.5
Sn 3d₅/₂	-	-	-	-	488.2	487.1
S 2p₁/₂	162.8	162.8	162.8	162.8	162.9	162.8
S 2p₃/₂	161.6	161.6	161.6	161.6	161.7	161.6
S 2p₁/₂	164.8	164.7	164.5	164.7	164.7	164.8
S 2p₃/₂	163.6	163.5	163.3	163.5	163.5	163.6

Figure 5.15 shows the Zn $2p$ spectra of the samples with different sulfurization temperatures which were fitted using a GL (80) function where a 23.0 eV spin-orbit splitting energy was used for all CZTS samples. The Zn $2p_{3/2}$ band, which spans the spectral region from 1021.6 and 1022.3 eV as given in the literature (Shin et al. 2011; Singh et al. 2012), was also observed in our samples between 1021.8-1022.2 eV energies which indicates +2 charge state for Zn in CZTS.

Figure 5.15. XPS peak fitting spectra of Zn 2p regions for CZTS thin films with different sulfurization temperature.

The Cu 2*p* regions of samples with different sulfurization temperature in Figure 5.16 were curve fitted with a spin–orbit splitting energy of 19.8 eV for all CZTS samples. The Cu 2*p* regions were fitted using a GL(90) function.

Figure 5.16. XPS peak fitting spectra of Cu 2p regions for CZTS thin films with different sulfurization temperature.

For the films sulfurized at a temperature $\geq$ 550 °C, the 2p band consists of two doublets. In the first doublet band, two Cu $2p_{3/2}$ peaks were observed at about 932 eV which is an evidence for Cu^{1+} charge state in CZTS (Singh et al. 2012; Das et al. 2012). In the Cu $2p$ spectra of films with sulfurization temperatures $\geq$ 540 °C, the well-known shake up satellite shoulder is also seen between 940-945 eV, indicating Cu(II) bonds. It is reported in the literature that these bonds are due to sulfur oxide formations on the surface (Krylova and Andrulevicius 2009). The existence of CuO phase was supported

by the second doublet seen in the Cu $2p$ spectra. The second Cu $2p_{3/2}$ band observed between 933.2-934.8 eV energy range shows a CuO formation on the CZTS surface which was displayed by the samples with sulfurization temperatures $\geq$ 550 °C (Krylova and Andrulevicius 2009); (Biesinger et al. 2010). The Cu $2p_{3/2}$ band of the samples with sulfurization temperatures $\geq$ 550 °C, exhibit a shoulder at $935.0 - 935.5$ eV range which is due to CuSO$_4$ formation (Krylova and Andrulevicius 2009). Usually, Ar$^+$ ion beam etching is needed to remove the secondary phases such as CuO and CuSO$_4$ on the surface. But it can alter the chemical state of the surface (Aygun et al. 2011), hence, it was not applied to the surface of any of our CZTS films before XPS measurements. Therefore, we can clearly attribute the observed peaks to the CuO and CuSO$_4$ phases.

XPS spectra of the Sn $3d$ bands for sample with different sulfurization temperature is given in Figure 5.17. The peak fitting was done using GL(55) function. Each band shows one or two couples of peaks which were fitted with a spin–orbit splitting energy value of 8.4 eV. For all CZTS films, the Sn $3d_{5/2}$ band displays a couple of peaks between 486.3-486.6 eV energy range. These were assigned to the Sn (IV) state in CZTS (Singh et al. 2012; Das et al. 2012). The $3d$ spectra of the CZTS films with sulfurization temperatures of 530 and 540 °C display a second couple of Sn $3d$ peaks at 487.8 and 488.4 eV energies. The Sn $3d_{5/2}$ peak observed at 487.0 eV is originated from Sn in SnS$_2$ phase (Shin et al. 2011). The peaks at 487.1 and 488.2 eV are attributed to SnS and Sn$_2$S$_3$ phases, respectively (Cruz et al. 2003). It has been proposed that Sn $3d_{5/2}$ peaks at 487.2 and 488.3 eV origante from SnS and SnS$_2$, respectively (Yang et al. 2013). Thus, according to all these references it is safe to say that there exist Sn based secondary phase formations in our samples which is consistent with the XRD and Raman results of the same CZTS films.

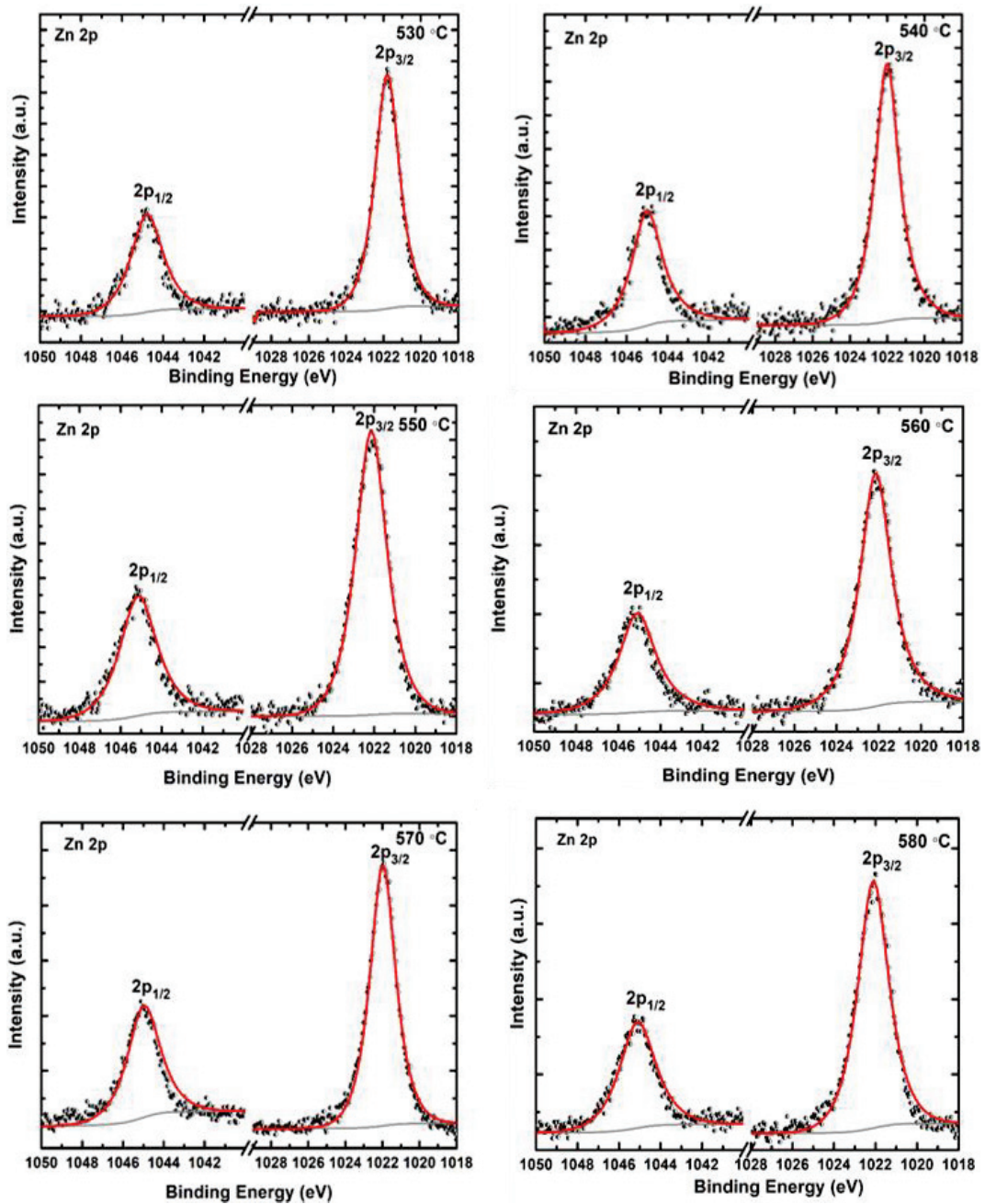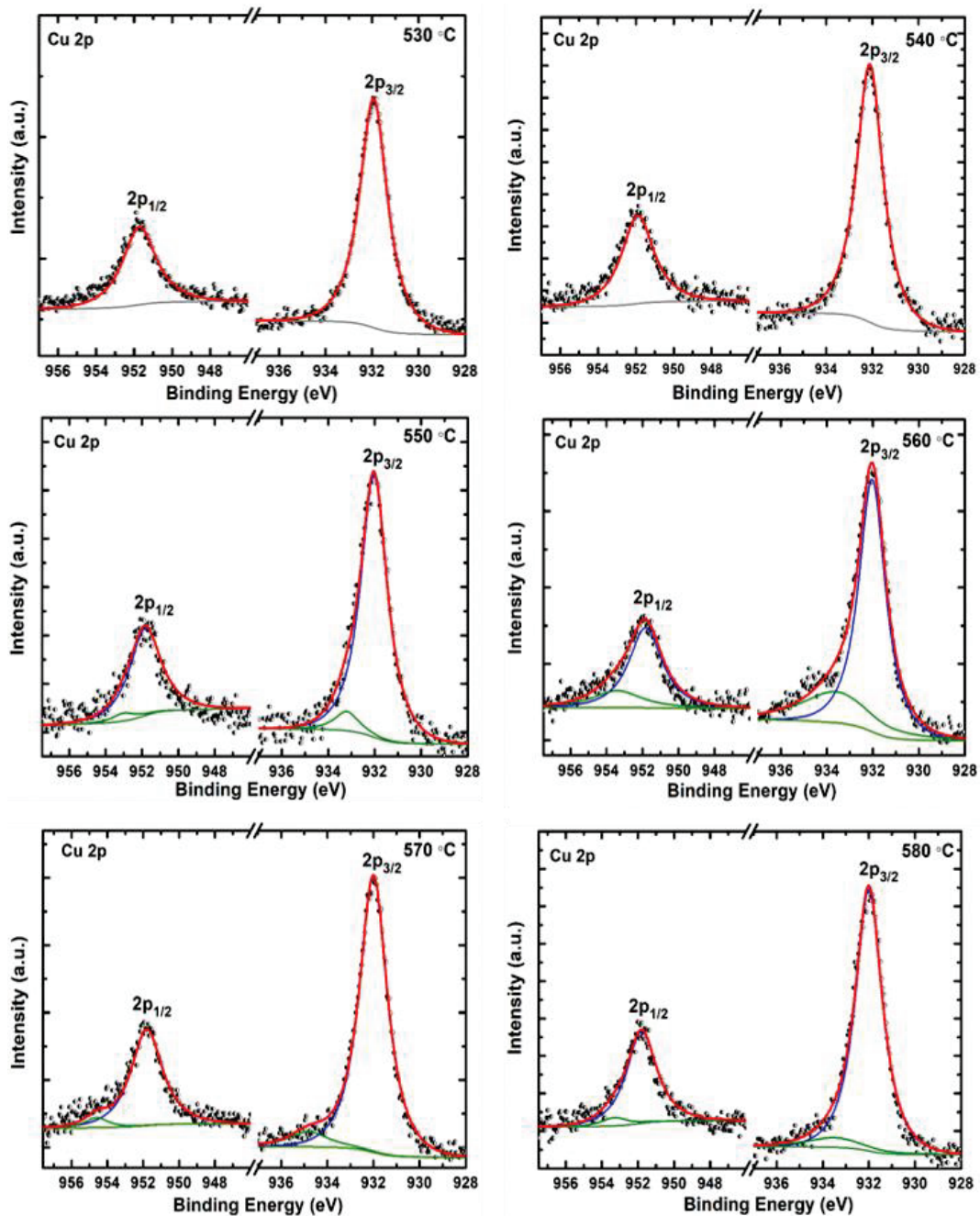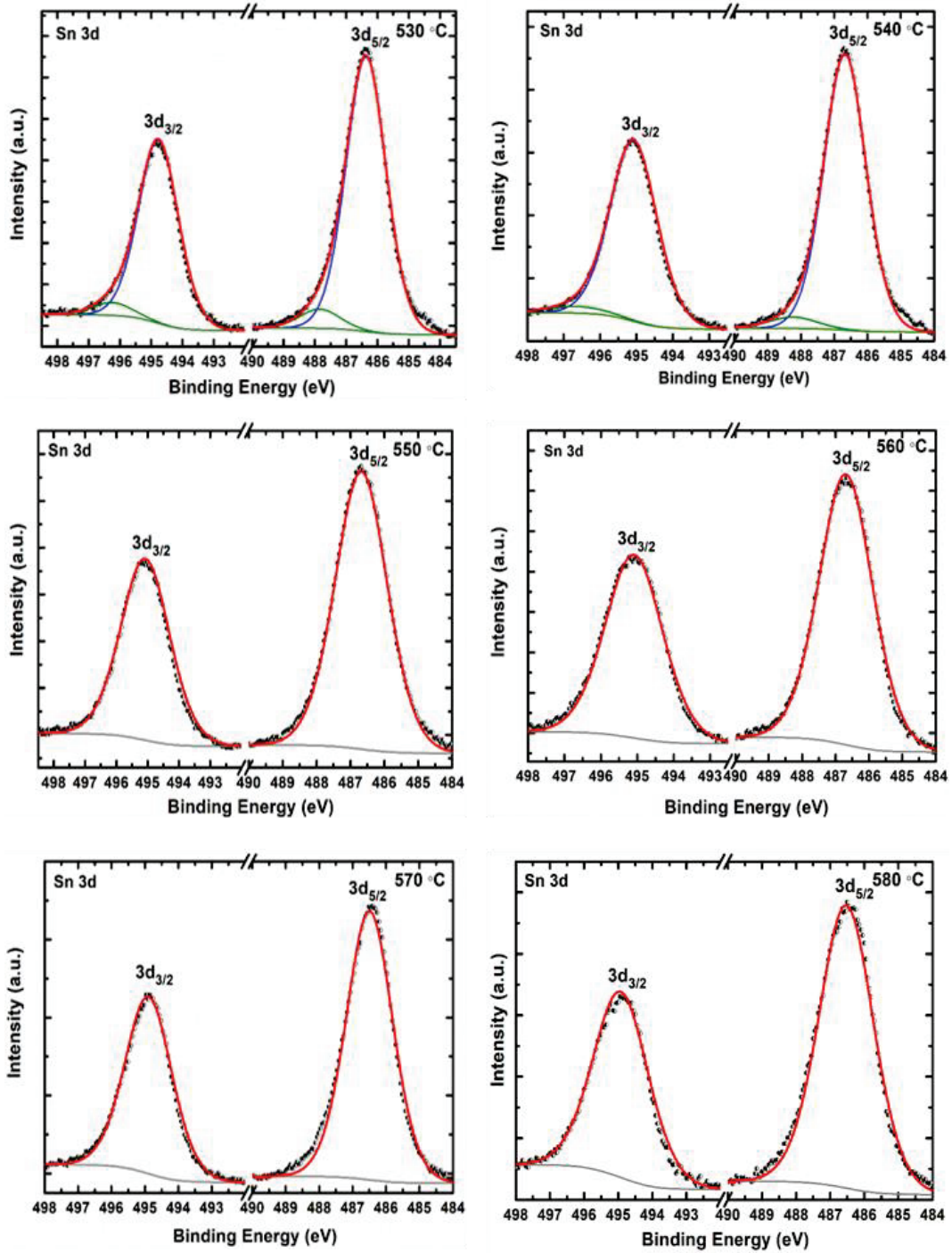Figure 5.17. XPS peak fitting spectra of Sn 3d regions for CZTS thin films with different sulfurization temperature.
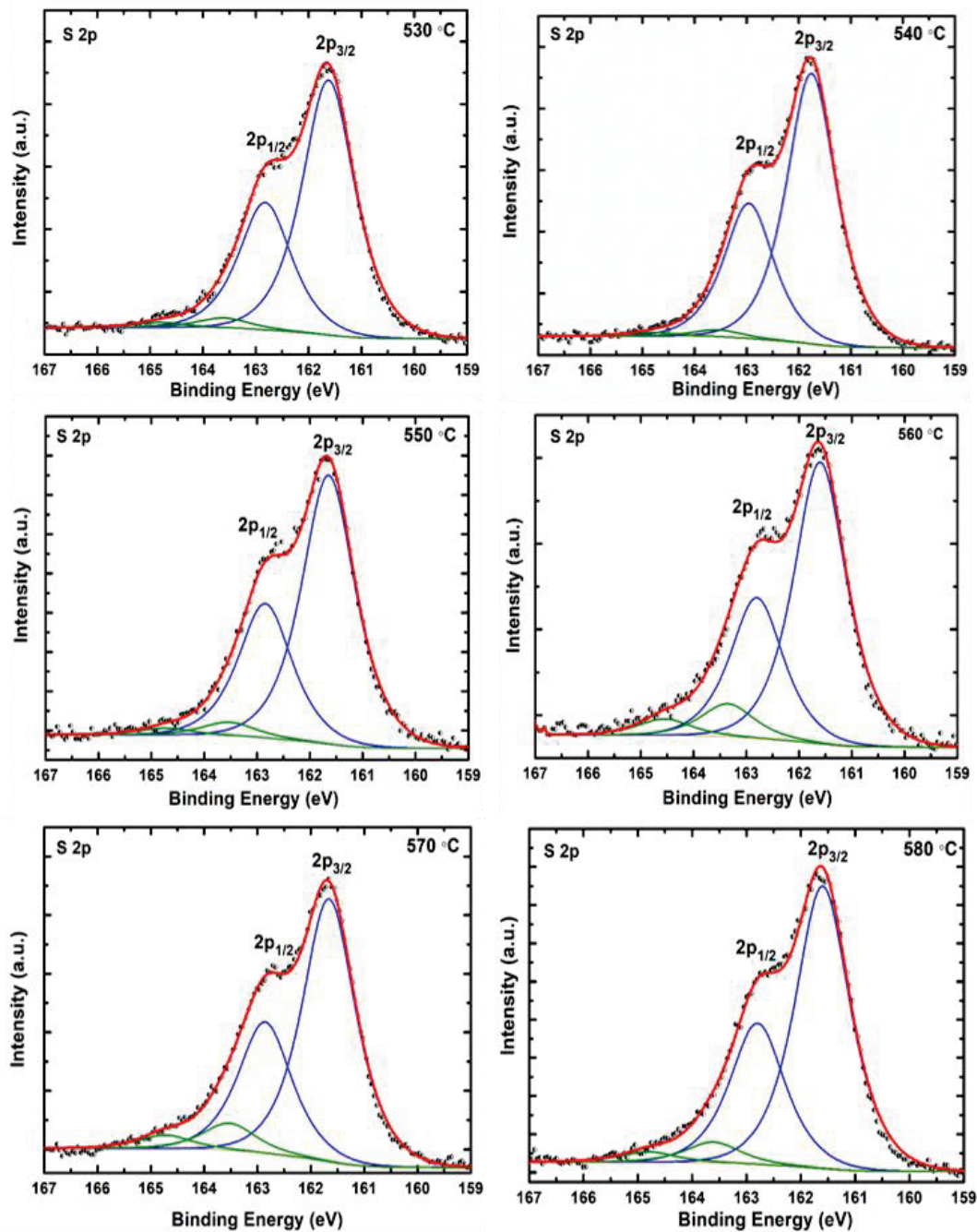
Figure 5.18. XPS peak fitting spectra of S 2p regions for CZTS thin films with different sulfurization temperature.

Figure 5.18 shows the The XPS spectra for S $2p$ energy state for the CZTS films. Each spectrum consists of two doublets with a spin orbit splitting energy of 1.2 eV. For the peak analysis a GL (75) line shape function was used. The $2p_{3/2}$ band, observed at a peak position of 161.7 or 161.6 eV, represents an expected monosulfide phase (S^{2-}) (Singh et al. 2012; Acres et al. 2010a). The second $2p_{3/2}$ band observed at a peak position between 163.3 (Acres et al. 2010b) and 163.6 eV (Mikhlin et al. 2004) for all samples. All CZTS films except for those with the sulfurization temperatures of 530 and 540 °C

contain another sulfur bond state at a higher binding energy region (168.8 eV) which implies the formation of copper sulfate ($CuSO_4$) as inferred from the Cu $2p$ peak analysis (Figure5.16). In addition, as mentioned above, the observed $CuSO_4$ phase may be related to CuO-S bonds in an oxidized CZTS surface. The CZTS films sulfurized at 580, 560 and 550 °C demonstrated a strong $CuSO_4$ formation whereas the films sulfurized at 570 °C showed almost none.

The result of XPS analysis, it can be said that all of the sulfurized CZTS films at different sulfurization temperatures are as a candidate for solar cell absorber layer. However, the one with the 570 °C sulfurization temperature is the most favorable one because it shows almost no secondary phase with very little sulfate formation.

CHAPTER 6

CONCLUSION

CZTS is a comparatively new quaternary kesterite structure compound semiconducting material. The kesterite CZTS is a promising candidate as an absorber layer for thin film solar cell applications. Since it contains earth-abundant and non-toxic elements, recently the interest in this structure has begun to increase. However, the current efficiency value of the kesterite-based solar cells are still lower than the other new generation thin film absorber layer such as CIGS and CdTe. For the kesterite-based solar cell to compete with the other, the current efficiency value of kesterite based solar cells has to be increased to get involve in the PV market. The CZTS thin film can be produced by non-vacuum or vacuum based method with one-stage or two-stage process. In two-stage process, the sputtering method offers the mass production due to its easy adaptation in roll-to-roll system and large scale area production. The high annealing or sulfurization process is important to fabricate high efficient photovoltaic devices in the two-stage process. The thermal process plays a key role to achieve efficient CZTS absorber layer because the reaction occurs during this process. Duration and temperature of sulfurization are critical parameters in the thermal process, since the decomposition of CZTS into binary and ternary phases, such as Cu_2S, ZnS, SnS and Cu_2SnS_3, occurs during the thermal process. These secondary phases can be detrimental to device performance. For that reasons, the deep investigation is needed to find optimal parameters for sulfurization process. The substrate is an important issue for thin film photovoltaic applications because to fabricate the homogenous films which required high temperature. Therefore, the substrate has to be chemically inert and vacuum compatible. Besides, thermal expansion coefficient of the substrate and absorber layer have to be same range in order to prevent crack formations and adhesion problem. The crack formation decreases the performance of the device because the shunt path occurs between the front and back contacts of the device. Therefore, the thermal expansion coefficient of the back contact and absorber layer have to be similar range.

We chose the Ti foil substrate due to its suitable thermal coefficient and it enable to grow uniform CZTS thin film without any crack formation and degradation. The barely

visible rutile phase of titanium was observed in XRD analysis. On the other hand, SEM images showed that any crack formations were not observed in our films. However, after chemical etching the surface of Ti foil substrate was degraded and some cavities occurred on the substrate. Our films have grown with imitating the substrate surface but any adhesion problem was not encountered.

The sulfurization temperature is a critical point to obtain efficient absorber layer. The grain sizes, crystallinity and composition are effected by sulfurization temperature. We focused the sulfurization temperature to produce good quality CZTS absorber layer on Ti foil substrate for the short sulfurization process. SEM images showed that all CZTS thin films had compact and dense surfaces without any cracks. Neither void formation nor degradation on those films were observed in those images. The grain sizes as observed from the XRD analysis also became larger with increasing sulfurization temperatures, up to 570 ºC, after which, they got smaller. We conclude from the XRD analysis that the best candidate for a CZTS absorber layer is the one sulfurized at 570 ºC. Since large grain size is a desired quality for better conductivity in an absorber layer of a solar cell, the knowledge of the best sulfurization temperature is very important for the production of good quality absorber layers. The XRD and Raman analysis showed that the crystal structure of the CZTS thin film with the sulfurization temperature of 570 ºC had almost a single phase although some secondary phase peaks were hardly visible. EDS results of this film indicate that it has a Cu-poor/Zn-rich composition which is desired as well for solar cell applications. The XPS spectrum of the CZTS film sulfurized at 570 ºC shows that it does not contain any considerable secondary phase on or near the surface. This result is consistent with the XRD and Raman analysis of the same sample which probe deeper under the surface.

The uniform CZTS thin films without any crack formation were grown on a Ti foil substrate with an optimal sulfurization temperature. It was concluded that, production of CZTS thin films on a Ti foil substrate is a current and important research area since it may enable flexible, and hence, more durable solar cells with desirable yield at lower costs for wide spread industrial applications. The results of this research provides an important step in that direction.

REFERENCES

Abusnina, Mohamed. 2016. "Synthesis and Characterization of Kesterite Cu_2ZnSnS_4 (CZTS) Thin Films for Solar Cell Application." *PhD Thesis*.

Acres, Robert G., Sarah L. Harmer, and David A. Beattie. 2010a. "Synchrotron XPS, NEXAFS, and ToF-SIMS Studies of Solution Exposed Chalcopyrite and Heterogeneous Chalcopyrite with Pyrite." *Minerals Engineering* 23 (11–13): 928–36. doi:10.1016/j.mineng.2010.03.007.

Acres, Robert G., Sarah L. Harmer, and David A. Beattie. 2010b. "Synchrotron XPS Studies of Solution Exposed Chalcopyrite, Bornite, and Heterogeneous Chalcopyrite with Bornite." *International Journal of Mineral Processing* 94: 43–51. doi:10.1016/j.mineng.2010.03.007.

Adachi, Sadao. 2015. *Earht Abundant Materials for Solar Cells*.

Altamura, Giovanni. 2014. "Development of $Cu_2ZnSn(S,Se)_4$ Thin Films Based Solar Cells." *PhD Thesis* doi:10.1109/PVSC.2016.7749619.

Altamura, Giovanni, Louis Grenet, Catherine Bougerol, Eric Robin, David Kohen, Hélène Fournier, Arnaud Brioude, Simon Perraud, and Henri Mariette. 2014. "$Cu_2ZnSn(S_{1-x}Se_x)_4$ Thin Films for Photovoltaic Applications: Influence of the Precursor Stacking Order on the Selenization Process." *Journal of Alloys and Compounds* 588: 310–15. doi:10.1016/j.jallcom.2013.11.068.

Altosaar, M., J. Raudoja, K. Timmo, M. Danilson, M. Grossberg, J. Krustok, and E. Mellikov. 2008. "$Cu_2Zn_{1-x}Cd_xSn(Se_{1-y}S_y)_4$ Solid Solutions as Absorber Materials for Solar Cells." *Physica Status Solidi (A) Applications and Materials Science* 205 (1): 167–70. doi:10.1002/pssa.200776839.

Araki, Hideaki, Aya Mikaduki, Yuki Kubo, Tatsuhiro Sato, Kazuo Jimbo, Win Shwe Maw, Hironori Katagiri, Makoto Yamazaki, Koichiro Oishi, and Akiko Takeuchi. 2008. "Preparation of Cu_2ZnSnS_4 Thin Films by Sulfurization of Stacked Metallic Layers." *Thin Solid Films* 517 (4). Elsevier B.V.: 1457–60. doi:10.1016/j.tsf.2008.09.058.

Aygun, Gulnur, Ayten Cantas, Yilmaz Simsek, and Rasit Turan. 2011. "Effects of Physical Growth Conditions on the Structural and Optical Properties of Sputtered Grown Thin HfO_2 Films." *Thin Solid Films* 519 (17): 5820–25. doi:10.1016/j.tsf.2010.12.189.

Bagdas Cantas, Ayten. 2017. "X-ray Photoelectron Spectroscopy Analysis of Magnetron Sputtered Cu_2ZnSnS_4 Based Thin Film Solar Cells with CdS Buffer Layer." *PhD Thesis*.

Bai, Zhizhong, Jun Yang, and Deliang Wang. 2011. "Thin Film CdTe Solar Cells with an Absorber Layer Thickness in Micro- and Sub-Micrometer Scale." *Applied*

Physics Letters 99 (14). doi:10.1063/1.3644160.

Berg, Dominik M., Monika Arasimowicz, Rabie Djemour, Levent Gütay, Susanne Siebentritt, Susan Schorr, Xavier Fontané, Victor Izquierdo-Roca, Alejandro Pérez-Rodriguez, and Phillip J. Dale. 2014. "Discrimination and Detection Limits of Secondary Phases in Cu_2ZnSnS_4 Using X-Ray Diffraction and Raman Spectroscopy." *Thin Solid Films* 569 Elsevier B.V.: 113–23. doi:10.1016/j.tsf.2014.08.028.

Berg, Dominik M, Rabie Djemour, Levent Gütay, Susanne Siebentritt, Phillip J Dale, Dominik M Berg, Rabie Djemour, et al. 2012. "Raman Analysis of Monoclinic Cu_2SnS_3 Thin Films." *Applied Physics Letters* 192103 (100). doi:10.1063/1.4712623.

Berg, Dominik Matthias. 2012. "Kesterite Equilibrium Reaction and the Discrimination of Secondary Phases from Cu_2ZnSnS_4." *Doctoral Thesis*

Biesinger, Mark C., Leo W M Lau, Andrea R. Gerson, and Roger St C Smart. 2010. "Resolving Surface Chemical States in XPS Analysis of First Row Transition Metals, Oxides and Hydroxides: Sc, Ti, V, Cu and Zn." *Applied Surface Science* 257 (3): 887–98. doi:10.1016/j.apsusc.2010.07.086.

Bremaud, D., D. Rudmann, M. Kaelin, K. Ernits, G. Bilger, M. Dbeli, H. Zogg, and A. N. Tiwari. 2007. "Flexible $Cu(In,Ga)Se_2$ on Al Foils and the Effects of Al during Chemical Bath Deposition." *Thin Solid Films* 515 (15 SPEC. ISS.): 5857–61. doi:10.1016/j.tsf.2006.12.152.

Buldu, Dilara Gokcen, Ayten Cantas, Fulya Turkoglu, Fatime Gulsah Akca, Ece Meric, Mehtap Ozdemir, Enver Tarhan, Lutfi Ozyuzer, Gulnur Aygun. 2017. "Influence of Sulfurization Temperature on Cu_2ZnSnS_4 Absorber Layer on Flexible Titanium Substrates for Thin Film Solar Cells" submitted to *Physica Scripta*.

Byungha Shin, Oki Gunawan, Yu Zhu, Nestor A. Bojarczuk, S. Jay Chey and Supratik Guha. 2013. "Thin Film Solar Cell with 8.4% Power Conversion Efficiency Using an Earth-Abundant Cu_2ZnSnS_4 Absorber." *Prog. Photovolt: Res. Appl.* 21 (February 2013): 72–76. doi:10.1002/pip.

Calderón, C., G. Gordillo, R. Becerra, and P. Bartolo-Pérez. 2015. "XPS Analysis and Characterization of Thin Films Cu_2ZnSnS_4 Grown Using a Novel Solution Based Route." *Materials Science in Semiconductor Processing* 39. Elsevier: 492–98. doi:10.1016/j.mssp.2015.05.064.

Chaar, L. El, L. A. Lamont, and N. El Zein. 2011. "Review of Photovoltaic Technologies." *Renewable and Sustainable Energy Reviews* 15 (5). Elsevier Ltd: 2165–75. doi:10.1016/j.rser.2011.01.004.

Chalapathi, U., S. Uthanna, and V. Sundara Raja. 2015. "Growth of Cu_2ZnSnS_4 Thin Films by a Two-Stage Process - Effect of Incorporation of Sulfur at the Precursor Stage." *Solar Energy Materials and Solar Cells* 132. Elsevier: 476–84. doi:10.1016/j.solmat.2014.09.035.

Chalapathy, R.B.V., Gwang Sun Jung, Young Min Ko, Byung Tae Ahn, and HyukSang Kwon. 2013. "Fabrication of Cu$_2$ZnSnS$_4$ Films by Rapid Thermal Annealing of Cu/ZnSn/Cu Precursor Layer and Their Application to Solar Cells." *Current Photovoltaic Research* 1 (2): 82–89.

Chaudhari, Sushmita, P K Kannan, and Suhash R Dey. 2016. "Investigation of Optimum Annealing Parameters for Formation of Dip Coated Cu$_2$ZnSnS$_4$ Thin Film" 612: 456–62.

Chen, Shiyou, X. G. Gong, Aron Walsh, and Su-huai Wei. 2010. "Defect Physics of the Kesterite Thin-Film Solar Cell Absorber Cu$_2$ZnSnS$_4$." *Applied Physics Letters* 96. doi:10.1063/1.3275796.

Chen, Shiyou, X. G. Gong, Aron Walsh, and Su Huai Wei. 2009. "Crystal and Electronic Band Structure of Cu$_2$ZnSnX$_4$ (X=S and Se) Photovoltaic Absorbers: First-Principles Insights." *Applied Physics Letters* 94 (4): 4–6. doi:10.1063/1.3074499.

Chen, Shiyou, Aron Walsh, Xin Gao Gong, and Su Huai Wei. 2013. "Classification of Lattice Defects in the Kesterite Cu$_2$ZnSnS$_4$and Cu$_2$ZnSnSe$_4$ Earth-Abundant Solar Cell Absorbers." *Advanced Materials* 25 (11): 1522–39. doi:10.1002/adma.201203146.

Chen, Shiyou, Lin Wang Wang, Aron Walsh, X. G. Gong, and Su Huai Wei. 2012. "Abundance of CuZn+ SnZn and 2CuZn +Sn Zn Defect Clusters in Kesterite Solar Cells." *Applied Physics Letters* 101 (22): 1–5. doi:10.1063/1.4768215.

Chen, Shiyou, Ji Hui Yang, X. G. Gong, Aron Walsh, and Su Huai Wei. 2010. "Intrinsic Point Defects and Complexes in the Quaternary Kesterite Semiconductor Cu$_2$ZnSnS$_4$." *Physical Review B - Condensed Matter and Materials Physics* 81 (24): 35–37. doi:10.1103/PhysRevB.81.245204.

Cheng, A.-J, M Manno, A Khare, C Leighton, S A Campbell, and E S Aydil. 2011. "Imaging and Phase Identification of Cu$_2$ZnSnS$_4$ Thin Films Using Confocal Raman Spectroscopy." *Journal of Vacuum Science & Technology A: Vacuum, Surfaces, and Films* 29 (5): 51203. doi:10.1116/1.3625249.

Choubrac, L., A. Lafond, C. Guillot-Deudon, Y. Moelo, and S. Jobic. 2012. "ChemInform Abstract: Structure Flexibility of the Cu$_2$ZnSnS$_4$ Absorber in Low-Cost Photovoltaic Cells: From the Stoichiometric to the Copper-Poor Compounds." *ChemInform* 43 (23): no-no. doi:10.1002/chin.201223001.

Cruz, M., J. Morales, J. P. Espinos, and J. Sanz. 2003. "XRD, XPS and 119 Sn NMR Study of Tin Sulfides Obtained by Using Chemical Vapor Transport Methods." *Journal of Solid State Chemistry* 175 (2): 359–65. doi:10.1016/S0022-4596(03)00329-3.

Das, S., C. Frye, P. G. Muzykov, and K. C. Mandal. 2012. "Deposition and Characterization of Low-Cost Spray Pyrolyzed Cu$_2$ZnSnS$_4$ (CZTS) Thin-Films for Large-Area High-Efficiency Heterojunction Solar Cells." *ECS Transactions* 45 (7):

153–61. doi:10.1149/1.3701535.

Emrani, Amin, Parag Vasekar, and Charles R. Westgate. 2013. "Effects of Sulfurization Temperature on CZTS Thin Film Solar Cell Performances." *Solar Energy* 98 (PC). Elsevier Ltd: 335–40. doi:10.1016/j.solener.2013.09.020.

Ennaoui, A., M. Lux-Steiner, A. Weber, D. Abou-Ras, I. Kötschau, H. W. Schock, R. Schurr, et al. 2009. "Cu_2ZnSnS_4 Thin Film Solar Cells from Electroplated Precursors: Novel Low-Cost Perspective." *Thin Solid Films* 517 (7): 2511–14. doi:10.1016/j.tsf.2008.11.061.

Ericson, Tove, Tomas Kubart, Jonathan J. Scragg, and Charlotte Platzer-Björkman. 2012. "Reactive Sputtering of Precursors for Cu_2ZnSnS_4Thin Film Solar Cells." *Thin Solid Films* 520 (24): 7093–99. doi:10.1016/j.tsf.2012.08.002.

Ericson, Tove, Jonathan J. Scragg, Tomas Kubart, Tobias Törndahl, and Charlotte Platzer-Björkman. 2013. "Annealing Behavior of Reactively Sputtered Precursor Films for Cu_2ZnSnS_4 Solar Cells." *Thin Solid Films* 535 (1). Elsevier B.V.: 22–26. doi:10.1016/j.tsf.2012.10.081.

Fernandes, P. A., P. M P Salomé, and A. F. da Cunha. 2009. "Growth and Raman Scattering Characterization of Cu_2ZnSnS_4 Thin Films." *Thin Solid Films* 517 (7): 2519–23. doi:10.1016/j.tsf.2008.11.031.

Fernandes, P. A., P. M P Salomé, and A. F. Da Cunha. 2010. "Cu_xSnS_{x+1} (X = 2, 3) Thin Films Grown by Sulfurization of Metallic Precursors Deposited by Dc Magnetron Sputtering." *Physica Status Solidi (C) Current Topics in Solid State Physics* 7 (3–4): 901–4. doi:10.1002/pssc.200982746.

Fernandes, P. A., P. M P Salomé, and A. F. Da Cunha. 2011. "Study of Polycrystalline Cu_2ZnSnS_4 Films by Raman Scattering." *Journal of Alloys and Compounds* 509 (28). Elsevier B.V.: 7600–7606. doi:10.1016/j.jallcom.2011.04.097.

Fernandes, P. A., P M P Salomé, and A F da Cunha. 2010. "A Study of Ternary Cu_2SnS_3 and Cu_3SnS_4 Thin Films Prepared by Sulfurizing Stacked Metal Precursors." *Journal of Physics D: Applied Physics* 43 (21): 215403. doi:10.1088/0022-3727/43/21/215403.

Fontane, X., L. Calvo-Barrio, V. Izquierdo-Roca, E. Saucedo, A. Perez-Rodriguez, J. R. Morante, D. M. Berg, P. J. Dale, and S. Siebentritt. 2011. "In-Depth Resolved Raman Scattering Analysis for the Identification of Secondary Phases: Characterization of Cu_2ZnSnS_4 Layers for Solar Cell Applications." *Applied Physics Letters* 98 (18): 1–4. doi:10.1063/1.3587614.

Fontané, X., V. Izquierdo-Roca, E. Saucedo, S. Schorr, V. O. Yukhymchuk, M. Ya Valakh, A. Pérez-Rodríguez, and J. R. Morante. 2012. "Vibrational Properties of Stannite and Kesterite Type Compounds: Raman Scattering Analysis of $Cu_2(Fe,Zn)SnS_4$." *Journal of Alloys and Compounds* 539: 190–94. doi:10.1016/j.jallcom.2012.06.042.

Ge, Jie, Wenlei Yu, Hong Cao, Jinchun Jiang, Jianhua Ma, Lihong Yang, Pingxiong Yang, Zhigao Hu, and Junhao Chu. 2012. "Fabrication of Cu_2ZnSnS_4 Absorbers by Sulfurization of Sn-Rich Precursors." *Physica Status Solidi (A) Applications and Materials Science* 209 (8): 1493–97. doi:10.1002/pssa.201228064.

Gemelli, E., and N.H.a. Camargo. 2007. "Oxidation Kinetics of Commercially Pure Titanium." *Matéria (Rio de Janeiro)* 12 (3): 525–31. doi:10.1590/S1517-70762007000300014.

Green, Martin A., Keith Emery, Yoshihiro Hishikawa, Wilhelm Warta, and Ewan D. Dunlop. 2016. "Solar Cell Efficiency Tables (Version 48)." *Progress in Photovoltaics: Research and Applications* 24 (7): 905–13. doi:10.1002/pip.2788.

Guc, Maxim, Sergiu Levcenko, I.V. Bodnar, Victor Izquierdo-roca, Xavier Fontane, L.V. Volkova, Ernest Arushanov, and Alejandro Pérez-Rodríguez. 2016. "Polarized Raman Scattering Study of Kesterite Type Cu_2ZnSnS_4 Single Crystals." *Scientific Reports* 5 (December 2015). Nature Publishing Group: 19414/1-7. doi:10.1038/srep19414.

Guilin, Chen, Wang Weihuang, Zhang Jin, Chen Shuiyuan, Huang Zhigao, and Rongkun Jian. 2017. "Ultra-High Sulfurization Temperature Drives the Growth of Oxide-Derived Cu_2ZnSnS_4 Thin Film with Very Large Grain." *Journal of Renewable and Sustainable Energy* 9 (1). doi:10.1063/1.4973716.

Gürel, Tanju, Cem Sevik, and Tahir Çagın. 2011. "Characterization of Vibrational and Mechanical Properties of Quaternary Compounds Cu_2ZnSnS_4 and $Cu_2ZnSnSe_4$ in Kesterite and Stannite Structures." *Physical Review B - Condensed Matter and Materials Physics* 84 (20): 1–7. doi:10.1103/PhysRevB.84.205201.

Hall, S R, J T Szymanski, and J M Stewart. 1978. "Kesterite, Cu(2) (Zn,Fe)SnS(4), and Stannite, Cu(2)(Fe,Zn)SnS(4), Structurally Similar but Distinct Minerals." *Canadian Mineralogist* 16 (2): 131–37.

Hartmann, M, Marion Schmidt, Axel Jasenek, Hans-Werner Schock, F. Kessler, K Herz, and Michael Powalla. 2000. "Flexible and Light Weight Substrates for Cu (In, Ga) Se_2 Solar Cells and Modules." *Proceedings of the 28th IEEE PVSC*, 638–41. doi:10.1109/PVSC.2000.915924.

He, Jun, Lin Sun, Ye Chen, Jinchun Jiang, and Junhao Chu. 2014. "Cu_2ZnSnS_4 Thin Film Solar Cell Utilizing Rapid Thermal Process of Precursors Sputtered from a Quaternary Target a Promising Application in Industrial Processes." *Royal Society of Chemistry* 4: 43080–86. doi:10.1039/c4ra07748b.

He, Jun, Lin Sun, Ye Chen, Jinchun Jiang, Pingxiong Yang, and Junhao Chu. 2015. "Influence of Sulfurization Pressure on Cu_2ZnSnS_4 Thin Films and Solar Cells Prepared by Sulfurization of Metallic Precursors." *Journal of Power Sources* 273: 600–607. doi:10.1016/j.jpowsour.2014.09.088.

Herz, K., A. Eicke, F. Kessler, R. Wachter, and M. Powalla. 2003. "Diffusion Barriers for CIGS Solar Cells on Metallic Substrates." *Thin Solid Films* 431–432 (May

2003): 392–97. doi:10.1016/S0040-6090(03)00259-1.

Himmrich, M., and H. Haeuseler. 1991. "Far Infrared Studies on Stannite and Wurtzstannite Type Compounds." *Spectrochimica Acta Part A: Molecular Spectroscopy* 47 (7): 933–42. doi:10.1016/0584-8539(91)80283-O.

Hiroi, Homare, Noriyuki Sakai, Takuya Kato, Hiroki Sugimoto, and Showa Shell Sekiyu K K. 2013. "High Voltage Cu_2ZnSnS_4 Submodules by Hybrid Buffer Layer." *2013 IEEE 39th Photovoltaic Specialists Conference (PVSC)*, 863–66. doi:10.1109/PVSC.2013.6744281.

Hodges, Deidra Ranel. 2008. "Development of CdTe Thin Film Solar Cells on Flexible Foil Substrates." *PhD Thesis*

Ikhlasul Amal, M., and Kyoo Ho Kim. 2013. "Structural and Optical Properties of Sulfurized Cu_2ZnSnS_4 Thin Films from Cu-Zn-Sn Alloy Precursors." *Journal of Materials Science: Materials in Electronics* 24 (2): 559–66. doi:10.1007/s10854-012-0858-7.

Ito, Kentaro, and Tatsuo Nakazawa. 1988. "Electrical and Optical Properties of Stannite-Type Quarternary Semiconductor Thin Films." *Japanese Journal of Applied Physics* 27: 2094–97. doi:10.1143/JJAP.27.2094.

Jackson, Philip, Dimitrios Hariskos, Erwin Lotter, Stefan Paetel, Roland Wuerz, Richard Menner, Wiltraud Wischmann, and Michael Powalla. 2011. "New World Record Efficiency for $Cu(In,Ga)Se_2$ thin-Film Solar Cells beyond 20%." *Prog. Photovolt: Res. Appl.* 19: 894–97. doi:10.1002/pip.

Jawhari, T, M Dimitrievska, A Fairbrother, and E Saucedo. 2014. "Multiwavelength Excitation Raman Scattering Study of Polycrystalline Kesterite Cu_2ZnSnS_4 Thin Films." *Applied Physics Letters* 21901: 1–5.

Jimbo, Kazuo, Ryoichi Kimura, Tsuyoshi Kamimura, Satoru Yamada, Win Shwe Maw, Hideaki Araki, Koichiro Oishi, and Hironori Katagiri. 2007. "Cu_2ZnSnS_4-Type Thin Film Solar Cells Using Abundant Materials." *Thin Solid Films* 515 (15 SPEC. ISS.): 5997–99. doi:10.1016/j.tsf.2006.12.103.

Katagiri, Hironori, and Kazuo Jimbo. 2011. "Development of Rare Metal-Free CZTS-Based Thin Film Solar Cells." *Conference Record of the IEEE Photovoltaic Specialists Conference*, 003516–21. doi:10.1109/PVSC.2011.6186707.

Katagiri, Hironori, Kazuo Jimbo, Win Shwe Maw, Koichiro Oishi, Makoto Yamazaki, Hideaki Araki, and Akiko Takeuchi. 2009. "Development of CZTS-Based Thin Film Solar Cells." *Thin Solid Films* 517 (7): 2455–60. doi:10.1016/j.tsf.2008.11.002.

Katagiri, Hironori, Kazuo Jimbo, Masami Tahara, Hideaki Araki, and Koichiro Oishi. 2009. "The Influence of the Composition Ratio on CZTS-Based Thin Film Solar Cells." *Materials Research Society Symposium Proceedings Vol. 1165* 1165: 1165-M04-1. doi:10.1016/j.solmat.2011.05.050.

Katagiri, Hironori, Nobuyuki Sasaguchi, Shima Hando, Suguro Hoshino, Jiro Ohashi, and Takaharu Yokota. 1997. "Preparation and Evaluation of Cu_2ZnSnS_4 Thin Films by Sulfurization of E-B Evaporated Precursors." *Solar Energy Materials and Solar Cells* 49 (1–4): 407–14. doi:10.1016/S0927-0248(97)00119-0.

Kazmerski, L. L., F. R. White, and G. K. Morgan. 1976. "Thin-Film CuInSe2/CdS Heterojunction Solar Cells." *Applied Physics Letters* 29 (4): 268–70. doi:10.1063/1.89041.

Kessler, Friedrich, and Dominik Rudmann. 2004. "Technological Aspects of Flexible CIGS Solar Cells and Modules." *Solar Energy* 77 (6): 685–95. doi:10.1016/j.solener.2004.04.010.

Khalil, M. I., O. Atici, A. Lucotti, S. Binetti, A. Le Donne, and L. Magagnin. 2016. "CZTS Absorber Layer for Thin Film Solar Cells from Electrodeposited Metallic Stacked Precursors (Zn/Cu-Sn)." *Applied Surface Science* 379. Elsevier B.V.: 91–97. doi:10.1016/j.apsusc.2016.04.062.

Khare, Ankur, Burak Himmetoglu, Matteo Cococcioni, and Eray S Aydil. 2012. "First Principles Calculation of the Electronic Properties and Lattice Dynamics of $Cu_2ZnSn(S_{1-x}Se_x)_4$." *Journal of Applied Physics* 111 (12): 123704. doi:10.1063/1.4728232.

Khare, Ankur, Burak Himmetoglu, Melissa Johnson, David J. Norris, Matteo Cococcioni, and Eray S. Aydil. 2012. "Calculation of the Lattice Dynamics and Raman Spectra of Copper Zinc Tin Chalcogenides and Comparison to Experiments." *Journal of Applied Physics* 111 (8). doi:10.1063/1.4704191.

Koseoglu, Fulya. 2017. " Magnetron Sputtering Growth of AZO/ZnO/Zn(O,S) Multilayers for Cu_2ZnSnS_4 Thin Film Solar Cells: Material and Device Characterization. " *PhD Thesis.*

Krylova, Valentina, and Mindaugas Andrulevičius. 2009. "Optical, XPS and XRD Studies of Semiconducting Copper Sulfide Layers on a Polyamide Film." *International Journal of Photoenergy* 2009 (Ii). doi:10.1155/2009/304308.

Kumar, Mukesh, Ashish Dubey, Nirmal Adhikari, Swaminathan Venkatesan, and Qiquan Qiao. 2015. "Strategic Review of Secondary Phases, Defects and Defect-Complexes in Kesterite CZTS–Se Solar Cells." *Energy Environ. Sci.* 8 (11). Royal Society of Chemistry: 3134–59. doi:10.1039/C5EE02153G.

Lafond, Alain, Léo Choubrac, Catherine Guillot-Deudon, Philippe Deniard, and Stephane Jobic. 2012. "Crystal Structures of Photovoltaic Chalcogenides, an Intricate Puzzle to Solve: The Cases of CIGSe and CZTS Materials." *Zeitschrift Fur Anorganische Und Allgemeine Chemie* 638 (15): 2571–77. doi:10.1002/zaac.201200279.

Liu, Fangyang, Yi Li, Kun Zhang, Bo Wang, Chang Yan, Yanqing Lai, Zhian Zhang, Jie Li, and Yexiang Liu. 2010. "In Situ Growth of Cu_2ZnSnS_4 Thin Films by Reactive Magnetron Co-Sputtering." *Solar Energy Materials and Solar Cells* 94 (12): 2431–34. doi:10.1016/j.solmat.2010.08.003.

Mikhlin, Yuri L., Yevgeny V. Tomashevich, Igor P. Asanov, Alexander V. Okotrub, Vladimir A. Varnek, and Denis V. Vyalikh. 2004. "Spectroscopic and Electrochemical Characterization of the Surface Layers of Chalcopyrite (CuFeS2) Reacted in Acidic Solutions." *Applied Surface Science* 225 (1–4): 395–409. doi:10.1016/j.apsusc.2003.10.030.

Mkawi, E. M., K. Ibrahim, M. K M Ali, K. M A Saron, M. A. Farrukh, and Nageh K. Allam. 2014. "Influence of Substrate Temperature on the Properties of Electrodeposited Kesterite Cu_2ZnSnS_4 (CZTS) Thin Films for Photovoltaic Applications." *Journal of Materials Science: Materials in Electronics* 26 (1): 222–28. doi:10.1007/s10854-014-2387-z.

Moholkar, A. V., S. S. Shinde, A. R. Babar, Kyu Ung Sim, Ye bin Kwon, K. Y. Rajpure, P. S. Patil, C. H. Bhosale, and J. H. Kim. 2011. "Development of CZTS Thin Films Solar Cells by Pulsed Laser Deposition: Influence of Pulse Repetition Rate." *Solar Energy* 85 (7): 1354–63. doi:10.1016/j.solener.2011.03.017.

Monshi, Ahmad, Mohammad Reza Foroughi, and Mohammad Reza Monshi. 2012. "Modified Scherrer Equation to Estimate More Accurately Nano-Crystallite Size Using XRD." *World Journal of Nano Science and Engineering* 2 (3): 154–60. doi:10.4236/wjnse.2012.23020.

Olekseyuk, I. D., I. V. Dudchak, and L. V. Piskach. 2004. "Phase Equilibria in the Cu_2S-ZnS-SnS_2 System." *Journal of Alloys and Compounds* 368 (1–2): 135–43. doi:10.1016/j.jallcom.2003.08.084.

Paier, Joachim, Ryoji Asahi, Akihiro Nagoya, and Georg Kresse. 2009. "Cu_2ZnSnS_4 as a Potential Photovoltaic Material: A Hybrid Hartree-Fock Density Functional Theory Study." *Physical Review B - Condensed Matter and Materials Physics* 79 (11): 1–8. doi:10.1103/PhysRevB.79.115126.

Persson, Clas. 2010. "Electronic and Optical Properties of Cu_2ZnSnS_4 and $Cu_2ZnSnSe_4$." *Journal of Applied Physics* 107 (5). doi:10.1063/1.3318468.

Platzer-Björkman, C., J. Scragg, H. Flammersberger, T. Kubart, and M. Edoff. 2012. "Influence of Precursor Sulfur Content on Film Formation and Compositional Changes in Cu_2ZnSnS_4 Films and Solar Cells." *Solar Energy Materials and Solar Cells* 98: 110–17. doi:10.1016/j.solmat.2011.10.019.

Repins, Ingrid, Carolyn Beall, Nirav Vora, Clay DeHart, Darius Kuciauskas, Pat Dippo, Bobby To, et al. 2012. "Co-Evaporated $Cu_2ZnSnSe_4$ Films and Devices." *Solar Energy Materials and Solar Cells* 101: 154–59. doi:10.1016/j.solmat.2012.01.008.

Schorr, Susan, and Gabriela Gonzalez-Aviles. 2009. "In-Situ Investigation of the Structural Phase Transition in Kesterite." *Physica Status Solidi (a)* 206 (5): 1054–58. doi:10.1002/pssa.200881214.

Schorr, Susan, Hans-Joachim Hoebler, and Michael Tovar. 2007. "A Neutron Diffraction Study of the Stannite-Kesterite Solid Solution Series." *European Journal of*

Mineralogy 19 (1): 65–73. doi:10.1127/0935-1221/2007/0019-0065.

Shockley, William, and Hans J. Queisser. 1961. "Detailed Balance Limit of Efficiency of P-N Junction Solar Cells." *Journal of Applied Physics* 32 (3): 510–19. doi:10.1063/1.1736034.

Scragg, J. J., Tomas Kubart, J. Timo Wätjen, Tove Ericson, Margareta K. Linnarsson, and Charlotte Platzer-Björkman. 2013. "Effects of Back Contact Instability on Cu_2ZnSnS_4 Devices and Processes." *Chemistry of Materials* 25 (15): 3162–71. doi:10.1021/cm4015223.

Scragg, J. J., J. Timo Wätjen, Marika Edoff, Tove Ericson, Tomas Kubart, and Charlotte Platzer-Björkman. 2012. "A Detrimental Reaction at the Molybdenum Back Contact in $Cu_2ZnSn(S,Se)_4$ Thin-Film Solar Cells." *Journal of the American Chemical Society* 134 (47): 19330–33. doi:10.1021/ja308862n.

Scragg, Jonathan J., Phillip J. Dale, and Laurence M. Peter. 2008. "Towards Sustainable Materials for Solar Energy Conversion: Preparation and Photoelectrochemical Characterization of Cu_2ZnSnS_4." *Electrochemistry Communications* 10 (4): 639–42. doi:10.1016/j.elecom.2008.02.008.

Scragg, Jonathan J., Tove Ericson, Xavier Fontané, Victor Izquierdo-Roca, Alejandro Pérez-Rodríguez, Tomas Kubart, Marika Edoff, and Charlotte Platzer-Björkman. 2014. "Rapid Annealing of Reactively Sputtered Precursors for Cu 2ZnSnS4 Solar Cells." *Progress in Photovoltaics: Research and Applications* 22 (1): 10–17. doi:10.1002/pip.2265.

Scragg, Jonathan James. 2010. "Studies of Cu2ZnSnS4 Films Prepared by Sulfurisation of Electrodeposited Precursors." *PhD Thesis*, 262.

Shin, Seung Wook, S. M. Pawar, Chan Young Park, Jae Ho Yun, Jong Ha Moon, Jin Hyeok Kim, and Jeong Yong Lee. 2011. "Studies on Cu_2ZnSnS_4 (CZTS) Absorber Layer Using Different Stacking Orders in Precursor Thin Films." *Solar Energy Materials and Solar Cells* 95 (12): 3202–6. doi:10.1016/j.solmat.2011.07.005.

Shockley, William, and Hans J. Queisser. 1961. "Detailed Balance Limit of Efficiency of P-N Junction Solar Cells." *Journal of Applied Physics* 32 (3): 510–19. doi:10.1063/1.1736034.

Siebentritt, Susanne, and Susan Schorr. 2012. "Kesterites a Challenging Material for Solar Cells." *Prog. Photovolt: Res. Appl.* 20: 512–19. doi:10.1002/pip.

Singh, Ajay, Hugh Geaney, Fathima Laffir, and Kevin M Ryan. 2012. "Colloidal Synthesis of Wurtzite Cu(2)ZnSnS(4) Nanorods and Their Perpendicular Assembly." *Journal of the American Chemical Society* 134 (6): 2910–13. doi:10.1021/ja2112146.

Singh, Om P, N Muhunthan, Vidya N Singh, and Bhanu P Singh. 2014. "Effect Of Annealing Time On The Composition , Microstructure And Band Gap Of Copper Zinc Tin Sulfide Thin Films." *Adv. MAter. Lett.* 6 (1): 2-7

doi:10.5185/amlett.2015.6584.

Sun, Kaiwen, Fangyang Liu, Chang Yan, Fangzhou Zhou, Jialiang Huang, Yansong Shen, Rong Liu, and Xiaojing Hao. 2016. "Influence of Sodium Incorporation on Kesterite Cu_2ZnSnS_4 Solar Cells Fabricated on Stainless Steel Substrates." *Solar Energy Materials and Solar Cells* 157. Elsevier: 565–71. doi:10.1016/j.solmat.2016.07.036.

Tajima, Shin, Umehara Mitsutaro, Masaki Hasegawa, Takahiro Mise, and Tadayoshi Itoh. 2017. "Cu_2ZnSnS_4 photovoltaic Cell with Improved Efficiency Fabricated by High-Temperature Annealing after CdS Buffer-Layer Deposition." *Prog. Photovolt: Res. Appl.* 25: 14–22. doi:10.1002/pip.2837.

Tanaka, Kunihiko, Minoru Kato, Koichi Goto, Yuya Nakano, and Hisao Uchiki. 2012. "Face-to-Face Annealing Process of Cu_2ZnSnS_4 Thin Films Deposited by Spray Pyrolysis Method." *Japanese Journal of Applied Physics* 51: 10NC26.

Thota, Narayana, M. Gurubhaskar, M. Anantha Sunil, P. Prathap, Y. P.Venkata Subbaiah, and Ashutosh Tiwari. 2017. "Effect of Metal Layer Stacking Order on the Growth of Cu_2ZnSnS_4 thin Films." *Applied Surface Science* 396: 644–51. doi:10.1016/j.apsusc.2016.11.001.

Tiwari, Devendra, Tapas K. Chaudhuri, T. Shripathi, U. Deshpande, and R. Rawat. 2013. "Non-Toxic, Earth-Abundant 2% Efficient Cu_2SnS_3 Solar Cell Based on Tetragonal Films Direct-Coated from Single Metal-Organic Precursor Solution." *Solar Energy Materials and Solar Cells* 113 (December): 165–70. doi:10.1016/j.solmat.2013.02.017.

Todorov, Teodor, Oki Gunawan, S. Jay Chey, Thomas Goislard De Monsabert, Aparna Prabhakar, and David B. Mitzi. 2011. "Progress towards Marketable Earth-Abundant Chalcogenide Solar Cells." *Thin Solid Films* 519 (21): 7378–81. doi:10.1016/j.tsf.2010.12.225.

Todorov, Teodor K., Kathleen B. Reuter, and David B. Mitzi. 2010. "High-Efficiency Solar Cell with Earth-Abundant Liquid-Processed Absorber." *Advanced Materials* 22 (20): 156–59. doi:10.1002/adma.200904155.

Tuna, Ocal, Yusuf Selamet, Gulnur Aygun, and Lutfi Ozyuzer. 2010. "High Quality ITO Thin Films Grown by Dc and RF Sputtering without Oxygen." *Journal of Physics D: Applied Physics* 43 (5): 55402. doi:10.1088/0022-3727/43/5/055402.

Valakh, M. Y., O. F. Kolomys, S. S. Ponomaryov, V. O. Yukhymchuk, I. S. Babichuk, V. Izquierdo-Roca, E. Saucedo, et al. 2013. "Raman Scattering and Disorder Effect in Cu_2ZnSnS_4." *Physica Status Solidi - Rapid Research Letters* 7 (4): 258–61. doi:10.1002/pssr.201307073.

Valle Rios, Laura Elisa, Kai Neldner, Galina Gurieva, and Susan Schorr. 2016. "Existence of off-Stoichiometric Single Phase Kesterite." *Journal of Alloys and Compounds* 657: 408–13. doi:10.1016/j.jallcom.2015.09.198.

Walker, Perrin, and William H Tarn. 1991. *Handbook of Metal Etchants*. *Technology*.

Walsh, Aron, Shiyou Chen, Su Huai Wei, and Xin Gao Gong. 2012. "Kesterite Thin-Film Solar Cells: Advances in Materials Modelling of Cu_2ZnSnS_4." *Advanced Energy Materials* 2 (4): 400–409. doi:10.1002/aenm.201100630.

Wang, Hongxia. 2011. "Progress in Thin Film Solar Cells Based on Cu_2ZnSnS_4" *International Journal of Photoenergy* 2011: 10. doi:10.1155/2011/801292.

Wang, K., O. Gunawan, T. Todorov, B. Shin, S. J. Chey, N. A. Bojarczuk, D. Mitzi, and S. Guha. 2010. "Thermally Evaporated Cu_2ZnSnS_4 Solar Cells." *Applied Physics Letters* 97 (14): 2013–16. doi:10.1063/1.3499284.

Wang, Wei, Mark T. Winkler, Oki Gunawan, Tayfun Gokmen, Teodor K. Todorov, Yu Zhu, and David B. Mitzi. 2014. "Device Characteristics of CZTSSe Thin-Film Solar Cells with 12.6% Efficiency." *Advanced Energy Materials* 4 (7): 1–5. doi:10.1002/aenm.201301465.

Wang, Weijing, Yahui Liu, Tianjan Xue, Jie Li, Desheng Chen, and Tao Qi. 2015. "Mechanism and Kinetics of Titanium Hydrolysis in Concentrated Titanyl Sulfate Solution Based on Infrared and Raman Spectra." *Chemical Engineering Science* 134 (June). Elsevier: 196–204. doi:10.1016/j.ces.2015.05.006.

Wang, Yejiao. 2016. "Fabrication of Cu2ZnSnSe4 Thin-Film Solar Cells by a Two-Stage Process." *PhD Thesis*, no. April.

Washio, Tsukasa, Hiroshi Nozaki, Tatsuo Fukano, Tomoyoshi Motohiro, Kazuo Jimbo, and Hironori Katagiri. 2011. "Analysis of Lattice Site Occupancy in Kesterite Structure of Cu_2ZnSnS_4 Films Using Synchrotron Radiation X-Ray Diffraction." *Journal of Applied Physics* 110 (7): 74511. doi:10.1063/1.3642993.

Weber, A., R. Mainz, and H. W. Schock. 2010. "On the Sn Loss from Thin Films of the Material System Cu-Zn-Sn-S in High Vacuum." *Journal of Applied Physics* 107 (1). doi:10.1063/1.3273495.

Wu, Changzheng, Zhenpeng Hu, Chengle Wang, Hua Sheng, Jinlong Yang, and Yi Xie. 2007. "Hexagonal Cu_2SnS_3 with Metallic Character: Another Category of Conducting Sulfides." *Applied Physics Letters* 91 (14): 1–4. doi:10.1063/1.2790491.

Wuerz, R., A. Eicke, M. Frankenfeld, F. Kessler, M. Powalla, P. Rogin, and O. Yazdani-Assl. 2009. "CIGS Thin-Film Solar Cells on Steel Substrates." *Thin Solid Films* 517 (7). Elsevier B.V.: 2415–18. doi:10.1016/j.tsf.2008.11.016.

Xie, M, D M Zhuang, M Zhao, Z L Zhuang, L Q Ouyang, X L Li, and J Song. 2013. "Preparation and Characterization of Cu_2ZnSnS_4 Thin Films and Solar Cells Fabricated from Quaternary Cu-Zn-Sn-S Target." *International Journal of Photoenergy* 2013. doi:10.1155/2013/929454.

Xu, Jiaxiong, Zhongming Cao, Yuanzheng Yang, and Zhiwei Xie. 2014. "Characterization of Cu_2ZnSnS_4 Thin Films on Flexible Metal Foil Substrates." *Journal of Materials Science: Materials in Electronics* 26 (2): 726–33.

doi:10.1007/s10854-014-2456-3.

Yang, Kee-jeong, Sim, J.-H, Jeon, B., Son, D-H , Kim, D-H, Sung, S-Joon, Hwang, D-K. 2014. "Effects of Na and MoS_2 on Cu_2ZnSnS_4 Thin-Film Solar Cell." *Prog. Photovolt: Res. Appl.* doi:10.1002/pip.2500.

Yang, Chongyin, Mingsheng Qin, Yaoming Wang, Dongyun Wan, Fuqiang Huang, and Jianhua Lin. 2013. "Observation of an Intermediate Band in Sn-Doped Chalcopyrites with Wide-Spectrum Solar Response." *Scientific Reports* 3: 1–7. doi:10.1038/srep01286.

Yang, K-J, J-H Sim, Dae Ho Son, Dae Hwan Kim, Gee Yeong Kim, William Jo, Soomin Song, et al. 2015. "Effects of the Compositional Ratio Distribution with Sulfurization Temperatures in the Absorber Layer on the Defect and Surface Electrical Characteristics of Cu_2ZnSnS_4 Solar Cells." *Prog. Photovolt: Res. Appl.* 23 (April 21): 1771–84. doi:10.1002/pip.

Yazici, Sebnem, Mehmet Ali Olgar, Fatime Gulsah Akca, Ayten Cantas, Metin Kurt, Gulnur Aygun, Enver Tarhan, Ekrem Yanmaz, and Lutfi Ozyuzer. 2015. "Growth of Cu_2ZnSnS_4 Absorber Layer on Flexible Metallic Substrates for Thin Film Solar Cell Applications." *Thin Solid Films* 589: 563–73. doi:10.1016/j.tsf.2015.06.028.

Yoo, Hyesun, and Junho Kim. 2010. "Growth of Cu_2ZnSnS_4 Thin Films Using Sulfurization of Stacked Metallic Films." *Thin Solid Films* 518 (22). Elsevier B.V.: 6567–72. doi:10.1016/j.tsf.2010.03.058.

Yoo, Hyesun, and Junho Kim. 2011. "Comparative Study of Cu_2ZnSnS_4Film Growth." *Solar Energy Materials and Solar Cells* 95 (1): 239–44. doi:10.1016/j.solmat.2010.04.060.

Zakaria, Zaihasraf, Puvaneswaran Chelvanathan, Mohammad Junaebur Rashid, Md Akhtaruzzaman, Mohammad Mezbaul Alam, Zeid Abdullah Al-Othman, Alamoud Abdulrahman, Kamaruzzaman Sopian, and Nowshad Amin. 2015. " Effects of Sulfurization on Cu_2ZnSnS_4 (CZTS) Thin Fims Deposited by Single Source Thermal Evaporation Method." *Japanese Journal of Applied Physics* 54 (8S1): 6–11. doi:http://dx.doi.org/10.7567/JJAP.54.08KC18.

Zhang, Y Z, Q Y Ye, Jiang Liu, Hao Chen, X L He, Cheng Liao, J F Han, Hao Wang, Jun Mei, and W M Lau. 2014. "Earth-Abundant and Low-Cost CZTS Solar Cell on Flexible Molybdenum Foil." *Rsc Advances* 4 (45): 23666–69. doi:10.1039/c4ra02064b.